CATALYTIC GAS-PHASE HYDRODEOXYGENATION OF PHENOL OVER SILICA SUPPORTED ZINC CATALYSTS AT ATMOSPHERIC PRESSURE

HAMED POURZOLFAGHAR

FACULTY OF ENGINEERING
UNIVERSITY OF MALAYA
KUALA LUMPUR

2021

CATALYTIC GAS-PHASE HYDRODEOXYGENATION OF PHENOL OVER SILICA SUPPORTED CATALYSTS AT ATMOSPHERIC PRESSURE

HAMED POURZOLFAGHAR

THESIS SUBMITTED IN FULFILMENT OF THE REQUIREMENTS FOR THE DEGREE OF DOCTOR OF PHILOSOPHY

CHEMICAL ENGINEERING DEPARTMENT
FACULTY OF ENGINEERING
UNIVERSITY OF MALAYA
KUALA LUMPUR

2021

UNIVERSITY OF MALAYA

ORIGINAL LITERARY WORK DECLARATION

Name of Candidate: Hamed Pourzolfaghar

Matric No: KHA140021

Name of Degree: DOCTOR OF PHILOSOPHY

Title of Project Paper/Research Report/Dissertation/Thesis ("this Work"):

CATALYTIC GAS-PHASE HYDRODEOXYGENATION OF PHENOL OVER SILICA SUPPORTED ZINC CATALYSTS AT ATMOSPHERIC PRESSURE

Field of Study:

BIOFUEL UPGRADING, CHEMICAL REACTION ENGINEERING

 I do solemnly and sincerely declare that:

(1) I am the sole author/writer of this Work;
(2) This Work is original;
(3) Any use of any work in which copyright exists was done by way of fair dealing and for permitted purposes and any excerpt or extract from, or reference to or reproduction of any copyright work has been disclosed expressly and sufficiently and the title of the Work and its authorship have been acknowledged in this Work;
(4) I do not have any actual knowledge nor do I ought reasonably to know that the making of this work constitutes an infringement of any copyright work;
(5) I hereby assign all and every rights in the copyright to this Work to the University of Malaya ("UM"), who henceforth shall be owner of the copyright in this Work and that any reproduction or use in any form or by any means whatsoever is prohibited without the written consent of UM having been first had and obtained;
(6) I am fully aware that if in the course of making this Work I have infringed any copyright whether intentionally or otherwise, I may be subject to legal action or any other action as may be determined by UM.

 Candidate's Signature   **Date:** 04/06/2021

Subscribed and solemnly declared before,

 Witness's Signature   **Date:**

Name:

Designation:

CATALYTIC GAS-PHASE HYDRODEOXYGENATION OF PHENOL OVER SILICA SUPPORTED ZINC CATALYSTS AT ATMOSPHERIC PRESSURE

ABSTRACT

Hydrodeoxygenation (HDO) is a promising process for bio-oil upgrading derived from biomass wood. Although the result of the process performance is encouraging, further investigation still continues especially in obtaining the best type of catalyst in an atmospheric process condition. In this study, the HDO of phenol-based bio-oil catalyzed by Zn/SiO_2 under atmospheric H_2 pressure was investigated in a continuous fixed bed reactor. The physicochemical properties of the catalysts were surveyed by XRD, BET, ICP-OES, EDX, H_2-TPD, NH_3-TPD, TGA, H_2-TPR, and FESEM. Following, the effects of various process parameters on the conversion efficiency and selectivity of the catalytic reaction products have been investigated. Finally, the stability and regenerability of the catalysts as well as the mechanism of the reaction have been surveyed.

Characteristics outcomes indicated that the prepared catalyst is able to convert the phenol into aromatic hydrocarbons in low pressure hydrogen. The optimization study using various independent variables revealed that the hydrogen volumetric flow rate slightly affects product distribution and conversion efficiency. Process temperature increases the reaction conversion efficiency without changing the selectivity. The optimization study indicated that a process with 3% Zn/SiO_2 as the catalyst, temperature at 500 ˚C, WHSV of 0.32 h^{-1}, and H_2 volumetric flow rate of 150 mL/min provides the highest possible conversion efficiency of phenol into aromatic hydrocarbons. The time-on-stream investigation illustrated that the silica-supported zinc was highly active up to 240 min of phenol HDO, with a conversion efficiency up to 80%, and after 420 min of TOS, the activity decreased to around a conversion rate of 43%. Reusability tests revealed that the

catalyst displayed outstanding reusability and could be regenerated fully after four reusing rounds.

HIDRODEOKSIGENASI BERFASA GAS BERMANGKIN FENOL MELALUI PEMANGKIN SILIKA DISOKONG OLEH ZINK PADA TEKANAN ATMOSFERA

ABSTRAK

Proses hidrodeoksigenasi (HDO) berpotensi untuk meningkatkan kualiti penjanaan minyak-bio berasaskan bio-jisim kayu. Walaupun hasil dapatan daripada proses ini memberasangkan, kajian terperinci masih perlu dilakukan untuk mencari jenis pemangkin yang sesuai pada tekanan atmosfera. Kajian ini menfokuskan kepada penghasilan fenol berasaskan minyak-bio melalui HDO yang dimangkinkan oleh pemangkin Zn/SiO_2 pada tekanan atmosfera oleh H_2 dalam reaktor katil tetap berterusan. Sifat-sifat fisiko-kimia pemangkin ini dikaji menggunakan pelbagai peralatan analitikal. Kesan-kesan penggunaan pelbagai parameter proses terhadap kecekapan penukaran dan selektiviti bagi hasil daripada tindak-balas katalitik turut disiasat. Akhir sekali, kestabilan dan keupayaan penjanaan semula berserta dengan mekanisma tindak-balas pemangkin ini turut dikaji.

Keupayaan pemangkin untuk menukarkan fenol kepada hidrokarbon aromatik dalam keadaan hidrogen brtekanan rendah dapat dibuktikan melalui ciri-ciri hasilan daripada tindak-balas pemangkin. Kajian pengoptimaan menggunakan pelbagai pembolehubah bebas menunjukkan kadar aliran isipadu hidrogen mampu menjejaskan pengagihan produk dan kecekapan penukaran pemangkin. Peningkatan suhu juga boleh meningkatkan kecekapan penukaran tindak-balas tanpa mengubah selektiviti pemangkin. Pengoptimuman tindak balas menunjukkan penggunaanan pemangkin Zn/SiO_2 berkadar 3% bersuhu 500 °C dengan WHSV berkuantiti 32 h^{-1}, dan kadar aliran isipadu H_2 sebanyak 150 mL/min mencapai kecekapan yang paling optimum untuk penukaran fenol kepada hidrokarbon aromatik. Selain itu, kaedah penyelidikan *time-on-stream*

menunjukkan silika disokong oleh zink mempunyai pengaktifan HDO fenol yang tinggi sehingga 240 minit melalui kecekapan penukaran sebanyak 80%. Pengaktifan ini berkurangan dengan kadar kecekapan penukaran sebanyak 43% selepas 420 minit masa TOS. Ujian kebolehgunaan semula mendedahkan pemangkin ini mempunyai kemantapan kebolehgunaan semula dan boleh dijana semula sepenuhnya selepas beberapa kali pusingan penggunaan.

Kata kunci: Hidrodoksigenasi atmosfera (HDO), Peningkatan minyak bio, Sebatian fenolik, Pemangkin zink, Zn/SiO_2.

DEDICATED TO

My dearest parents

Whose endless love and care supported me all through the way

ACKNOWLEDGEMENTS

TABLE OF CONTENTS

LIST OF FIGURES

LIST OF TABLES

LIST OF SYMBOLS AND ABBREVIATIONS

Abbreviation /Symbol		Description
Å	:	Angstrom
Ar	:	Argon gas
BET	:	Brunauer–Emmett–Teller
C	:	Carbon
CNFs	:	Carbon nanofibers
CNG	:	Compressed natural gas
DDO	:	Direct deoxygenation
DME	:	Demethylation
DMO	:	Demethoxylation
DOE	:	di-*n*-octyl ether
EDX	:	Energy-dispersive X-ray spectroscopy
EPA	:	United States Environmental Protection Agency
FAME	:	Fatty acid methyl esters
FCC	:	Fluid Catalytic Cracking
FESEM	:	Field Emission Scanning Electron Microscope
FT oil	:	Fisher-Tropsch oil or green motor fuel from biomass
Ga	:	Gallium
GC-FID	:	Gas chromatography - Flame-ionization detection
HDN	:	Hydrodenitrogenation
HDO	:	Hydrodeoxygenation
HDS	:	Hydrodesulfurization

HHV	:	Higher heat value/Calorific value
HPLC	:	High Performance Liquid Chromatography
HV	:	Heating value
ICP-OES	:	Inductively coupled plasma atomic emission spectroscopy
ID	:	Internal diameter
IUPAC	:	International Union of Pure and Applied Chemistry
LPG	:	Liquefied petroleum gas
max	:	Maximum
Mo	:	Molybdenum
MSDS	:	Material safety data sheet
N_2	:	Nitrogen gas
NH_3	:	Ammonia gas
nm	:	nanometer
O_2	:	Oxygen gas
OFAT	:	One factor at a time method
Pd	:	Palladium
PPE	:	Personal protective equipment
R	:	Gas constant ($N{\cdot}m{\cdot}kmol^{-1}{\cdot}K^{-1}$)
STP	:	Standard temperature and pressure
SCCM	:	Standard cubic centimeters per minute
TCD	:	Thermal conductivity detector
TGA	:	Thermogravimetry analysis
TMB	:	Trimethylbenzene
TOS	:	Time-on-stream
TPD	:	Temperature programmed desorption
TPR	:	Temperature programmed reduction

WHSV	:	Weight hourly space velocity
XRD	:	X-ray powder diffraction
Zn	:	Zinc metal

LIST OF APPENDICES

CHAPTER 1: INTRODUCTION

1.1   Background

Fast pyrolysis is the most promising thermochemical process among other procedures to directly produce liquid from lignocellulosic biomass, in high yield of up to 75 wt.%, commonly referred to bio-oil. Likewise, it has become of considerable interest due to its moderate operating temperature of around 500 ˚C and very short reaction time of up to 2 seconds (Bridgwater, 2012; Elliott, 2007; Limayem & Ricke, 2012; Mohan et al., 2006; Naik et al., 2010; Popov et al., 2013). Bio-oil is commonly a mixture of primarily phenolic oligomers derived from lignin in an aqueous phase comprising predominantly carbohydrate derived compounds (Abnisa et al., 2013, 2014; Furimsky, 2000; Rover et al., 2015). It can be used either as whole bio-oil, fractionated bio-oil, or extracted specific chemicals/chemical feedstock (Krutof & Hawboldt, 2020; No, 2014). The potential applications of the bio-oils include fuels in boilers, engines, and turbines for heat and power generation (Bridgewater, 2004; David Chiaramonti et al., 2007; Czernik & Bridgwater, 2004; Mohan et al., 2006; Oasmaa et al., 2005). Furthermore, since bio-oil contains several chemical compounds, it has potential to be applied as the source of chemical such as preservatives, liquid smoke, resin precursors, additives in fertilizing and pharmaceutical industries, and flavoring agents in food industries. This can be performed by chemical extraction or reactions of bio-oil (Jiang et al., 2020; Pattiya, 2018). Bio-oil can also be converted to transportation biofuel by upgrading processes. Several deteriorated properties such as high acidity, low higher heating value (HHV), high viscosity, and poor storage stability have made the bio-oil undesirable to instant usage as high grade fuels, mainly due to high amounts of oxygenated compounds as well as complex mixtures of chemical compounds (Ko et al., 2012; Saber et al., 2016; X. Zhang et al., 2016).

Hydrodeoxygenation (HDO) and catalytic cracking with zeolite are the two main processes for bio-oil upgrading (Choudhary & Phillips, 2011; Q. Zhang et al., 2007). The former is a hydrogenolysis route which uses high hydrogen pressure to exclude oxygen from oxygenated compounds, resulting a high grade product compared to bio-oil (Furimsky, 2000). In the latter process, different kinds of zeolites (HZSM-5, H-mordenite, H-Y, MgAPO-36, SAPO-11, and ZnHZSM-5) are applied for the deoxygenation process without demanding hydrogen (Adjaye & Bakhshi, 1995; Guo et al., 2004; Katikaneni et al., 1995; Shemfe et al., 2017; Williams & Horne, 1994). Due to many drawbacks of catalytic cracking with zeolite such as very short lifetime of catalyst, low grade products and a low H/C ratio, HDO is considered as the most effective route for upgrading bio-oil (De et al., 2015).

High pressure HDO uses high pressure of hydrogen to remove oxygen atoms from oxygenated compounds as well as hydrogenation of aromatic rings. It can reduce oxygen contents of several classes of oxygenated groups include esters, phenols, aldehydes, acids, and ketones. Depending on the composition of the organic compound, many reactions can be occurred during this process such as hydrogenation, decarboxylation, dehydration, hydrogenolysis, and hydrocracking. Various categories of catalysts have been applied by researchers for high pressure HDO which present various characteristics (He & Wang, 2012; Mortensen et al., 2011; Ruddy et al., 2014).

A continuous low or even atmospheric HDO of the vapor phase is preferred for bio-oil upgrading because it can be easily combined with conventional pyrolysis setups and operated under near-atmospheric pressure. Moreover, this method is a flexible strategy for sequential processing in bio-refineries, cost-effective (in terms of consumption of lower hydrogen and using cheaper equipment for the process), and safer than high-

pressure setups (Eschenbacher et al., 2020; Karnjanakom et al., 2016). The procedure of atmospheric/low-pressure HDO resembles that of conventional HDO (high-pressure HDO). However, the catalyst, the process conditions, the mechanism of the reaction, and the function of hydrogen in the upgrading mechanism of atmospheric/low-pressure HDO are different from those of high-pressure HDO (Chandra-Sekhar et al., 2014; Shin-Kuan, W., 2013).

Selecting a stable, cost-effective, abundant, and active and selective catalyst is crucial because the catalyst should withstand specific operation conditions, such as low H_2 pressure and moderate-to-high temperatures (Korea et al., 2019). Various kinds of catalyst supports have been developed and applied in the atmospheric HDO of bio-oil oxygenated compounds; these catalyst supports include SiO_2, active carbon, Al_2O_3, TiO_2, ZrO_2, CeO_2, and MgO (Zhou et al., 2016b). Among these supports, SiO_2 is frequently used due to its abundance, lack of deactivation caused by coke deposition, and low price. Olcese et al. reported that low-acidity supports, such as silica, would be a good carrier for transition metals by acting as active sites (R. N. Olcese et al., 2012b; Valencia et al., 2019). Many types of the catalyst active sites have been applied that could be categorized into four types including metal oxides, transition-metal sulfides, phosphides, and precious metals. Nonetheless, exploring new catalysts for HDO remains a hot research topic.

Due to the complicated bio-oil HDO pathway, application of the bio-oil as the feed results in numerous concurrent reactions during the upgrading process. Therefore, most studies have used model compounds to attain sufficient information for improving the perception of the HDO reaction networks and mechanisms. Some of the most applied model compounds are anisole, phenol, guaiacol, m-cresol, and furan, to name a few. Since phenolic compounds are the most abundant compounds in the bio-oil, researchers tend to

apply phenols rather that pyrolysis oil as the model compound of bio-oil on the laboratory scales (Z. Li, Jiang, et al., 2020).

1.2   Problem statement

Atmospheric hydrodeoxygenation (HDO) is a promising process for bio-oil upgrading. It may overcome the disadvantages of the conventional HDO process such as high pressure and expensive equipment. Several research investigations have been performed in this discipline in the last decade. In these surveys, various kinds of catalysts have been tested including transition metal oxides, precious metals, phosphides, and bifunctional. Due to the lack of high pressure of hydrogen in this process, having a robust, efficient, selective, and stable catalyst is crucial for practical applications in larger scales and continues state. In recent investigations, zinc metal has shown promising results, in bifunctional catalysts, in terms of catalytic activity and stability for the conversion of oxygenated compounds in vegetable oil to hydrocarbon fuels and the aromatization of chemical compounds. However, so far, it has not been applied as the sole active site for the bio-oil HDO purpose. Selection of a proper support for zinc metal is also expected to improve its favorable characteristics.   Various kinds of catalyst supports have been applied in the atmospheric HDO of bio-oil oxygenated compounds. Among the supports, SiO_2 is frequently used due to its abundance, proper surface area, and lack of deactivation caused by coke deposition.

Because of the complexity of the bio-oil, generally an appropriate model compound applies to represent a fixed characteristic for the bio-oil. Therefore, in this study, phenol has been selected as the best choice for simulating the bio-oil characteristics since it is the most persistent, yet fairy abundant compounds in the bio-oil.

The current investigation aims to study the characteristics of the silica-based zinc catalysts for HDO of phenol at low hydrogen pressure in a continues fixed bed reactor. Furthermore, independent process parameters optimization, conversion efficiency, products selectivity, stability, regenerability, and mechanism studies have also been performed for atmospheric HDO of phenol using the Zn/SiO_2 as the catalyst.

1.3   Research objectives

The aim of this investigation is to study the performance of Zn/SiO_2 for HDO of phenol in an atmospheric pressure of H_2 gas as a co-reactant. Hence the objectives of this study are to:

1.   To synthetize and characterize the silica-based zinc catalysts prepared by impregnating the zinc dust in the SiO_2 as the support.

2.   To study on process parameter effects on catalytic performance and product yield such as active site loading (Zn), temperature, partial pressure, reaction time, hydrogen flow rate, and feed to catalyst ratio in a continues fixed bed reactor.

3.   To investigate the stability and regenerability of the catalyst as well as the mechanism study of the reaction.

1.4   Scope of the study

The scopes of the present project are as below:

1-   Phenol will be used in this survey as the model compound due to its high severity in conversion in comparison to other model compounds applies in this field. 1% phenol

in n-decane solution has been selected as the feed since the phenol solubility decreases with more than 1% in n-decane.

2- The current process has two types of products include liquid and gas. Only the liquid products will be analyzed in this investigation, although there might be insignificant amount of the products in the gas phase.

3- The independence factor ranges in this study have been selected based on the literature survey.

1.5   Thesis organization

The format of this thesis follows the conventional style format as mentioned in the University of Malaya guideline. The overall outline as well as the organizational pattern of this thesis are discussed in this section. The thesis comprises five chapters, and each chapter is introduced as follows.

CHAPTER 1 briefly introduces hydrodeoxygenation process, especially the atmospheric H_2 pressure and the limitations encountered with commercializing of this process. It also presents research problem statement, aim and objectives of this study.

CHAPTER 2 contains broad literature survey of atmospheric hydrodeoxygenation process, followed by an overview of the applied process conditions, catalysts and the like. Furthermore, phenol has been introduced as the model compounds for bio-oil and its chemical structure and reactions has been reviewed comprehensively.

CHAPTER 3 explains all experimental and analytical procedures for the synthesis, characterization and catalyst activity of Zn/SiO_2 in HDO of phenol. Details on raw materials, equipment and other related procedures are also presented.

CHAPTER 4 presents result, and data obtained from laboratory experiments. In this chapter, the results are presented in the following parts:

In the first part, the physiochemical properties of the prepared catalysts were surveyed by various analytical methods include XRD, BET, ICP-OES, EDX, H_2-TPD, NH_3 NH_3-TPD, TGA, H_2-TPR, and FESEM.

The second part of the chapter studies the effect of various process parameters on the conversion efficiency and selectivity of the catalytic reaction products. The process parameters have been surveyed in this project are active site loading on the support surface, the reaction temperature, weight hourly space velocity (WHSV), and H_2 volumetric flow rate.

The next part of this chapter deals with the results of stability and regenerability tests of the selected catalysts. Besides, the mechanism of the reaction also has been investigated. Section 4.5 discusses all the finding and results attained in this study to explain and evaluate them. Furthermore, this section shows how the results support the literature and also answers to the main questions of this research.

CHAPTER 5 provides a conclusion of the results and findings in this research and subsequently, recommendations are given for possible future research in this area.

CHAPTER 2: LITERATURE REVIEW

2.1 Introduction

HDO of oxygenated compounds at atmospheric pressure of H_2 gas has been studied by many researchers in the last decade (Eschenbacher et al., 2020; Jiamin et al., 2020; Olbrich et al., 2016; Zhou et al., 2016a). They have applied various types of reactors, process conditions, catalysts, and analytical methods in their investigations (Z. Li, Yi, et al., 2020). Selecting a stable, cost-effective, abundant, and active catalyst is crucial because the catalyst should withstand specific operation conditions, such as low H_2 pressure and moderate-to-high temperatures. Consequently, it is crucial to review the previous studies in order to find out the applied technologies, equipment and method modifications, active sites, and supports. Furthermore, this section will also review the theoretical background of the analytical methods applied in this study.

2.2 Biomass

2.2.1 Feedstocks

The main biofuels feedstocks are waste materials, forest products, energy and sugar crops and aquatic biomass (Vorobiev & Lebovka, 2020). The cheapest biofuel feedstocks are cellulosic biomass; however, the conversion technology of a cellulosic biomass is expensive (Ali et al., 2020). Triglyceride based biomass is expensive, but also cheap to convert into fuel (Soni et al., 2020). Biomass is a rich carbon source and receives its carbon from the photosynthesis process, as shown in the following reaction (Eq. 2-1).

$$CO_2 + H_2O \xrightarrow{Light} CH_2O + O_2 \qquad (2\text{-}1)$$
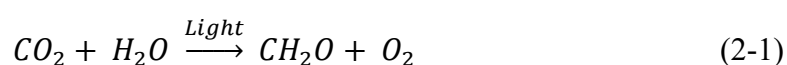
This process creates two types of metabolites; primary and secondary. The main products are primary metabolites, and these are composed of different types of polymers, for example cellulose, hemicellulose, starch and lignin (Everard & Loescher, 2017). These primary metabolites can be converted to biofuels. Other products from the photosynthesis process are secondary metabolites, for example resins, alkaloids, sterols and plant acids. These secondary metabolites can be used to produce high value chemicals such as pharmaceutical and cosmeceutical products (Croteau et al., 2000). Naik et al., (2010) divide biomass into 2 different generation biofuels and a comparison between the different generations biofuel and petroleum-based fuel is illustrated in Figure 2.1. First generation biofuels consist of biodiesel, bioethanol and biogas. These fuels have been produced at a large scale worldwide and are considered "established technologies". Biodiesel is produced through transesterification of vegetable oils and can be used as a substitute of conventional diesel. Bioethanol is produced through fermentation of sugar and starch and can be used as a substitute for gasoline and feedstock to ethyl tertiary butyl ether. There are, however, controversies about 1st generation biofuels because they are competing with food crops, and it is uncertain how much they decrease the production of CO_2. The second generation does not compete with food crops and is carbon neutral. It uses cheap feedstock such as abundant plant waste, and it can utilize all parts of the plant, such as seeds, barks and leaves. Lignocellulosic materials from the cell walls are used as feedstock in pyrolysis and liquefaction to produce bio-oil and in gasification to produce Fischer-Tropsch oil. The production of second-generation biofuels is, however, not yet cost effective due to many technological barriers.
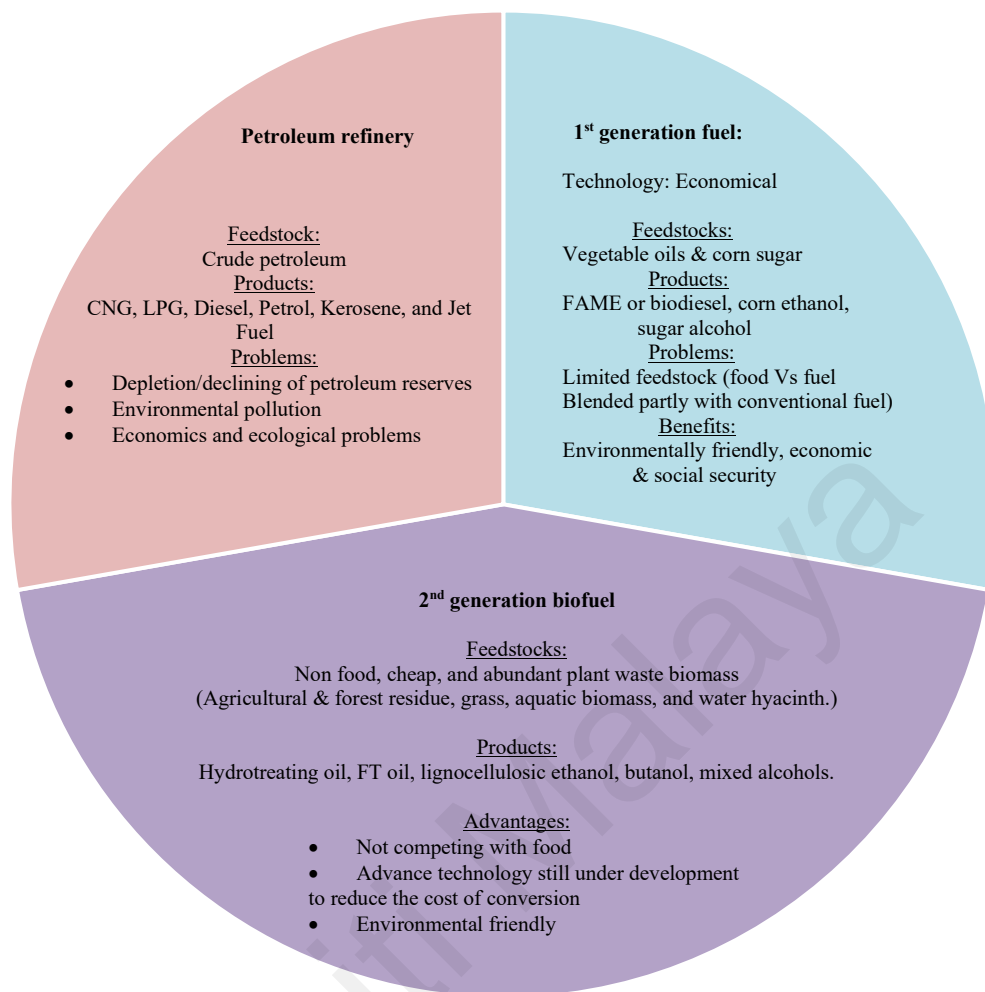
Figure 2.1: A comparison between the different generations of biofuel and petroleum-based fuel.

2.2.2 Pyrolysis

Pyrolysis has become of major interest due to the flexibility in operation, versatility of technology, and adaptability to a wide variety of feedstocks and products (Adams et al., 2018; Czajczyńska et al., 2017). Pyrolysis operates in anaerobic conditions where heat is usually provided externally and the constituents of biomass are thermally cracked to gases and vapors, which usually undergo secondary reactions, thereby giving a broad spectrum of products. There are a number of conditions and circumstances which have a major impact on the products and the process performance. These include feedstock,

technology, reaction temperature, additives, catalysts, hot-vapor residence time, solid residence time, and pressure.

Pyrolysis has been applied for thousands of years for charcoal production, but it is only in the last decades that fast pyrolysis for liquids has been developed. Fast pyrolysis is a method carried out at atmospheric pressure by which small biomass particles are heated in the absence of oxygen, vaporized, and condensed into liquid. The residence time of the reaction is approximately one second. Pyrolysis densifies the biomass feedstock to reduce storage space and transport costs. Pyrolysis liquid, unprocessed bio oil, pyrolysis oil, wood liquid, wood oil, liquid smoke, wood distillates, pyroligneous acid, liquid wood, biocrude, and pyrolytic oil are some synonyms for bio-oil which can be produced from fast pyrolysis of lignocellulosic biomass with yield up to 75 wt.% (Abnisa et al., 2011; D. Chiaramonti et al., 2003; Gollakota et al., 2016; Liu et al., 2014). Bio-oil is an intricate mixture comprising beyond 300 organic compounds including phenolics (phenol, catechol, anisole, syringol, and guaiacol), oxygenates (alcohols, acids, esters, aldehydes and ketons), hydrocarbons (aromatics, alkene) furans, sugars, high molecular species (lignin derived oligomers, lignin, hemicellulose and cellulose) and water (H. Wang et al., 2013). The composition and yield of bio oil strictly depend on the pyrolysis process conditions (the heat transfer rate, the time, the temperature, the condensation, and the char removal efficiency), the moisture content, the particle size, and the feedstock chemical composition (Debdoubi et al., 2006; Demirbas, 2007; Huber et al., 2006; Jacobson et al., 2013).

Oxygen is the most problematic element, as bio-oils contains 10-40% oxygen. This influences the heating value (HV), acidity, viscosity, polarity, and homogeneity of the bio oil (Graèa et al., 2013). The high water content leads to a polar nature for bio oils,

properties of bio oil such as good lubricity, less toxicity, and greater bio degradation resulting in immiscibility of bio oil with crude petroleum oil (Mortensen et al., 2011). Moreover, the high water-content causes lower HV, which is around half of the value of heavy petroleum fuel oil. Acetic acid and formic acid are known as the main reasons for low pH of bio-oils (2 - 4) that cause harsh conditions for equipment used for processing, transport, and storage. Olefins, phenols, and aldehydes in bio-oil are unsaturated, unstable, while easily forming macro-molecules through polymerization, particularly in the presence of acids, which will also grow the viscosity of bio-oil and diminish liquidity. Considering some favorable comparison with heavy petroleum fuel oil, the application of bio-oil is still limited by some undesired properties which are mainly due to oxygenated compounds.

2.3   Upgrading of bio-oils

As discussed earlier, some undesirable properties of bio-oil, such as chemical instability and a strong tendency to re-polymerize are caused by the high oxygen content. High viscosities, acidity, water content and low heating value are all major defects making it very hard to use bio-oils as fuels. Therefore, fast pyrolysis oils must be refined to produce deoxygenated products that are compatible with existing transportation fuels.

The general methods for bio-oil upgrading include physical, chemical and catalytic process. Physical upgrading includes filtration, solvent addition and emulsion. Liquid filtration is extremely difficult because of the physicochemical properties of bio-oil, while hot-vapor filtration can lower the average molecular weight of the liquid product and improve its stability during accelerated aging studies (Whiffen, 2013). For solvent addition and emulsion, solvents and surfactants are added into bio-oil to improve stability. Chemical upgrading mainly involves esterification, aqueous phase processing, mild

cracking, and gasification. Catalytic upgrading pathways include HDO, zeolite cracking and steam reforming, of which the last one is a route to produce H_2, not transportation fuel. Zeolite cracking is related with fluid catalytic cracking (FCC) of petroleum fractions, where oxygen atoms are removed by simultaneous dehydration-decarboxylation reactions over cracking catalysts (generally acidic zeolite) at atmospheric pressure without external H_2. However, a major defect of this method is the low hydrocarbon yield due to severe carbonaceous deposits and dealumination of zeolite. Hydrotreating is also a conventional process for petroleum reforming, including hydrodesulfurization (HDS), hydrodenitrogenation (HDN), and HDO to remove sulfur, nitrogen, and oxygen heteroatoms respectively. Unlike petroleum oil, the content of sulfur and nitrogen in bio-oils is negligible whereas O content is extremely high. Hence, HDO becomes a crucial research topic. During HDO, reactions may occur including deoxygenation (C-O cleavage), hydrogenation (saturation of C=O and aromatic rings), hydrogenolysis, and hydrocracking.

2.4   Hydrodeoxygenation

Hydrodeoxygenation reactions are an effective process for the removal of the oxygen atoms from oxygenated compounds by catalytic reaction with hydrogen. The process can be represented by the following theoretical reaction (Eq. 2-2):

$$C_1H_{1.33}O_{0.43} + 0.77H_2 \rightarrow CH_2 + 0.43H_2O \tag{2-2}$$
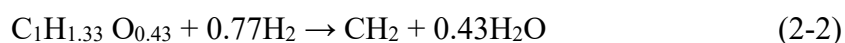
where $C_1H_{1.33}O_{0.43}$ represents pyrolysis vapor/raw bio-oil and "CH_2"denotes for unspecified hydrocarbon product.

HDO is closely related to the hydrodesulfurization (HDS) process from the refinery industry, used in the elimination of sulfur from organic compounds (Mortensen et al., 2011). Both HDO and HDS use hydrogen for the exclusion of the heteroatom, forming respectively H_2O and H_2S. Water is formed in the conceptual reaction, so (at least) two liquid phases will be observed as product: one organic and one aqueous. The appearance of two organic phases has also been reported, which is due to the production of organic compounds with densities less than water. In this case a light oil phase will separate on top of the water and a heavy one below. The formation of two organic phases is usually observed in instances with high degrees of deoxygenation, which will result in a high degree of fractionation in the feed.

Regarding operating conditions, a high pressure is generally used, which has been reported in the range from 75 to 300 bar in the literature (de Miguel Mercader et al., 2011). The high pressure has been described as ensuring a higher solubility of hydrogen in the oil and thereby a higher availability of hydrogen in the vicinity of the catalyst. This increases the reaction rate and further decreases coking in the reactor. High degrees of deoxygenation are favored by high residence times.

The catalysts originally tested were based on sulfided CoMo or NiMo supported on alumina or aluminosilicate and the process conditions are similar to those used in the desulfurization of petroleum fractions (Ma et al., 2015). However a number of fundamental problems arose, including that the catalyst supports of typically alumina or aluminosilicates were found to be unstable in the high water content environment of bio-oil and the sulfur was stripped from the catalysts requiring constant re-sulfurization. Significant research has been carried out to develop catalysts for the process aiming at improving catalyst activities and upgrading the fuel properties as well as prolonging the

catalyst life span. There are three main categories of catalyst employed in HDO, which are transition metal sulfide, noble metals, and transition metal phosphides and carbides (Badawi et al., 2011; Boullosa-Eiras et al., 2014; P. Bui et al., 2012; Gutierrez et al., 2009; Mortensen et al., 2016; Romero et al., 2010; J. Zhang et al., 2017).

The reaction pathway of bio-oil HDO is still not clear due to its complicated nature resulting in numerous concurrent reactions during the upgrading process. Therefore, rather than employing pyrolysis oil at lab-scale, most studies use model compounds to obtain sufficient information in order to understand HDO reaction networks and mechanisms. Meanwhile, model compounds experiments contribute to screening and designing HDO catalysts (Shafaghat et al., 2015). Currently, model compounds are selected among the most active compounds which will cause the instability of bio-oil. These compounds with different functional groups allow one to investigate the relative activities and selectivity of different reactions, such as dehydration, decarboxylation, hydrogenation, hydrogenolysis and hydrocracking. Phenol has been applied by researchers as model compound of bio-oil, as phenol and its derivatives (phenols) has been recognized among the most persistent, yet fairly abundant, compounds in the bio-oil. Figure 2.2 represent a schematic of conversion of phenol to hydrocarbons using a metal supported catalyst (Mortensen et al., 2013).
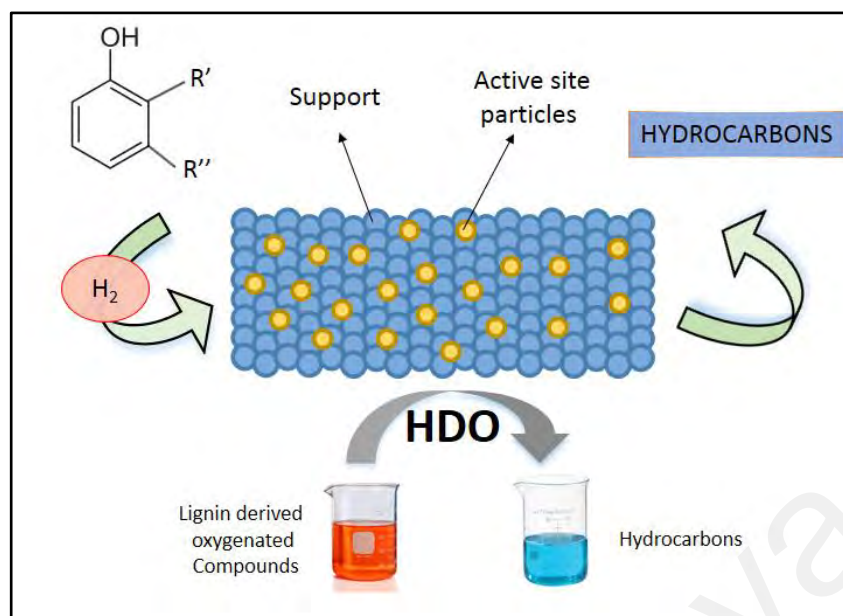
Figure 2.2: Schematic for conversion of phenol to hydrocarbons using a metal supported catalyst.

2.4.1   HDO of phenols as the model compound

Pyrolysis oils derived from the pyrolysis of forest residues have a very complex structure. The exact composition of pyrolysis oil will vary depending on feedstock composition, feedstock location, and pyrolysis conditions such as temperature, heating rate, and residence time (Furimsky, 2000). Thus, from a fundamental research standpoint, it is not practical to test the hydrodeoxygenation of pyrolysis oil for catalyst screening. This is because pyrolysis oil contains a large quantity of individual oxygenated compounds that would be difficult to identify and quantify. Overall, pyrolysis oil contains approximately 3-10 wt.% phenolic compounds (Furimsky, 2000). Phenols are also the most refractory compounds in pyrolysis oil and, thus, have been used as model compounds in many research based studies to represent pyrolysis oil feedstocks in catalyst assessments (Romero et al., 2009; W. yan Wang et al., 2009; Y. Q. Yang et al., 2008). Phenols consist of a hydroxyl group (-OH) attached to an aromatic hydrocarbon group. Since phenols have high activation energies for the HDO reaction over catalysts,

thus, they are ideal model chemicals for HDO catalyst testing. Table 2.3 represent relative reactivities of oxygen compounds for hydrodeoxygenation over a commercial catalyst (Whiffen, 2013).

Table 2.1: Relative reactivities of oxygen compounds for hydrodeoxygenation over a commercial catalyst.

Group	E_a (kj/mol)	Structure
Ketone	50	
Carboxylic acid	109	
methoxyphenol	113	
4-Methoxyphenol	142	
2-Ethylphenol	151	
Dibenzofuran	142	

2.4.2 Atmospheric HDO of oxygenated compounds

A continuous low or even atmospheric HDO of vapor-phase is preferred as it could be easily combined with conventional pyrolysis setups, operates at near atmospheric pressure, as well as enabling a flexible strategy for sequential processing in respective bio-refineries. Furthermore, it is cheaper and safer than high pressure set ups. Unstable operation of the reactor caused by pressure buildup in the upgrading reactor as well as catalyst deactivation caused by destructive components especially phenolic compounds are the main challenges of the researchers at low pressure conditions. What follows is a succinct account of the most outstanding process criteria being applied in recent studies.

As can be observed from Table 2, the criteria being discussed encompass the active phase, the support, H_2 partial pressure, the temperature, the feed composition, efficiency, and major products. The subsequent sections elaborate precisely on the most essential process criterion, the active phase, which brings us better understanding of catalyst selection for atmospheric HDO.

Table 2-2: Latest development systems for atmospheric H_2 hydrodeoxygenation.

Entry	Active phase	Support	H₂ partial pressure (kpa)	T (K)	Feed Composition	X (%)	Remarks	Major products	Ref
1	MoO₃	-	19.6	673	Acetone 2-hexanone Cyclohexanone Anisole 2- methyl furan 2,5-dimethylfuran	96.8 81.2 100 65 53.1 43.4	MoO₃ displays great tolerance to water poisoning and coke creation. By calcination process, MoO₃ can easily be regenerated fully.	Propylene Benzene Pentenes Hexenes	(Prasomsri et al., 2013)
2	Mo₂C	-	104	533-553	m-cresol, anisole, 1,2-dimethoxybenzene, guaiacol	>90	The applied operation conditions and the catalyst in this study can result to high product selectivity to aromatics.	Benzene Toluene	(C. J. Chen et al., 2016)
3	NiMo	Al₂O₃	20.68-103	723.15	Acetic acid	60-65	By elevating the partial pressure of H₂, acid acetic conversion rate increases. Maximum conversion rate occurs at H₂ partial pressure 103 kpa.	Ethanol Acetaldehyde Acetone Ethyl acetate	(Joshi & Lawal, 2012)
4	MoO₃	-	140	593-623	Phenol, m-cresol, anisole, guaiacol, diphenyl ether	28.7 - 97.5	MoO₃ is capable of selectively converting model compounds into aromatic hydrocarbons with high yields under atmospheric H₂ pressures.	Benzene Toluene Phenol Methane	(Prasomsri et al., 2014)
5	Mo₂C	-	140	420–520	Anisole	-	low reaction temperature, and low H₂ pressure were required to break the phenolic C–O bond.	Benzene	(Lee et al., 2014)
6	MoO₃	-	140	723	Acetone, Guaiacol	52	The level of HDO of the biomass pyrolysis vapors was not significant at temperatures below 400 °C. At 450 °C catalyst temperature and 93 vol % H₂ concentration, the wood pyrolysis vapor was more active toward cracking forming gas species instead of performing the desired HDO forming hydrocarbons.	Phenol Benzene Propene Propane	(Zhou et al., 2016b)

Table 2.2: Continued,

Entry	Active phase	Support	H_2 partial pressure (kpa)	T (K)	Feed Composition	X (%)	Remarks	Major products	Ref
7	MoO_3	γ-Al_2O_3 SiO_2 TiO_2 ZrO_2 CeO_2	140	593	m-cresol	8-78	The data from product distribution specify that the deoxygenation process on all catalysts involved a selective C-O bond cleavage rather than a path involving hydrogenation/dehydration as observed for supported noble metals.	Toluene	(Shetty et al., 2015)
8	Pt	γ-Al_2O_3	0-140	573	Guaiacol	-	By elevating the hydrogen partial pressure, selectivity for HDO enhanced gradually.	anisole phenol	(Nimmanwudipong et al., 2011b)
9	Pt	HBETA SiO_2	140	673	Anisole	80 – 100	Rate of HDO and methyl transfer reactions were accelerated by addition of Platinum to the zeolite. This results to lower hydrogen consumption as well as lower carbon losses as methane.	benzene toluene xylenes	(X. Zhu et al., 2011)
10	Pt	Al_2O_3	140	573	Guaiacol	-	The results indicate that there is no reaction in the absence of hydrogen	Anisole Benzene toluene	(Nimmanwudipong et al., 2011a)
11	Pt	MgO γ-Al_2O_3	140	573	Guaiacol	70	Pt/MgO catalyzed the formation of the cyclic deoxygenated product cyclopentanone at a relatively high selectivity along with C4 hydrocarbons and carbon monoxide.	Phenol catechol cyclopentanone	(Nimmanwudipong et al., 2012)
12	Pt	Al_2O_3	40	573	Guaiacol, anisole, 4-methylanisole, cyclohexanone	-	Metal function and hydrogen are essential factors for any hydrogenolysis reaction	Phenol Benzene Anisole	(Runnebaum et al., 2012)
13	Pt	γ-Al_2O_3 SiO_2 H-BEA	140	573	m-cresol	0-80	High acid sites density results to coke formation which is detrimental for catalyst stability.	Toluene	(Zanuttini et al., 2014)

Entry	Active phase	Support	H$_2$ partial pressure (kpa)	T (K)	Feed Composition	X (%)	Remarks	Major products	Ref
14	Pt	γ-Al$_2$O$_3$	140	573	m-cresol	74 – 90	By increasing the metal loading from 0.05 wt.% to 1.7 wt.%, high selectivity turned from light hydrocarbons into toluene.	Toluene Benzene Methylcyclohexane	(Zanuttini et al., 2013)
15	Fe	SiO$_2$	70	673	Guaiacol	77.7	-	Benzene Toluene	(R. N. Olcese et al., 2013)
16	Fe	SiO$_2$, Activated carbon	70	673	Guaiacol	100	By increasing the metal loading from 10 wt.% to 15 wt.%, high selectivity turned from phenol and cresols into benzene and toluene.	Benzene Phenols	(R. Olcese et al., 2013)
17	Fe	SiO$_2$	20-90	623–723	Guaiacol	74	Partial pressure of H$_2$ has negligible effect on product distribution.	benzene toluene xylenes	(R. N. Olcese et al., 2012b)
18	Ga	HBETA SiO$_2$ ZSM-5	140	673-823	m-cresol	80-85 (HBETA)	Without hydrogen partial pressure, the hydrogenolysis process is quickly depleted.	toluene benzene xylene	(Ausavasukhi et al., 2012)
19	Ru	TiO$_2$	58	673	Biomass pyrolysis vapors	-	With methoxy methyl groups transferred to the ring, the phenolic compounds in the bio-oil were transformed to less oxygenated compounds.	-	(Wan et al., 2013)
20	W	Carbon	140	653	propanol/propanal	-	The catalyst is very selective in breaking the C–O/C=O bond of propanol and propanal, resulting to the production propene as the main product.	propene	(Ren et al., 2014)
21	Ni	Al$_2$O$_3$ SiO$_2$ HZSM-5 ZSM55	100	488-533	1-octanol	87.4	Decreasing of pressure and WHSV, and also increasing of nickel loading and the reaction temperature resulted to increase in the conversion rate.	Octenes	(Chandra-Sekhar et al., 2014)

Table 2.2: Continued,

Entry	Active phase	Support	H₂ partial pressure (kpa)	T (K)	Feed Composition	X (%)	Remarks	Major products	Ref
22	Zn Ce Ni	Al₂O₃	0-140	838	Sunflower stalk bio-oil	92	2.5 wt.% metal (Zn, Ce or Ni) loading on the support exhibited the highest catalyst selectivity and activity.	Benzene Toluene Xylene	(Karnjanakom et al., 2016)
23	Cu Fe Pd Pt Pd/Fe Ru	Carbon	140	523- 723	Guaiacol	65	Base metal catalysts exhibit lower activity than the precious metal catalysts, but selectively form benzene along with small amounts of toluene, trimethylbenzene (TMB), and cresol without forming ring saturated or ring-opening products.	Toluene Benzene	(Sun et al., 2013)
24	Pt (Co, Ni)	γ-Al₂O₃	50/50 (H₂ to N₂ ratio)	533	m-cresol	38	The additions of Ni and Co into Platinum modified the product distribution as well as improving the overall HDO conversion.	Toluene methylcyclohexane.	(Do et al., 2012)
25	Pt, Sn	monolith	101	673	Anisole, Guaiacol	74 (anisole) 90 (guaiacol)	In case of CNFs coating, surface area of the monolith increased dramatically (more than 10 times), which results to a higher metal loading in active phase incorporation.	Phenol benzene	(Resasco, 2011)
26	Ni/P	SiO₂	101	573	Guaiacol	-	Maximum deactivation rate (78%) of guaiacol belongs to Ni/P=1 sample whereas the Ni/P=3 sample had the lowest.	-	(Wu et al., 2014)
27	Ni₂P Co₂P Fe₂P WP MoP	SiO₂	112	573	Guaiacol	80 70 64 60 54	The activity order of the applied catalysts for guaiacol HDO are: Ni₂P>Co₂P>Fe₂P, WP, MoP.	Phenol benzene	(H. Y. Zhao et al., 2011)

Entry	Active phase	Support	H₂ partial pressure (kpa)	T (K)	Feed Composition	X (%)	Remarks	Major products	Ref
28	Pd-FeO$_x$	SiO$_2$	100	573-623	Furan	100	Using 5%Pd-2.5%FeOx/SiO$_2$ as catalyst resulted to 100% conversion of furan.	Methyl-decane Methyl-nonane	(J. Yang et al., 2017a)
29	Ni$_2$P	Alumina, Zirconia, Silica	-	573	Guaiacol	-	Ni$_2$P/SiO$_2$ enhances DMO and DDO reactions, while Ni$_2$P/ZrO$_2$ and Ni$_2$P/Al$_2$O$_3$ promote DME.	Catechol anisole cresol phenol benzene cyclohexanone cyclohexanol	(Wu et al., 2013)
30	Ni$_2$P	SiO$_2$	112	573	Guaiacol	100	Selectivity profile by using this catalyst is pentenes as primary products, 2-pentanone as a secondary product, and pentane as a final product.	Phenol benzene	(P. Bui et al., 2012)
31	Ni$_2$P	SiO$_2$	140	573	2-MTHF	-	The Ni$_2$P catalyst is outstanding in producing desired alkanes in the HDO of the biomass model compound 2-methyltetrahydrofuran.	n-butane n-pentane	(P. P. Bui et al., 2016)
32	Pd-Co Pd-Fe	Al-MCM-41	100	673	Guaiacol	98%	The Pd-Fe/Al-MCM-41 presented as a suitable catalyst for upgrading of lignin-derived bio-oil since its higher deoxygenated products and lower gas-phase yields than Pd-Co/Al-MCM-41.	Phenol Benzene	(Ye Li et al., 2020)

As it can be observed from Table 2, various kinds of catalyst support have been applied in atmospheric HDO of bio-oil oxygenated compounds including SiO_2, γ-Al_2O_3, Zeolites, carbon, TiO_2, ZrO_2, MgO, CeO_2, and monolith. Based on Table 2, H_2 partial pressure fluctuates from 0 to 140 kpa in different studies. In most of the cases, the balance gas is N_2. The majority of researches has acknowledged that the higher partial pressure, the higher selectivity. The temperature fluctuates between 420 K and 838 K, while the prevalent temperature is 573 K. Taking into account the feed composition, it is realized that guaiacol is the most common model compound applied in these papers. However, various kinds of feeds have been used in this process including m-cresol, anisole, 2-hexanone, cyclohexanone, phenol, pyrolysis bio-oil vapors, furan, propanol, and 2-mthf. Based on the mentioned feeds in this process, certain main products are expected such as benzene, toluene, propene, and phenols.

2.4.2.1 Active sites applied in atmospheric HDO

Selection of a stable and active catalyst is crucial since it should overcome specifics operation conditions such as low H_2 pressure and moderate to high temperatures. Until now, various kinds of catalysts have been tested in this process such as metal oxides, transition metal sulfides, phosphides, and precious metals. Characterization of the applied catalysts are meaningful since it helps to understand the common nature of each catalyst facing different bio-oil model oxygenated compounds. To suit this purpose, almost all the so far applied catalysts for low H_2 pressure HDO have been reviewed and discussed in the following sections.

2.4.2.2 Molybdenum

Molybdenum has been used by many researchers for HDO of various oxygenated components such as 2,5-dimethylfuran, 1,2-dimethoxybenzene, 2-methylfuran, diphenyl

ether, 2-hexanonephenol, acetic acid, m-cresol, cyclohexanone, acetone, guaiacol, and anisole (C. J. Chen et al., 2016; Lee et al., 2014; Prasomsri et al., 2013, 2014; H. Y. Zhao et al., 2011; Zhou et al., 2016b). T. Prasomsri et al., (2013) reported that MoO_3 effectively converts bio-mass derived oxygenated compounds (Acetone, 2-hexanone, Cyclohexanone, Anisole, 2- methyl furan, 2,5-dimethylfuran) into unsaturated hydrocarbons (Propylene, Benzene, Pentenes, and Hexenes). According to their results, MoO_3, at low H_2 pressures, converts Phenolics and cyclic ketons to aromatics, and cyclic ethers and linear ketons to olefins with high yield. In another study by T.Prasomsri et al., (2014), it was pinpointed that MoO_3 is capable of selectively converting various oxygenated compounds to aromatic hydrocarbons without ring saturated products. The results revealed that MoO_3 specifically cleaves Phenolic Ph-OMe (CAromatic and OMethoxy) bond over the weaker aliphatic Ph-o-Me (OPhenolate and CMethoxy) bond which results in higher aromatic products. G. Zhou et al., (2016b) recently studied the atmospheric HDO of two bio-oil model compounds as well as a real biomass vapor in a fixed bed catalyst reactor at 773 K. They found that the best process conditions for conversion of the real biomass pyrolysis vapor are 723 K and 89% vol. H_2 concentration resulting in 16.2 wt% organic liquid with 11.5 wt% oxygen content. They also overstated that water inhibition, steric hindrance effects, and strong adsorption of pyrolysis vapor molecules to the catalyst active sites are the main reasons for harder upgrading of the pyrolysis vapor in comparison with the model compounds.

2.4.2.3 Platinum

Platinum is another frequently used metal as an active site for atmospheric HDO of model compounds. T. Nimmanwudipong et al., (2011b) studied the conversion of a model compound using platinum supported on Alumina. They found that the platinum function catalyzes the hydrogenolysis and hydrogenation reactions while the alumina support

catalyzes the transalkylation reaction. From the experiments results, they concluded that the HDO selectivity rises with decreasing temperature elevating H_2 partial pressure. In another study by T.Nimmanwudipong et al., (2011a), a comparative study was undertaken by using Pt/Al_2O_3 with H_2, HY zeolite, and Pt/Al_2O_3 without H_2 as the catalyst. Their results indicated that H_2 is significant for oxygen removal from guaiacol. Also, the acidic catalysts without metal function (HY zeolite) produces similarly to those identified in the conversion catalyzed by the Pt/Al_2O_3 in the absence of H_2 (only transalkylation products). T. Nimmanwudipong et al., (2012) further studied the HDO of guaiacol catalyzed by Pt/MgO in atmospheric H_2 pressure. The study results could be summarized as follows: (I) the selectivity to deoxygenated products in the reactions on Pt/MgO was higher, almost double the value achieved with $Pt/C-Al_2O_3$, (II) sequential reactions (ring opening, ring closing, and decarbonylation) occurred on Pt/MgO, (III) Pt/MgO catalyzed the formation of cyclopentanone at a relatively high selectivity, (IV) basic supports had higher conversion efficiency rather than acidic ones for noble metal hydrodeoxygenation catalysts. Runnebaun et al., (2012) scrutinized HDO of model compounds representative of lignin-derived bio oils such as guaiacol, anisole, 4-methylanisole, and cyclohexane using $Pt/\gamma-Al_2O_3$ as the catalyst. Here it was found that when selective deoxygenation is a goal, partial pressure of H_2 plays an important role in increasing the conversion efficiency. They also pointed out that $\gamma-Al_2O_3$ is not active for oxygen removal reactions and only catalyzes the transalkylation reactions.

2.4.2.4   Other metals

Lately, some transition/post-transition metal based catalysts such as Fe, Ga, W, and Ni have been employed by some researches (Ausavasukhi et al., 2012; Chandra-Sekhar et al., 2014; R. Olcese et al., 2013; R. N. Olcese et al., 2012b, 2013; Ren et al., 2014). R.N. Olcese et al., (2013; 2012b, 2013) investigated HDO of guaiacol over Fe/SiO_2,

concluding that Fe/SiO_2 is an active and selective catalyst for the conversion of guaiacol even at high temperatures [673 K]. Although, Fe/SiO_2 is less active in comparison with the co-based catalysts, it is a more versatile catalyst. It also enjoys the benefits of being low-cost and environmentally friendly. Ausavasukhi et al., (2012) studied HDO of m-cresol using gallium (Ga) modified catalysts. They found that the yield of the desired products such as toluene and benzene undergo a rise with Ga content, H_2 partial pressure, space time (W/F), and reaction temperature. According to their results, SiO_2 is not a proper support for Ga due to its inability to stabilize suitable Ga species which are the active sites for hydrogenolysis under atmospheric H_2 flow. In another study by Palla et al., (Chandra-Sekhar et al., 2014), the supported Ni catalysts (Ni/SiO_2, $Ni/ɤ-Al_2O_3$, and Ni/HZSM) were examined in HDO of 1-octanol as a model aliphatic alcohol of bio oil at atmospheric H_2 pressure. Table 2.3 tabulates the products and their selectivity percentages. According to the results, Ni/ZSM55 has the highest conversion efficiency among the other catalysts. Furthermore, the main products of HDO of 1-Octanol are n-Heptane, heptane, n-octane, octenes, DOE, and 1-octanal.

Table 2.3: The role of various supports on hydrodeoxygenation of 1-octanol (Chandra-Sekhar et al., 2014)**.**

Catalyst	Conversion rate	Selectivity (%)					
		n-Heptane	Heptenes	n-octane	Octenes	1-octanol	DOE[1]
Ni/ ɤ-Al$_2$O$_3$	45.1	50.9	24.9	0.7	0.4	10.7	10.1
Ni/SiO$_2$	43	52.7	32.8	0.3	0.2	10.8	2.6
Ni/ZSM23	40.2	8.2	0	5.9	73.2	6.2	6.5
Ni/ZSM55	61.5	10.6	0	4.0	69.5	6.2	6.9

1 : di-*n*-octyl ether

2.4.2.5 Bi-functional

Bi-functional catalysts such as Pt-Co/γ-Al$_2$O$_3$, Ni$_2$P/SiO$_2$, Pd-FeO$_X$/SiO$_2$, and Ru/TiO$_2$ represent superior stabilities and activities among the other catalysts which can convert the oxygenated compounds through more than one reaction mechanism resulting in a surge in the yield of the desired products. M.A. Gonzalez-Borja and D.E. Resasco (2011) elaborated on HDO of anisole and guaiacol using monolithic Pt-Sn catalysts at atmospheric pressure. The authors concluded that bimetallic Pt-Sn/CNF/Inconel catalyst is able to fully deoxygenate anisole and guaiacol at atmospheric pressure for a long time on stream (TOS). Nonetheless, the monometalic catalysts applied in this study (Pt/Inconel, and Sn/Inconel) deactivate much faster than the bimetallic catalysts and also have shorter TOS. In addition, Do et al., (2012) investigated HDO of m-cresol on Pt/γ-Al$_2$O$_3$, Pt-Co/γ-Al$_2$O$_3$, Pt-Ni/γ-Al$_2$O$_3$ at near atmospheric H$_2$ pressure. They reported that HDO proceeds through two successive routes; hydrogenation of aromatic rings on the metal sites and dehydration of intermediates on the support (γ-Al$_2$O$_3$). Addition of 3D metals, including Co and Ni, into the catalyst significantly improved the products (toluene, and methylcyclohexane) distribution and the conversion rate. In another study by N. Joshi and A. Lawal (2012), pre-sulfided NiO/MoO$_3$/Al$_2$O$_3$ was used as catalyst for HDO of acetic acid. Acetaldehyde, ethyl acetone, and acetone are the main products of HDO of acetic acid at 723 K and 80% H$_2$ gas. Supported nickel phosphide catalysts (Ni$_2$P/ZrO$_2$, Ni$_2$P/Al$_2$O$_3$, Ni$_2$P/SiO$_2$) were used in HDO of guaiacol by Wu et al., (2013). According to the analysis results obtained from this study, Ni$_2$P/ZrO$_2$ is the most whilst Ni$_2$P/SiO$_2$ is the least reactive catalyst, based on the pseudo first order kinetics results at 573 K. However, TOS results revealed that Ni$_2$P/SiO$_2$ promotes direct deoxygenation (DDO) as well as DMO routes for removing oxygen, resulting in benzene and phenol, respectively. They established that Ni$_2$P/SiO$_2$ is the most promising catalyst, in comparison with its counterparts, for HDO of Guaiacol in atmospheric pressure. In the

other study conducted by S.K. Wu et al., (2013), the effect of phosphorous composition of nickel phosphide catalysts was scrutinized. Using various initial Ni/P molar ratios, they prepared three catalysts with different active phases (Ni_2P, $Ni_{12}P_5$, and Ni_3P). The authors reported that although Ni_2P has the highest deactivation rate, its product distribution is more stable compared to the other catalysts, which is mainly due to its bi-functional nature (protonation on PO-H and hydrogenation on Ni). In a study by Wan et al., (2013), 5% Ru/TiO_2 was applied for HDO of oak and switchgrass pyrolysis vapors at low H_2 pressures. They found that noble metals play a role in generating vacancy sites on the support surface (TiO_2) that promotes ketonization besides its main role which is to function for deoxygenation. Furthermore, according to the Van krevel diagram results, catalytic treatment of the pyrolysis vapors contributed to a rise in O/C and H/C in the combined aqueous phase (0.93 and 1.92 respectively). In a very recent investigation by Yang et al., (2017b), a new bi-functional catalyst ($Pd-FeO_X/SiO_2$) was used for atmospheric HDO of furfural. Based on their results, $5\%Pd-2.5\%FeO_X/SiO_2$ represents a full conversion of furfural with high efficiency of jet fuel range alkenes at 573 K- 623 K. The modification of Pd/SiO_2 with FeOX results in (I) restraining of the decarbonylation reactions, (II) lowering the coordination number of Pd-Pd species, (III) promoting the hydrogenation of carbonyl group over Pd, and (IV) generating Pd-Fe alloy. All these effects contribute to a high HDO activity of the catalyst at atmospheric pressure.

2.5   Catalyst preparation methods

Contemporary catalysts are applying advanced materials derived from commercially accessible chemicals (Mbaraka & Shanks, 2006). The diversity of these chemicals for the preparation is quite extensive, and indeed some catalysts could be prepared by various phases. However, some general fundamental phases must be followed.

Two main approaches could be considered for theses phases, (1) empirical practice, or (2) knowledge-based procedures (Perego & Villa, 1997). In the second step, using detailed knowledge of the scientific laws govern chemical and physical transformations based on the fundamentals of inorganic or solid-state chemistries.

Overall, the applied catalysts in the industry should have the precise texture (surface area, pore structure, and bulk density) and shape (Leofanti et al., 1998). Consequently, at the beginning of a catalyst preparation, it is vital to contemplate the suitable texture and shape which are essential for the material and this must be based on a knowledge of the chemistry of the target catalyzed reaction. The principal variables are temperature, pH, aging time, pressure, and solute concentration in solution (Schmal, 2016).

Based on the various preparation methods include bulk preparation process, impregnation process, and physical mixing; three types of catalyst can be distinguished (Molina, 2014):

1. Bulk catalysts and supports
2. Impregnated catalysts
3. Mixed-agglomerated catalysts

Bulk catalysts comprise mainly active substances, but some inert binder is often added to aid the forming and/or shaping operation (Courty & Marcilly, 1983). This is the case, for instance, for silica-alumina for catalyst-cracking (Xu et al., 2017), copper and chromium oxide for the water gas shift reaction (M. Zhu & Wachs, 2018), iron molybdate for the oxidation of methanol to formaldehyde vanadyl (Soares et al., 2005), and pyrophosphate for butane oxidation to maleic anhydride (Goo et al., 2020). However, in

some cases, bulk catalysts are used as prepared, without the need for addition of the binder. Typically, this involves catalysts prepared by high temperature fusion, e.g. the iron-based ammonia synthesis catalyst (Cui et al., 2017). The need for the addition of binder, or the requirement for pelleting, solely depends on the strength required for the catalyst under the reaction conditions and the reactor type it is used in. This requires consideration of attrition resistance, and catalysts required for use in entrained-bed reactors will need different strength characteristics than those used in fixed-bed reactors.

Impregnated catalysts comprise supports which are first prepared by bulk preparation methods and then impregnated with the catalytically active material. The active materials can be deposited on the supports by various methods. Most of the methods involve aqueous solutions and liquid solid interface. In some cases, deposition is done from the gas phase and involves gas- solid interface (Anggoro et al., 2019; Komiyama, 1985).

Mixed agglomerated catalysts are prepared by physically mixing the active substances with a powdered support or precursors of support in ball mill. The final mixture is then agglomerated and activated (Malani et al., 2019).

Supported catalysts are prepared for a large variety of reasons such as obtaining bifunctional catalysts, high dispersion of the active phase, better diffusion of gases through the bed, better mechanical resistance to attrition (moving or fluidized beds reactors), better thermal conductivity, improved catalytic properties induced by active phase-support interaction, to name but a few of the many potential applications/requirements of heterogeneous catalysts (de Jongh & de Jong, 2018; Hutchings & Védrine, 2004).

In following, we discuss some general principles concerning the impregnation methods specifically incipient wetness impregnation (used in this investigation) for the preparation of heterogeneous catalysts. Impregnation and drying is a frequently used preparation method among others due to its simple execution and low waste streams. The first step is contacting a metal precursor solution with a porous support. Common precursors include inorganic metal salts, such as metal sulfates, carbonates, chlorides, nitrates, or acetates, and organic metal complexes, such as metal acetylacetonates (Friščić, 2011). The most commonly used solvent for inorganic salts is water because of the high solubility of many precursors, whereas organic solvents are mainly used for organometallic precursors. To prevent premature deposition of the metal precursor in bulk solution, concentrations below (super) saturation are required. Two main impregnation methods are distinguished, namely, wet impregnation (WI), whereby an excess amount of solution is used, and pore volume impregnation (PVI), in which an amount to just fill the pore volume of the support is used. The latter method is also known as incipient wetness impregnation (IWI) or dry impregnation (DI), because the impregnated material keeps a dry character at a macroscopic scale. Uptake of the liquid into the pores of the support occurs due to the capillary pressure difference Δp across a hemispherical meniscus in a pore with radius r_p according to the Young− Laplace equation (Eq. 2-3) (Mo et al., 2019):

$$\Delta p = (2\gamma_{lv}/r_p). \cos \theta \tag{2-3}$$

where γ_{lv} is the surface tension between the liquid and vapor interface and θ is the wetting angle between the solid and the liquid. If $\theta < 90°$, the liquid is considered as wetting and will penetrate the support spontaneously, which is the case with water in combination with most oxidic supports. If the liquid is nonwetting ($\theta > 90°$), the capillary

pressure becomes negative and an external pressure is needed to force the liquid into the pores. This can occur for hydrophobic supports such as carbon materials, for which a less polar solvent such as ethanol or 2-propanol may be more appropriate, although this usually comes at the expense of a lower precursor solubility.

From Eq. 2-3, the pressure difference depends inversely on the pore size, so that liquid is preferentially sucked up by the smallest pores. The rate at which the liquid fills the pores is generally fast and is often not considered critical for catalyst synthesis. According to the Washburn equation (Munnik et al., 2015), infiltration of a wetting liquid into a porous body of a few millimeters can occur in seconds to minutes, as has been experimentally verified (Haneveld et al., 2008). However, when the support is prewetted with the same solvent before loading of the precursor via wet impregnation, capillary forces do not play a role and the only driving force for the precursor to enter the support is diffusion, which can take significantly longer.

2.6   Reaction mechanisms for HDO of phenol

Two main parallel routes were suggested in early studies for HDO of phenol. One route is a hydrogenolysis reaction of phenol to benzene, and another route is a combined hydrogenation-hydrogenolysis reaction via cyclohexanone and cyclohexene to cyclohexane (Wildschut et al., 2010).

By using different catalysts and reaction conditions, the reaction routes can vary and cause different intermediate and end products. Senol et al., (2007) used a plug-flow reactor for the gas phase and a batch reactor for the liquid phase. They discovered that cyclohexene and cyclohexane were the main products with the use of sulfide NiMo, and benzene was the end product with the use of CoMo. Cyclohexanone was detected as an

intermediate, but not as an end product (Şenol et al., 2007). Wildschut et al., (2010) used a Ru/C catalyst on HDO reaction of phenol and discovered no benzene in the product. Instead, they proposed a reaction pathway via cyclohexanol to cyclohexane. Gevert et al., (1987) used a batch reactor with a sulfided CoMo catalyst and proposed a similar route for methyl substituted phenols, as seen in Figure 2.3.
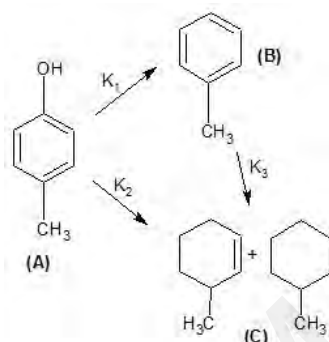
Figure 2.3: Reaction pathways for methyl phenol to methyl cyclohexene and methyl cyclohexane via a toluene route.

They derived the following equations (Eq. 2-4) for mole fractions of phenol (X_A), aromatics (X_B) and cyclohexane/cyclohexene (X_C) with first order rate constants.

$$X_B = \frac{k_1}{k_1 + k_2} (1 - x_A) \; and \; X_C = \frac{k_2}{k_1} X_B \qquad (2\text{-}4)$$

Boullosa-Eiras et al., (2014) tested MoO_3/TiO_2 for HDO of phenol in a temperature range between 350 and 450 °C at a pressure of 25 bar. They reported phenol HDO for all the tested materials proceeded dominantly through direct hydrogenolysis to benzene as primary product. Relatively small amounts of non-aromatics were also produced (cyclohexane, cyclohexene and methyl cyclopentane).

2.7 Application of Zn as the active site for HDO processes

Zinc, a transition metal in group 12 of the periodic table is the 24th most abundant element in earth's crust and has five stable isotopes. It is cost effective and efficient during upgrading of vegetable bio oils to hydrocarbon fuels as well as aromatization of chemical compounds (Fanchiang & Lin, 2012; Yuning Li et al., 2009; Luzgin et al., 2009; Ni et al., 2011; Sio & Yue-juan, 2017; Smiešková et al., 2004; Viswanadham et al., 1996; Yi-hao et al., 2017; Yiwen et al., 2010; X. Zhao et al., 2015). Until now, many researchers have alluded to the characteristics of this element in HDO process. In the following, some of the most important studies on the role of Zn as the active site for HDO processes have been outlined.

In a study by Parsell et al., (2013), HDO of lignin using Pd/Zn catalyst was performed and they could reach 80-90% conversion yield. Based on their studies, two pathways proposed for the reaction mechanism of β-O-4 lignin substrate over Zn/Pd/C catalyst. Pathway (a) involves substrate binding to Zn^{II} sites and hydrogen spillover from Pd sites. Pathway (b) represents desorption of Zn ions solution, activation of substrate via binding, and it is the Zn bond substrate that reacts with Pd sites on the catalyst surface. Figure 2.4 represent the proposed mechanism.
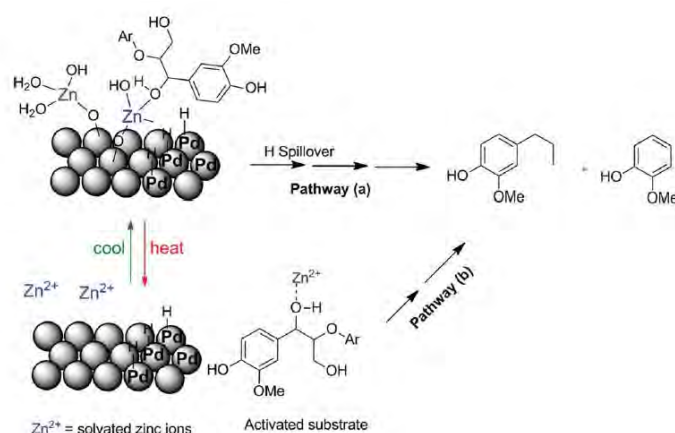
Figure 2.4: Proposed mechanisms for hydrodeoxygenation of β-O-4 lignin substrate over Zn/Pd/C catalyst.

They indicated that a combined Zn/Pd/C catalyst is far more effective than Pd/C alone for the cleavage of β-O-4 lignin molecules and the subsequent HDO of the aromatic fragments without loss of aromatic functional group. Furthermore, they found that the catalyst ids robust and fully recyclable after each catalytic reaction without the need to additional Zinc.

Mirzayanti et al., (2017) also proved that applying Zn as the active site increases the process performance for hydrocracking of Kapuk seed oil. They reported that the best catalytic performance occurred on catalytic hydrocracking of the bio oil using Zn-Mo/HZSM-5 with loading 2.99% wt. for Zn and 7.55% wt. for Mo.

In a study by Cheng et al., (2017), the synergistic effect of Zn and Ni on Al_2O_3 support has been investigated on HDO of pine sawdust bio oil using a series of Ni and/or Zn loaded Al_2O_3 catalysts. They reported that the 15%Ni-5%Zn/Al_2O_3 catalyst generated the highest upgraded bio-oil yield at 44.64 wt.% and produced the upgraded bio-oil with the highest hydrocarbon content at 50.12%.

From the previous studies, it can be perceived that no research has been performed applying the zinc metal as a single active site in HDO of the bio-oil model compounds. Furthermore, most of the previous studies, using zinc as the active site, have been performed in high pressure HDO. Application of the zinc as the single active site for the HDO process will help to depict the clear role of the zinc in the conversion efficiency of the oxygenated compounds as well as the reaction mechanism.

2.8   Catalyst stability

Long term stability of the selected catalyst for hydrodeoxygenation process is one of the most important challenges, a key factor for its successful industrial application, in this concept. Particularly, there are two main possible causes of catalyst deactivation. It might be due to the formation of carbon species on the catalysts or due to impurities in the feed. However, limited research has been conducted in this direction for the bio-oils upgrading process during which catalyst deactivation is a prevalent issue. In a study by Shetty et al., (2015), the authors reported that MoO_3/ZrO_2 and MoO_3/TiO_2 feature the maximum initial site time yields (23.4 and 13.9 h^{-1}) and minimum first-order deactivation rate constants (0.013 and 0.006 h^{-1}) of all catalysts tested after ca.100 h on stream. Furthermore, they stated that the supports play an important role in stabilizing partially reduced, coordinatively unsaturated (CU) sites in surface oligomeric Mo moieties.

Karnjanakom et al., (2016) tested the reusability of four catalysts (Al_2O_3-0.5, 2.5 wt.% Zn/Al_2O_3-0.5, 2.5 wt.% Ce/Al_2O_3-0.5 and 2.5 wt.% Ni/Al_2O_3-0.5) for 4 cycles at the same operation conditions. According to the results, the metal-doped microporous rod-like γ-Al_2O_3 alumina catalyst (2.5 wt.% metal (Zn, Ce or Ni)/Al_2O_3-0.5) had long-term stability in their performance. Moreover, the authors reported that the regeneration of spent catalysts (4th reuse) by calcination at 650 °C in air for 30 min recovered their activity perfectly.

Mortensen et al., (2014) investigated the stability of Ni/ZrO_2 over bio-oil impurities such as potassium, chlorine, and sulfur. The authors reported that without impurities in the feed good stability of the Ni/ZrO_2 catalyst could be achieved over more than 100 h of operation, particularly for a sample prepared with small Ni particles, which minimized carbon deposition. Exposing the catalyst to 0.05 wt% sulfur in the feed resulted in rapid

deactivation with complete loss of activity due to the formation of nickel sulfide. Exposing Ni/ZrO_2 to chlorine-containing compounds on-stream led to a steady decrease in activity over 40 h of exposure. Removal of the chlorine species from the feed led to the regaining of activity. In two experiments, potassium, as either KCl or KNO_3, was impregnated on the catalyst prior to testing. In both cases deactivation was persistent over more than 20 h of testing and severely decreased the deoxygenation activity while the hydrogenation of guaiacol was unaffected. Overall, sulfur was found to be the worst poison, followed by potassium and then chlorine. Thus, removal/limitation of these species from bio-oil is a requirement before long term operation can be achieved with this catalyst.

CHAPTER 3: RESEARCH METHODOLOGY

3.1 Introduction

In this section, firstly, the applied materials for this research and the preparation methods for the catalyst samples have been introduced. In continue, the procedure and conditions for each applied analysis method have been precisely described. The applied analysis methods include X-ray diffraction (XRD), N_2 physisorption (BET), inductively coupled plasma-optical emission spectrometry (ICP-OES), Energy Dispersive X-Ray Spectroscopy (EDX), H_2 temperature-programmed desorption (H_2-TPD), NH_3 temperature-programmed desorption (NH_3-TPD), thermogravimetry analysis (TGA), H_2 temperature-programmed reduction (H_2-TPR), field-emission scanning electron microscopy (FESEM), and gas chromatography flame ionization detector (GC-FID). Finally, the main experiment procedures and conditions (Catalyst activity testing and optimizing the process parameters) have been detailed in this section. Figure 3.1 represent the methodology flowchart of this investigation.
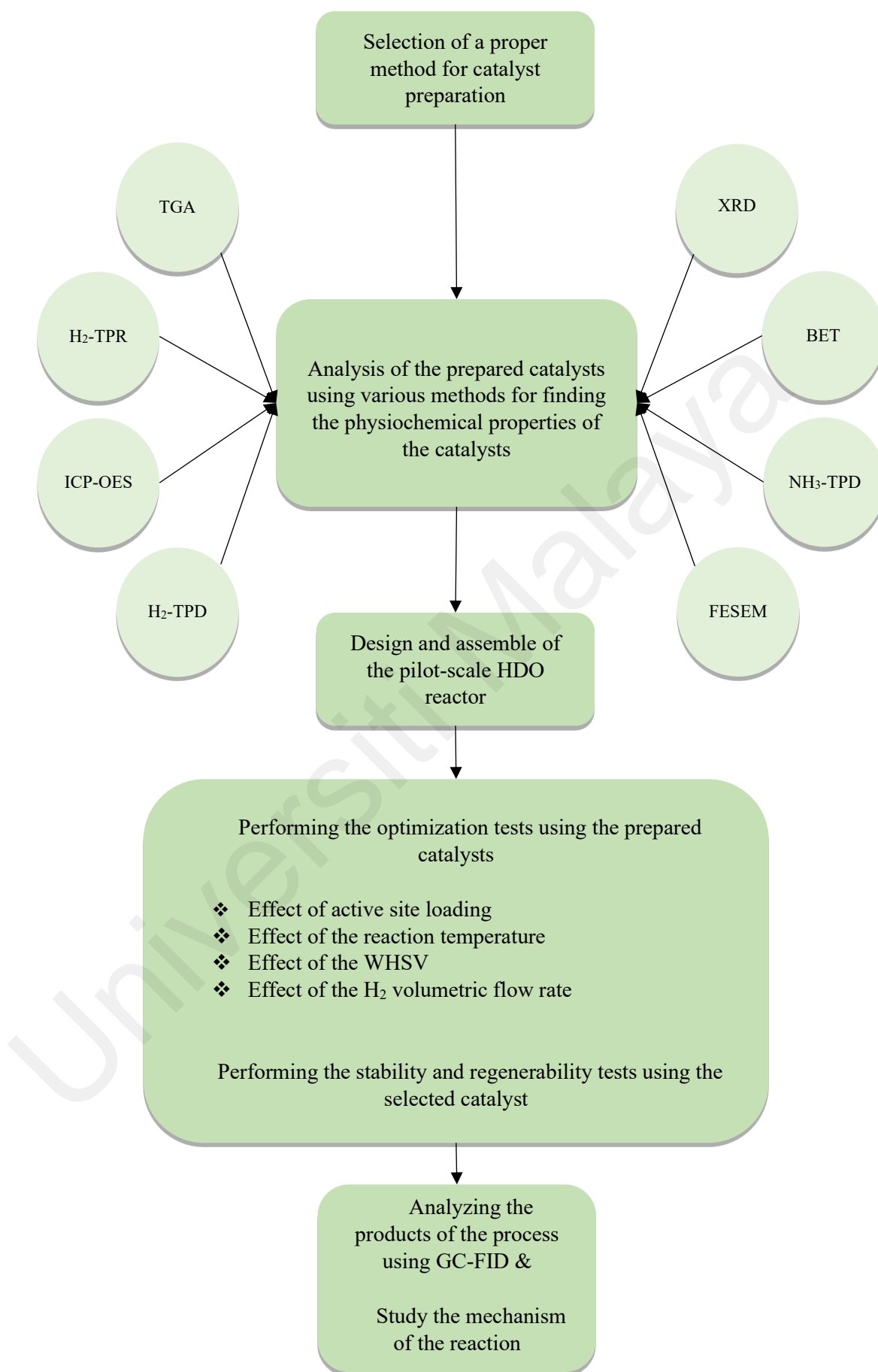
Figure 3.1: Methodology flow chart of this study.

3.2   Materials

Zinc powder used to synthesize Zn/SiO_2 was purchased from Sigma Aldrich. U.S. Silicon dioxide (SiO_2) was purchased from R & M chemicals. n-decane ($\geq$95%) employed as the neutral feed was purchased from Aldrich. Analytical grade acetone used as a solvent in gas chromatography was supplied from Merck. Liquefied Phenol ($\geq$ 89%) used as feed was purchased from Sigma Aldrich. High purity benzene (99.8%), cyclohexane and cyclohexene employed as the standard for gas chromatography were supplied by Sigma Aldrich. Silicon pellet and Quartz wool were supplied by R & M chemicals. Hydrogen, nitrogen, argon, compressed air, hydrogen in air and oxygen in argon are the gases have been applied in this study.

Table 3-1: List of chemicals used in this project.

Chemical	Chemical formula	State	Purpose	Supplier	Purity
Acetone	C_3H_6O	l	GC solvent	Merck	Analytical grade
Air (compressed)	$O_2 + N_2$	g	GC	Gaslink	100%
Argon	Ar	g	TGA, GC	Gaslink	100%
Benzene	C_6H_6	l	GC standard	Sigma Aldirch	99.8%
Hydrogen	H_2	g	HDO feed, TGA, GC	Gaslink	100%
Hydrogen in air	H_2 + Air	g	TPR	Gaslink	100%
n-decane	$C_{10}H_{22}$	l	HDO feed	Aldrich	$\geq$95%
Nitrogen	N_2	g	Inert in HDO, GC	Gaslink	100%
Oxygen in argon	O_2 + Ar	g	TPR	Gaslink	100%
Phenol	C_6H_5OH	l	HDO feed	Sigma Aldirch	$\geq$89%
Silicon dioxide	SiO_2	s	Support	R & M	100%
Zinc powder	Zn	s	precursor	Sigma Aldirch	100%
Cyclohexane	C_6H_{12}	l	GC standard	Sigma Aldirch	100%
Cyclohexene	C_6H_{10}	l	GC standard	Sigma Aldirch	100%
Nitric acid	HNO_3	l	ICP-OES	R & M	65%
Ethylene glycol	$C_2H_6O_2$	l	Chiller liquid	Sigma Aldirch	99.8%

3.3 Preparation of catalysts

Zinc supported catalysts were prepared in different loading of active cites (Zn) (0.5, 1, 2, 5, and 10 percent of Zinc on SiO_2 as the catalyst's support). Two different preparation procedures have been applied to prepare some preliminary samples for Zn/SiO_2 catalysts in order to compare the various procedures for incipient wetness impregnation method mentioned in literatures. The purpose of applying the two procedure to make the catalysts (Method A & B) is to find out a system that results to higher loading of the active phase (Zinc). Figure 3.2 represent the synthesis procedures for the methods A and B.

3.3.1 Method A (no initial calcination of the support)

Eight grams of SiO_2 weighted and then mixed with enough distilled water. Then, 1 g Zn dust weighted and mixed with some water and was shook to mixed well. The mixed Zinc then added to the SiO_2 and mixed well on the heat (60 ˚C) and magnetic stirrer. After mixing well, around 2 h, it transferred to the oven, 105 ˚C, and dried for 16 h. The dried sample then transferred to the furnace at 500 ˚C for calcination for 5 h. The sample then analyzed with XRD and EDX analysis equipment to identify its components.

3.3.2 Method B (with initial calcination of the support)

Eight grams of SiO_2 weighted and then mixed with enough distilled water. It then mixed well on the heat and magnetic stirrer. After mixing well, around, 2 h, it transferred to the oven, 105 ˚C, and dried for 16 h. After drying, it then mixed with some water and 1 g of Zinc dust (mixed with water), and mixed well on the magnetic stirrer. After mixing well, around, 2 h, it again transferred to the oven, 105 ˚C, and dried for 16 h. The sample then transferred to the furnace and it calcinated for 5 h under 500 ˚C. The sample then analyzed with XRD and EDX to identify its components.
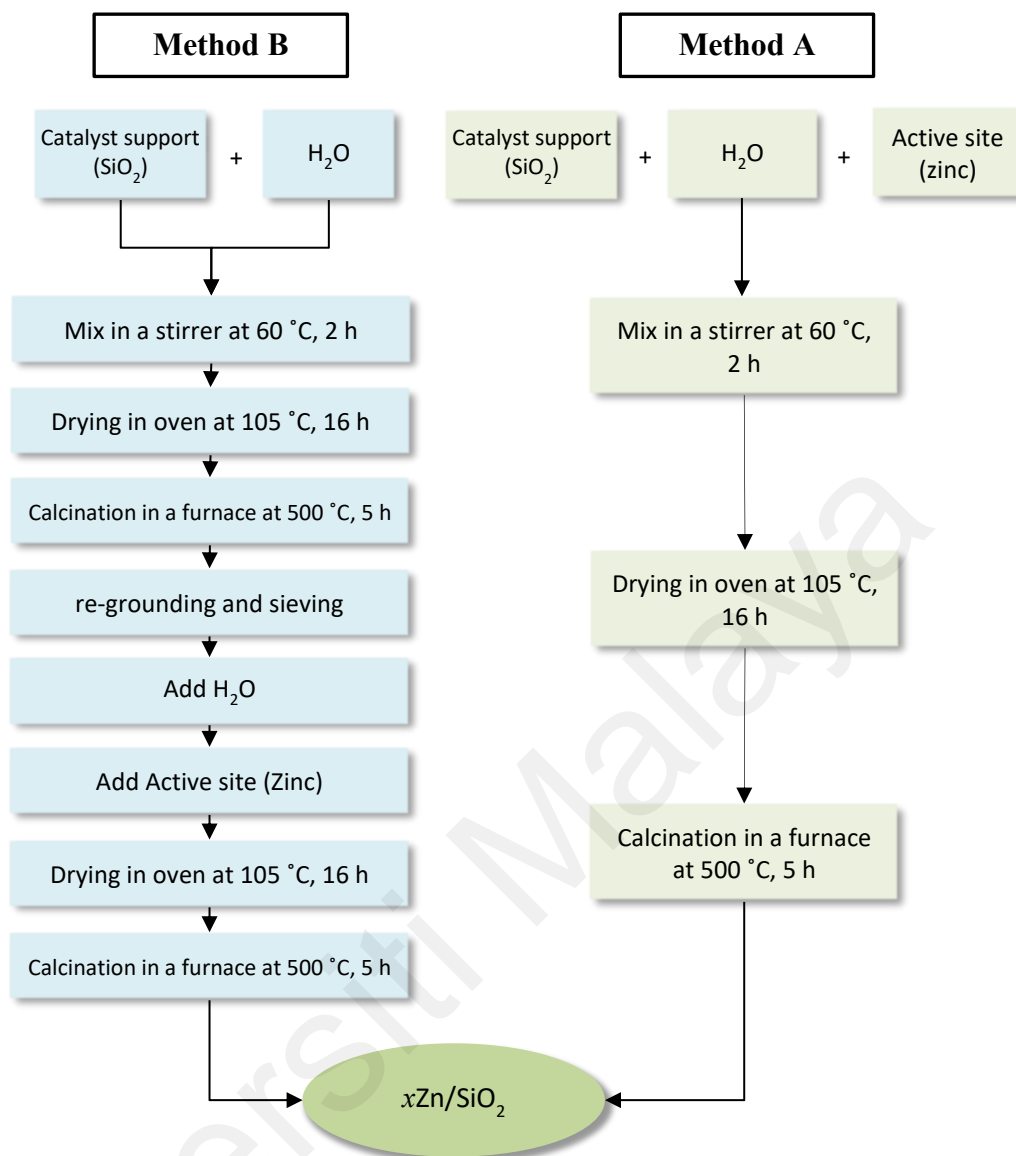
Figure 3.2: Flowchart for synthesis procedure of xZn/SiO$_2$ catalysts.

3.4 Characterization methods

The catalyst samples were characterized by different characterization methods. Pure supports and calcinated impregnates were characterized by XRD, N$_2$-adsorption, FESEM/EDX, H$_2$-TPR, H$_2$-TPD, NH$_3$-TPD, TGA, and ICP-OES. Feed and the process liquid products have been analyzed using GC-FID.

3.4.1   XRD

X-ray powder diffraction (XRD) is a characterization technique used to identify crystalline phase and cell dimensions of an unknown material to detect their chemical composition and other information. XRD analysis is based on interference of incident beams of monochromatic X-rays with one another, as they pass through the atomic planes, as they leave the crystal. Figure 3.3 represent a schematic of X-ray Diffractometer and its various component parts.
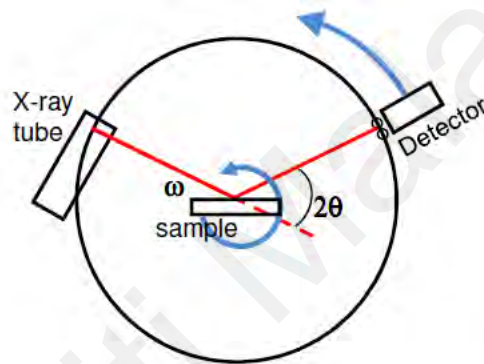
Figure 3.3: A schematic of X-ray Diffractometer and its various component parts**.**

By calculating the intensities and angles of the diffracted beams using the Bragg's law (Eq. 3-1), the lattice spacing can be determined.

$$n\lambda = 2d \, \sin \theta \tag{3-1}$$

In Bragg's law, *n* represents the order of reflection, which is a positive integer, λ stands for the wavelength of the x-ray, *d* represents the distance among two lattice plans and θ is the angle among reflecting lattice plans and the incoming x-rays. Due to the random orientation of the powdered sample, all possible diffraction directions of the lattice are attaining by scanning the material through a range of 2 theta angles. Alteration of the

diffraction peaks to d-spacings results to the identification of the mineral because each mineral has a set of unique d-spacings. Naturally, this is achieved by evaluation of d-spacings with standard reference patterns. The samples of the catalysts were characterized through X-ray diffraction spectrometry (XRD) using PANalytical X'Pert with Cu-Kα radiation. The samples were measured within $5° < 2\theta < 80°$. The step size was set to $0.0260°$ with a time step of 0.1 s, whereas the slit was 0.1 mm. Scherrer's formula (Eq. 3-2) was used to approximate the crystallite size of each sample. In this formula, d_{xrd} stands for the crystalline size nm, λ denotes the wavelength of the radiation, k is a constant equal to 0.94, β_{hkl} represents the half of the peak width at the maximum intensity, and θ is the peak position.

$$d_{xrd} = \frac{k\lambda}{\beta_{hkl}cos\theta}$$ (3-2)

3.4.2   N₂-adsorption

Brunauer Emmett Teller (BET) theory serves as a basis for determining the total surface area of porous and finely divided materials using physical adsorption of N_2 gas on the material surface. The concept of the BET theory derives from the Langmuir theory. The Langmuir theory hypotheses monolayer adsorption, constant heat of adsorption, and dynamic equilibrium among gas and adsorbed molecules. However, The BET formula does not consider monolayer adsorption, but multilayer adsorption with the following assumptions (Eq. 3-3):

- Infinite layers of gas molecules adsorb on a surface

- Interaction of the gas molecules with the adjacent layers only.

- No interaction between the adsorbed gas molecules.

- Constant enthalpy of adsorption for the first layer.

- The first layer enthalpy is greater than the other layers.

- The second and higher layers enthalpy is the same as the enthalpy of the liquefaction.

$$\frac{P}{V(P_0-P)} = \left[\frac{(C-1)}{V_m C}\right] \frac{P}{P_0} + \frac{1}{V_m C} \tag{3-3}$$

Equation 2-6 represent the BET equation where V stands for total volume of the adsorbed gas at STP, P_0 represent the saturation vapor pressure, V_m is the monolayer volume of the adsorbed gas at STP, and C is the BET constant which is defined by Eq. 3-4.

$$C = e^{\frac{q_1-q_L}{RT}} \tag{3-4}$$

where q_1 is the heat of adsorption for the first layer and q_L is that for the second and higher monolayers which is equal to the heat of liquefaction. Using the Eq. 2-6, the BET plot can be plotted as a straight line with $\frac{P/P_0}{V(1-P/P_0)}$ on the y-axis and P_0/P on the x-axis with a slope $\frac{C-1}{V_m C}$ and an intercept $\frac{1}{V_m C}$. By finding the V_m, the specific surface area can be calculated using Eq. 3-5.

$$A \left[\frac{m^2}{g}\right] = V_m \left[\frac{cm^3 STP}{g}\right] \left[\frac{6.023 \cdot 10^{23} molecules}{21400 \, cm^3 STP}\right] \left[\frac{cross \, section, m^2}{molecule}\right] \tag{3-5}$$

In 2015, the new IUPAC technical report proposed updated classification of physisorption isotherms which is shown in Figure 3.4. However, the original IUPAC resort for the physisorption isotherms were grouped into six types only.
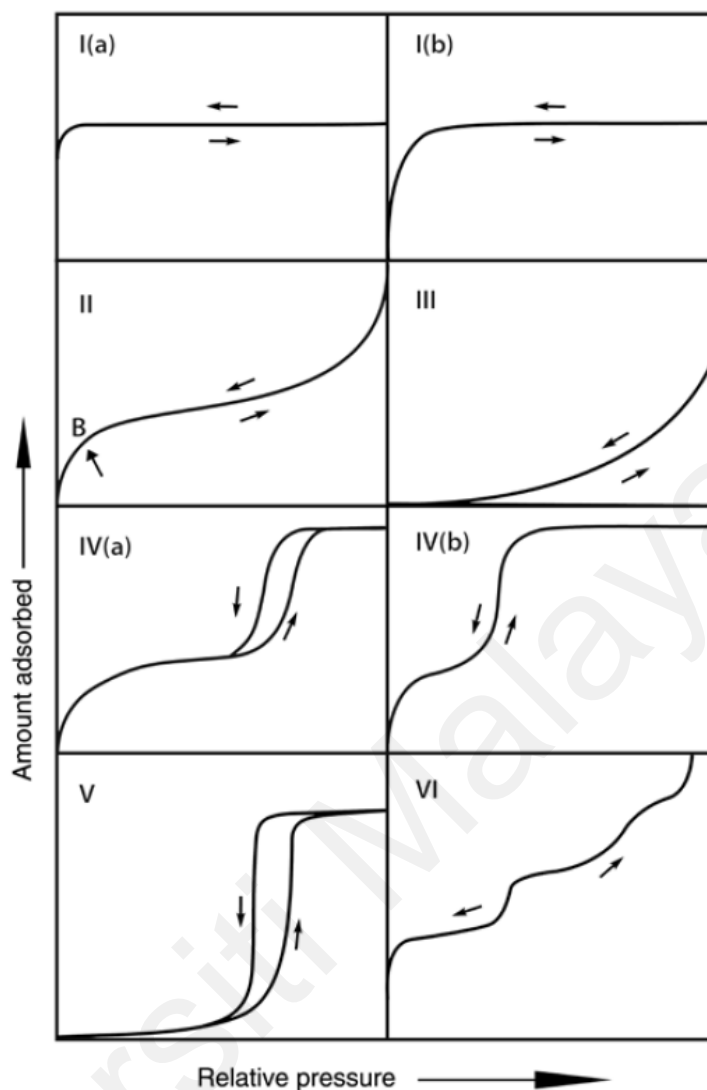
Figure 3.4: The latest IUPAC classification of physisorption isotherms (2015) (Thommes et al., 2015).

Reversible Type I isotherms are given by microporous solids having relatively small external surfaces. Type I(a) isotherms are given by microporous materials having mainly narrow micropores (of width < ~ 1 nm); Type I(b) isotherms are found with materials having pore size distributions over a broader range including wider micropores and possibly narrow mesopores (< ~ 2.5 nm). Reversible Type II isotherms are given by the physisorption of most gases on nonporous or macroporous adsorbents. In the case of a Type III isotherm, there is no Point B and therefore no identifiable monolayer formation;

the adsorbent-adsorbate interactions are now relatively weak, and the adsorbed molecules are clustered around the most favorable sites on the surface of a nonporous or macroporous solid. Type IV isotherms are given by mesoporous adsorbents. In the case of a Type IV(a) isotherm, capillary condensation is accompanied by hysteresis. With adsorbents having mesopores of smaller width, completely reversible Type IV(b) isotherms are observed. Type V isotherms are observed for water adsorption on hydrophobic microporous and mesoporous adsorbents. The reversible stepwise Type VI isotherm is representative of layer-by-layer adsorption on a highly uniform nonporous surface.

In this survey, the prepared samples of the catalysts were characterized through N_2-adsorption to detect their BET surface areas, pore volumes, and pore sizes. The samples were degassed at 90 °C for 1 h and 200 °C for 4 h before the analysis. The measurements were conducted at -196 °C. The N_2-adsorption apparatus used here was a Micromeritics TrisStar II 3020 V1.04.

3.4.3   FESEM/EDX

The elemental composition of the calcinated SiO_2 and xZn/SiO_2 was estimated via energy dispersive X-ray spectroscopy (EDX) using an Oxford-Horiba Inca XMax50 EDX at 20 kV. The morphology of the coated samples and bare SiO_2 was examined by a field-emission scanning electron microscope (FESEM) using a QUANTA 450 FEG.

Field Emission Scanning electron microscopy in combination with energy-dispersive X-ray spectrometry (FESEM/EDX) is a well-established and versatile method for the examining the localized morphology and elemental distributions of heterogeneous catalysts at the microscopic scale (Figure 3.5). Information about particle size distribution, deposition on the substrate surface, and elemental compositions can be

obtained easily. FESEM uses a focused beam of electrons to generate an image or to analyze the specimen. For operation, the gun head, the column, and specimen chamber have to be evacuated. The prevacuum pump and turbo pump evacuate the specimen chamber. Vacuum in the specimen chamber is measured by penning gauge. Column chamber valve closes and N_2 gas flows into the specimen chamber through vent valve. Schottky emitter emits electrons. The beam of electrons passes through the multihole aperture. Stigmator makes sure that the beam is rotationally symmetrical. Anode and linear tube are connected to form the beam booster. Beam booster provides better protection against external stray fields. Condenser lens controls the amount of demagnification. Objective lens focuses the electron beam onto the specimen. Deflection system consists of a set of scan coils to move the electron beam in a point-to-point scan process.

Figure 3.5: An image of the Quanta FEC 450 FESEM equipment.

Energy Dispersive X-Ray Spectroscopy (EDX) is a chemical microanalysis method applied in conjunction with FESEM. The method detects X-rays released from the surface during bombardment by an electron beam to characterize the elemental composition of the analyzed volume (up until 1 μm).

A detector calculates the relative abundance of emitted X-rays against their energy. The detector is typically a lithium-drifted silicon, solid-state device. When an incident X-ray strikes the detector, it creates a charge pulse that is proportional to the energy of the X-ray. The charge pulse is converted to a voltage pulse by a charge-sensitive preamplifier. The signal is then sent to a multichannel analyzer where the pulses are sorted by voltage. The energy, as determined from the voltage measurement, for each incident X-ray is sent to a computer for display and further data evaluation. The spectrum of X-ray energy versus counts is evaluated to determine the elemental composition of the sampled volume.

3.4.4 H$_2$-TPR

Temperature-programmed reduction (TPR) is an analytical method widely applied for the characterization of porous catalysts. The TPR tool results in quantitative data of the reducibility of the oxide's surface, as well as the heterogeneity of the reducible surface. In this method, a reducing gas mixture (5% or 10% H$_2$ in Ar or N$_2$ gas) streams over the catalyst. A thermal conductivity detector (TCD) is used to measure changes in the thermal conductivity of the gas stream. The TCD signal is then converted to concentration of active gas using a level calibration. Integrating the area under the concentration vs. time (or temperature) yields total gas consumed. The reduction of a metal oxide MO$_n$ by H$_2$ is described by Eq. 3-6:

$$MO_n + H_2 \rightarrow M + H_2O \tag{3-6}$$

A typical TPR profile is illustrated in Figure 3.6. This Figure represents a TPR spectrum where the peak maximum indicates the temperature that corresponds to the maximum rate of reduction.
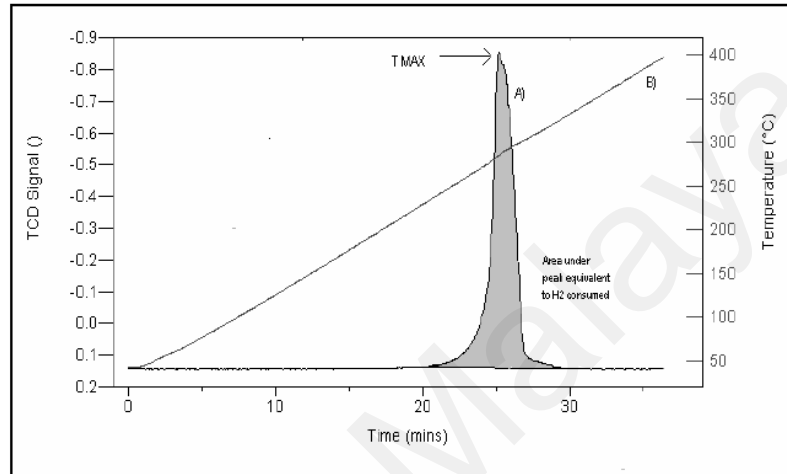
Figure 3.6: A typical TPR profile. Trace A shows the TCD signal as a function of time. Trace B represents the temperature as a function of time.

The rate expression for the reduction reaction, which has been given by Hurst et al., (1982) and by Wimmers et al., (1986), is presented by Eq. 3-7.

$$-\frac{d[MO_n]}{dt} = k_{red}\,[H_2]^p f([MO_n]) \tag{3-7}$$

Where

[MO$_n$]   metal oxide concentration

[H$_2$]   hydrogen gas concentration

k_{red} rate constant of the reduction reaction

p order of the reaction in hydrogen gas

f a function describes the dependence of the rate of reduction on the
    concentration of metal oxide

t time

If we write alpha for the degree of reduction, assume that the reaction is conducted in excess hydrogen ($p = 0$), use the fact that the temperature increases linearly in time (dt = betha dt) and replace k_{red} by the Arrhenius equation, we see the temperature dependence of the reduction process (Eq. 3-8).

$$\frac{d\alpha}{dT} = \frac{v}{\beta}\, e^{-E_{red}/RT} f(1-\alpha) \tag{3-8}$$

Where

α reduced material fraction

$f(1-\alpha)$ function of the fraction of unreduced material

v pre-exponential factor

β heating rate

E_{red} activation energy

R gas constant

T temperature

Hydrogen temperature-programmed reduction (H_2-TPR) was conducted by a Micromeritics Chemisorb 2720 apparatus. Prior to hydrogen adsorption, using the pure nitrogen at 500 ˚C, the samples were outgassed for 30 min. Subsequently, the catalysts were reduced, using 5% hydrogen diluted in argon gas, for one hour and 500 ˚C. In the following, the catalysts were cooled and, to remove the physically adsorbed molecules, flushed with N_2 gas at a flow rate of 20 mL/min. Finally, the catalysts were heated up to 900 ˚C in the nitrogen atmosphere. A thermal conductivity detector (TCD) monitored and recorded the H_2 consumption during the reduction process. The experiment procedure and operational details of H_2 temperature programmed reduction (H_2-TPR) are included in Appendix A.1.

3.4.5 H_2-TPD

Temperature Programmed Desorption (TPD) is a characterization method which has conventionally been used to provide information on the binding energies of atomic and molecular species adsorbed on a solid surface. The process of thermal desorption, on which this technique is based, is the mechanism with which an adsorbate leaves the substrate upon annealing and enters the gas phase. Desorption takes place if a molecule has enough energy to overcome the activation barrier for desorption. In a typical thermal desorption experiment, the sample is first exposed to a flux of molecules at a given temperature, until the desired initial surface coverage is reached. The sample is subsequently placed in front of a quadrupole mass spectrometer and its temperature is increased at a constant rate, in such a way to induce the thermal desorption of the adsorbed species (either atoms or molecules). During the experiment, the partial gas pressures are measured, in such a way to monitor the desorption rate of each atomic/molecular species as a function of the temperature.

A basic assumption in TPD, in fact, is that the desorption rate of an adsorbate is proportional to the corresponding measured partial pressure. This conditions rigorously met only if a high enough pumping speed is attainable in the chamber. Figure 3.7 represent the schematics of flow-through TPD reactor and vacuum TPD cell.
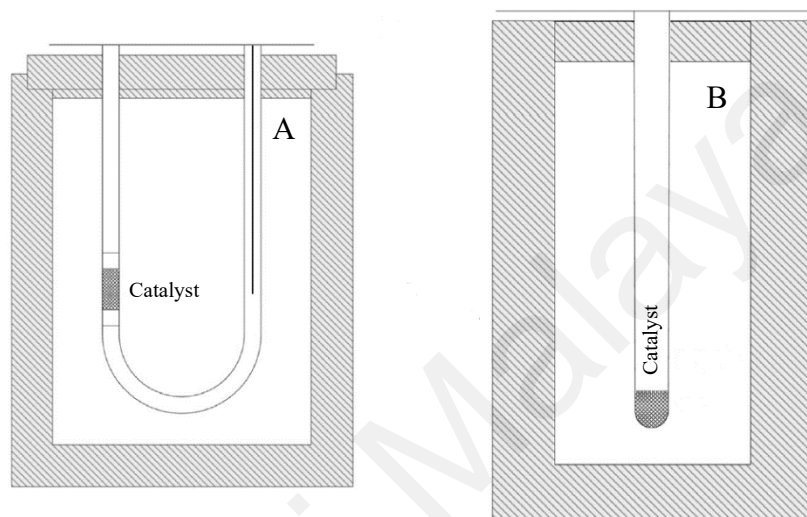
Figure 3.7: A schematics of flow-through TPD reactor and vacuum TPD cell.

Another important requirement in TPD is to keep a constant heating rate during the experiment, a condition that can be realized by an electronically controlled ramping of the temperature.

Provided these requirements are satisfied, the measured increase in partial pressure as a function of time can be fitted to the model equation above in order to obtain the relevant parameters, in particular the desorption energy. The analysis of the desorption curves (in particular the position of the desorption maxima and the shape of the spectra) also provides information on the desorption kinetics and on the adsorption mechanisms of the different species on the substrate.

Thermal desorption is described based on the Arrhenius equation (Eq. 3-9):

$$r(\theta) = -\frac{d\theta}{dt} = \upsilon(\theta)e^{-E_{act}(\theta)/RT}\theta^n \qquad (3\text{-}9)$$

Where

r(θ)	desorption rate
n	desorption order
θ	surface coverage
υ(θ)	pre-exponential factor
E_{act}	desorption activation energy
R	gas constant
T	temperature (K)

The simplified Arrhenius equation of the thermal desorption can be achieved considering the following assumptions:

- Activation energy and pre-exponential factor are dependent of the coverage
- Linear heating rate: $T(t) = T_0 + (\beta t)$ where β is the heating rate, T_0 represents the start temperature, and t indicates time.
- Indefinitely large of the gas pump rate, results to no gas re-adsorption

Then, the simplified thermal equation is (Eq. 3-10):

$$r(t) = -\frac{d\theta}{dt} = \upsilon_n e^{-E_{act}/RT}\theta^n \qquad (3\text{-}10)$$

Where

r(t)	desorption rate
n	desorption order
θ	surface coverage
v_n	pre-exponential factor
E_{act}	desorption activation energy
R	gas constant
T	temperature (K)

Hydrogen temperature programmed desorption was performed using the Micromeritics Chemisorb 2720 instrument under 5 vol% H_2/Ar gas flow. Prior to H_2 adsorption, the samples (50 mg) were outgassed in pure N_2 (20 mL/min) at 500 ˚C for 30 min. The outgassed samples were subsequently reduced with 5 vol% H_2/Ar gas mixture (20 mL/min) at 500 ˚C for 1 h and then cooled to room temperature. Subsequently, the catalyst was flushed with pure N_2 gas (20 mL/min) to remove all physically adsorbed molecules. The catalyst was then heated to 900 °C at various heating rates with pure N_2 at a flow rate of 20 mL/min. H_2 desorption was monitored using a thermal conductivity detector (TCD). The experiment procedure and operational details of H_2 temperature programmed desorption (H_2-TPD) are included in Appendix A.2.

3.4.6   NH₃-TPD

Determining the quantity and strength of the acid sites on porous materials is crucial to understand and predict the performance of a catalyst. The activity depends on many factors, but the Brønsted-acid site density is usually one of the most crucial parameters. TPD of ammonia is a widely used method for characterization of site densities in solid

acids due to the simplicity of the technique. Ammonia often overestimates the quantity of acid sites. Its small molecular size allows ammonia to penetrate all pores of the solid where larger molecules commonly found in cracking and hydrocracking reactions only have access to large micropores and mesopores. Also, ammonia is a very basic molecule which is capable of titrating weak acid sites which may not contribute to the activity of catalysts. The strongly polar adsorbed ammonia is also capable of adsorbing additional ammonia from the gas phase. Using the same apparatus and concepts of H_2-TPD, and replacing the Hydrogen gas with Ammonia gas, NH_3-TPD characterization method could be performed.

Theoretical equation of the TPD ammonia by taking the re-adsorption into account will results to the following equation (Eq. 3-11) that describes desorption-adsorption processes.

$$NH_3^* \underset{k_a}{\overset{k_d}{\rightleftarrows}} NH_3 (g) + {}^* \qquad (3\text{-}11)$$

In this equation, the NH_3^* (θ) denotes for the adsorbed ammonia, * stands for the vacant site, and NH_3 represents the ammonia in the gas phase. k_a and k_d are the rate constants for adsorption and *desorption*, respectively.

The time derivation of the *NH_3* coverage (θ) is given by (Eq. 3-12) (L. Chen et al., 2019):

$$\frac{d\theta}{dt} = k_a \frac{P_g}{P^0} (1 - \theta) - k_d \theta \qquad (3\text{-}12)$$

Where P_g represents the pressure of ammonia and P^0 stands for the pressure at standard conditions. Using the ideal gas law, P_g can be written as RTC_g where R is the gas constant, T is the temperature and C_g is the ammonia concentration. The concentration can be calculated assuming equilibrium between the gaseous and adsorbed ammonia (Eq. 3-13):

$$C_g = \frac{\theta}{1-\theta} \frac{P^0}{RT} K \tag{3-13}$$

Where K is the equilibrium constant given by enthalpy and entropy changes ($\Delta H \ and \ \Delta S$) upon adsorption (Eq. 3-14):

$$K = \frac{k_d}{k_a} = \exp\left(-\frac{\Delta H}{RT}\right) \exp\left(\frac{\Delta S}{R}\right) \tag{3-14}$$

The mass balance in the following gas is (Eq. 3-15):

$$FC_g = -A_0 W \frac{d\theta}{dt} = -\beta A_0 W \frac{d\theta}{dT} \tag{3-15}$$

Where F is the flow rate of the carrier gas, A_0 is the concentration of the adsorption sites, W is the catalyst weight and β is the heating rate. The concentration can in this way written (Eq. 3-16):

$$C_g = -\frac{\beta A_0 W}{F} = \frac{d\theta}{dT} = \frac{\theta}{1-\theta} \frac{P^0}{Rt} \exp\left(-\frac{\Delta H}{RT}\right) \exp\left(\frac{\Delta S}{R}\right) \tag{3-16}$$

The concentration depends on temperature and site-coverage. The site coverage is obtained iteratively through (Eq. 3-17):

$$\theta_{i+1} = \theta_i + \left(\frac{d\theta}{dT}\right)_i \Delta T \tag{3-17}$$

This relation connects C_g and T, which gives the TPD profile.

The total acidity of the prepared catalysts has been tested using the NH_3-TPD method. Prior to outgassing the catalyst (50 mg) in the quartz U-tube, it was heated from the room temperature up to 300 ℃. Then, under flow rate of 20 mL/min of Helium, the sample was degassed for 30 min at 300 ℃. Subsequently, the catalyst was cooled down to the room temperature and it was ready for Ammonia chemisorption step. A 5% NH_3/He gas mixture has been selected for this step and the ammonia chemisorbed on the sample for 30 min. To remove the physiosorbed molecules, the sample was purged using the helium gas at 100 ℃ (30 min). Finally, applying the heating rate of 40 ℃/min, the sample was heated up to 900 ℃ in the helium atmosphere (20 mL/min). For this analysis, a Micromeritics apparatus has been used (Model: Chemisorb 2720).

3.4.7   TGA

Thermogravimetry (TGA) analysis is a technique which measures the change in the mass of a sample over a range of temperatures or time. A TGA machine consists of a sample pan which hangs off a hook and is connected by a microgram balance arm to a tare pan (Figure 3.8).
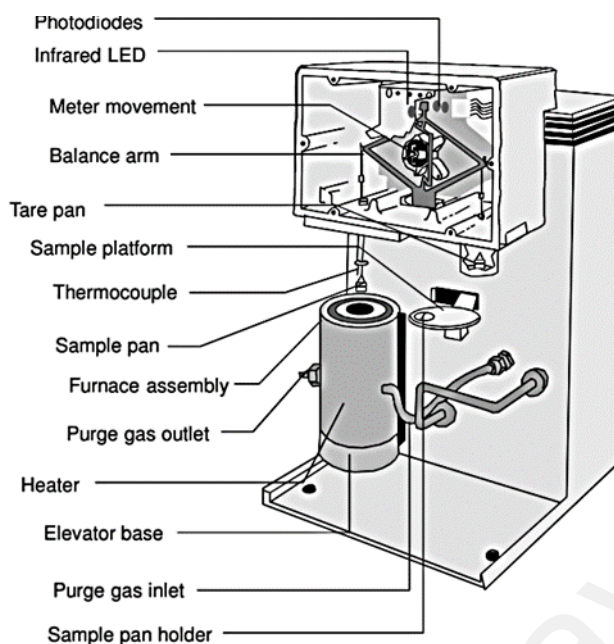
Figure 3.8: A schematic of a TGA analysis apparatus (Ye Li et al., 2020).

The basic principle of TGA is that as a sample is heated, its mass changes. This change can be used to determine the composition of a material. Thermograms are unique for each compound and communicate material thermal stability, oxidative stability, multi-component composition, product lifetime, decomposition kinetics, and moisture and volatile content. Generic thermograms have multiple sections.

1.   Below 150 ˚C, physiosorbed water, low molecular weight volatile compounds, solvents, and trapped gases evolve.

2.   Between 150 ˚C-250 ˚C, mass loss is due to chemisorbed water and low molecular weight compounds like additives and volatile decomposition products.

3.   Above 250 ˚C, compounds begin to decompose between the onset and endset temperature. Multiple onset and endset temperatures are possible for multi-component systems and for reactions with intermediate steps.

4.   The remaining material above the endset temperature includes non-volatile inorganic ashes and metals.

5. In an oxidizing environment, metallic compounds increase the oxidation state and gain mass.

Thermogravimetric (TGA) analysis was employed for the bare SiO_2 and freshly calcinated catalysts to examine the extent of water and organic compounds on the samples. A TGA Q500 V20.10 (TA instruments) instrument has been applied in this survey. In a typical run, 80 mg of a sample was placed in the sample holder and it was heated with a heating rate of 20 ℃/min up to 800 ℃. The experiment procedure of TGA analysis is included in Appendix A.3.

3.4.8   ICP-OES

It has been around 3 decades since ICP optical emission spectrophotometers (ICP-OES) began to be widely used and is now one of the most versatile methods of inorganic analysis. Its features are often compared to atomic absorption spectrophotometers. Compared to atomic absorption spectrophotometers, in which the excitation temperature of air-acetylene flame measures 2000 to 3000 K, the excitation temperature of argon ICP is 5000 to 7000 K, which efficiently excites many elements. Also, using inert gas (argon) makes oxides and nitrides harder to be generated.

ICP, abbreviation for Inductively Coupled Plasma, is one method of optical emission spectrometry. When plasma energy is given to an analysis sample from outside, the component elements (atoms) are excited. When the excited atoms return to low energy position, emission rays (spectrum rays) are released and the emission rays that correspond to the photon wavelength are measured. The element type is determined based on the position of the photon rays, and the content of each element is determined based on the rays' intensity.

To generate plasma, first, argon gas is supplied to torch coil, and high frequency electric current is applied to the work coil at the tip of the torch tube. Using the electromagnetic field created in the torch tube by the high frequency current, argon gas is ionized, and plasma is generated. This plasma has high electron density and temperature (10000K) and this energy is used in the excitation-emission of the sample. Solution samples are introduced into the plasma in an atomized state through the narrow tube in the center of the torch tube. Equipment for ICP optical emission spectrometry consists of a light source unit, a spectrophotometer, a detector and a data processing unit. There are several types of equipment based on differences in the Spectrophotometer and the detector.

The metal content of the prepared catalysts was determined through inductively coupled plasma–optical emission spectrometry (ICP–OES) analysis (Optima 7000 DV, Perkin Elmer). The sample (100 mg) was digested with 10 mL of nitric acid (HNO_3). The solution then was filled to 50 mL with deionized distilled water and then analyzed using ICP–OES. The calibration standards for zinc were prepared by adding an appropriate amount of zinc to deionized distilled water (14 mL) and HNO_3 (7 mL). The solution was later brought to a volume of 1000 mL with deionized water. The calibration standard solutions were prepared with five levels including 10, 50, 100, 200, and 400 ppm. The blank sample was prepared with deionized distilled water.

3.4.9   GC-FID

Gas Chromatography is a technique for quality control as well as identification and quantitation of compounds in a mixture. A broad variety of samples can be analyzed if the compounds are sufficiently thermally stable and reasonably volatile. In this technique, a mobile and a stationary phase are required. The mobile phase is comprised of an inert

gas i.e., helium, argon, or nitrogen. The stationary phase consists of a packed column in which the packing or solid support itself acts as stationary phase or is coated with the liquid stationary phase. The separation of compounds is based on the different strengths of interaction of the compounds with the stationary phase. The stronger the interaction is, the longer the compound interacts with the stationary phase, and the more time it takes to migrate through the column. Flame Ionization Detector (FID) is very sensitive towards organic molecules but relative insensitive for a few small molecules i.e., N_2, NO_x, H_2S, CO, CO_2, H_2O. If proper amounts of hydrogen/air are mixed, the combustion does not afford any or very few ions resulting in a low background signal. If other carbon containing components, are introduced to this stream, cations will be produced in the effluent stream. The more carbon atoms are in the molecule, the more fragments are formed and the more sensitive the detector is for this compound. Since there is no direct relationship between the number of carbon atoms and the size of the signal, the individual response factors for each compound have to be experimentally determined for each instrument. In addition, several gases are usually required to operate a FID: hydrogen, oxygen (or compressed air), and a carrier gas.

Many factors influence the separation of the components in a mixture include vapor pressure, polarity of compounds, polarity of the stationary phase, column temperature, carrier gas flow rate, column length, and amount of material injected.

The liquid samples from activity testing have been analyzed using GC-FID (Agilent 7890A- Gas Chromatograph) in order to measure the conversion efficiency of the HDO of phenol in various operation conditions. GC-FID analysis conditions were firstly taken from the method 8014A, EPA publication SW_846. However, the method was modified by some trial and error to identify all components in the samples include phenol, benzene,

n-decane and acetone. Table 3.2 represents the various conditions have been tested for this study.

Table 3-2: GC-FID methods and their conditions tested in this study.

Conditions	Method 8014 A	Modified method I	Modified method II
Column	DB-5	DB-5	DB-5
Carrier gas	Nitrogen	Helium	Helium
Flow rate	6 ml/min	6 ml/min	6 ml/min
Makeup gas	Hydrogen	Hydrogen	Hydrogen
Flow rate	30 ml/min	30 ml/min	30 ml/min
Oven initial Temperature	80 ˚C	40 ˚C	40 ˚C
Temperature program	1.5 min hold 80 ˚C to 230 ˚C at 6 ˚C/min 230 ˚C to 275 ˚C at 10 ˚C/min 4.5 min hold	2 min hold 40 ˚C to 240 ˚C at 10 ˚C/min 10 min hold	3 min hold 40 ˚C to 150 ˚C at 30 ˚C/min 5 min hold
Injection temperature	200 ˚C	200 ˚C	200 ˚C
Detector temperature	300 ˚C	300 ˚C	300 ˚C
Injection volume	1microliter	1microliter	1microliter
Detector type	FID	FID	FID

From preliminary experiments, modified method II was selected for further investigations in this study. Before analyzing the samples, run time and standard curve of each main component should be detected by standard samples. Table 3.3 represent the samples have been prepared for this purpose. The results for each sample in given in attachments A.4 to A.16.

Table 3-3: Sample's name, the components, and their purposes for GC-FID analysis (gas chromatography spectrograms of the samples are available in Appendix B.4).

No.	Sample Name	Components	Purpose
1	Pure acetone	Pure acetone	To identify the run-time of acetone
2	10000 ppm phenol	Phenol, acetone	To draw the phenol standard curve
3	5000 ppm phenol	Phenol, acetone	To draw the phenol standard curve
4	2500 ppm phenol	Phenol, acetone	To draw the phenol standard curve
5	20000 ppm n-decane	n-decane, acetone	To identify the run-time of n-decane as well as draw the n-decane standard curve
6	10000 ppm n-decane	n-decane, acetone	To draw the n-decane standard curve
7	5000 ppm n-decane	n-decane, acetone	To draw the n-decane standard curve
8	20000 ppm benzene	Benzene, acetone	To draw the benzene standard curve
9	10000 ppm benzene	Benzene, acetone	To draw the benzene standard curve
10	5000 ppm benzene	Benzene, acetone	To draw the benzene standard curve
11	2500 ppm benzene	Benzene, acetone	To draw the benzene standard curve
12	20000 ppm Cyclohexene	Cyclohexene, acetone	To draw the benzene standard curve
13	10000 ppm Cyclohexene	Cyclohexene, acetone	To draw the benzene standard curve
14	5000 ppm Cyclohexene	Cyclohexene, acetone	To draw the benzene standard curve
15	2500 ppm Cyclohexene	Cyclohexene, acetone	To draw the benzene standard curve
16	20000 ppm Cyclohexane	Cyclohexane, acetone	To draw the benzene standard curve
17	10000 ppm Cyclohexane	Cyclohexane, acetone	To draw the benzene standard curve
18	5000 ppm Cyclohexane	Cyclohexane, acetone	To draw the benzene standard curve
19	2500 ppm Cyclohexane	Cyclohexane, acetone	To draw the benzene standard curve
20	Feed	n-decane, phenol (1% v/v), acetone	To detect the feed spectrum
21	product	n-decane, phenol, benzene, acetone	To simulate the expected product

3.5   Catalyst activity testing and optimizing the process parameters

A continuous bench-scale fixed bed reactor was designed, fabricated, and used in this work to test the catalysts at atmospheric pressure. The experiments were carried out on the pilot plant laboratory at the department of chemical engineering, University Malaya. Figure 3.9 represents a process flow diagram of the rig.
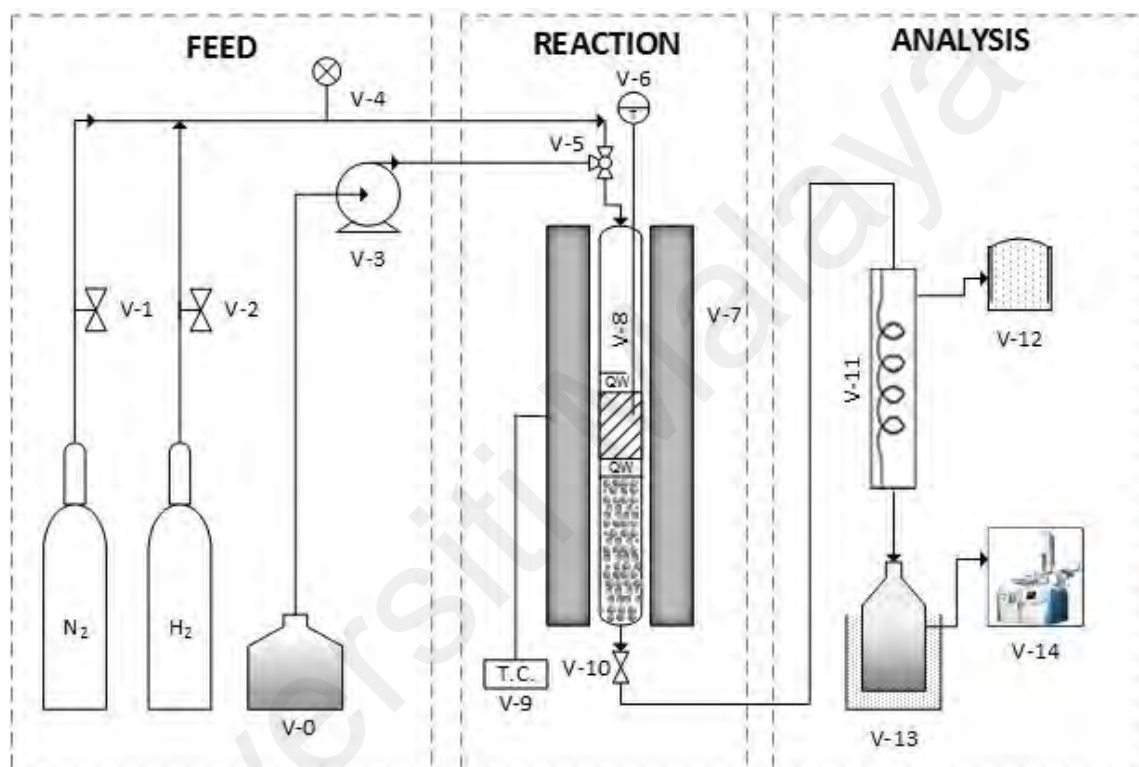
Figure 3.9: Process flow diagram of the rig (V_0 = feed, V_1 = flow controller for the carrier gas, V_2 = flow controller for the reactant gas, V_3 = HPLC pump, V_4 = flowmeter, V_5 = gas-feed mixer, V_6 = thermometer, V_7 = furnace chamber, V_8 = Stainless steel reactor containing the inert ceramic balls, quartz wool, and the catalyst, V_9 = Temperature controller, V_{10} = valve, V_{11} = condenser, V_{12} = gas collector, V_{13} = liquid product container with the ice trap, V_{14} = off-line GC/FID).

The reactor was made of a stainless-steel tube with an ID of 0.80 cm and length of 77 cm according to Figure 3.10. It was externally heated with a two-zone electric furnace, where the actual HDO temperature was monitored by a Type K external thermocouple located next to the catalyst position in the reactor. One g of the xZn/SiO$_2$ was packed in the center of the reactor on a bed of silicon beads. The catalyst also sandwiched by two

layers of quartz wool at both ends to avoid of the catalyst's relocation. The reaction temperature used for the experiments varied from 200 ˚C to 600 ˚C. At each standard experiment and before initiating the feed, the catalyst was firstly purged with N_2 (150 mL/min) for 1h and then reduced/activated *in situ* for 2h in flowing H_2 (100 mL/min) at 500 ˚C. The temperature then set to the designed temperature for each experiment. The gas flow rates (N_2 and H_2) were controlled with mass flow controllers (GFC series, Dwyer). Feed was injected using an intelligent HPLC pump (PU-980, JASCO) at various flow rates (0.1 – 0.5 mL/min). All experiments were done at 1 vol.% of phenol solved in n-decane as the feed (calculations for preparation of the feed solution is available in Appendix B.1). The upgraded vapor mixture, exhaust from the bottom of the reactor, were then condensed by a condenser (contains Ethylene glycol as the coolant liquid) at -4 ˚C, and the liquid products collected for further analysis by GC-FID. Three injections were made for each sample, and the average measured amount has been used. Before analyzing the samples, standard curve has been prepared for phenol, benzene, cyclohexane, cyclohexene, and n-decane. Also, the run time of each component has been detected using standard solutions. The standard curves are given in appendix B.3.

0.4 cm

Thermocouple

60.4 cm

77 cm

Quartz wool ← 0.5 cm
Catalyst ← 0.6 cm
Quartz wool ← 0.5 cm

Silicon pellet ← 15 cm

0.8 cm
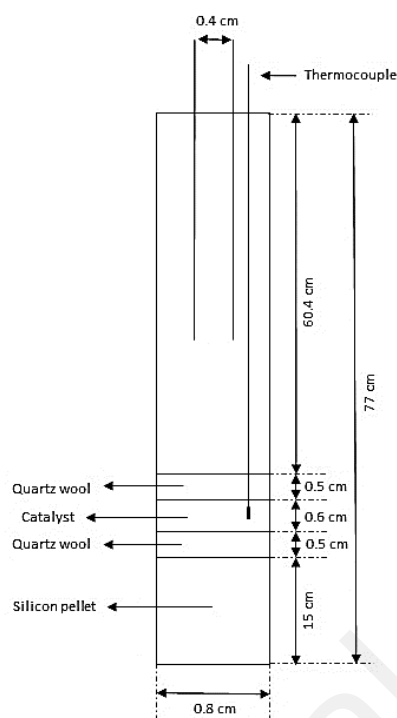
Figure 3.10: Schematic of the reactor dimensions.

3.6　Catalyst stability and reusability study

To perform the stability test of the prepared catalysts in this study, a freshly prepared 3% Zn/SiO_2 catalyst was selected. The collected data from the HDO reaction at various times on stream (TOSs) were used for calculating the conversion efficiency of the phenol. The obtained results will reveal the variation in activity and selectivity of the catalyst applied with TOS. A reusability study was done in the fixed-bed reactor and the sample applied for the stability test was regenerated at 500 ˚C under the air atmosphere (for 1 h in an electrical furnace). Preliminary experiments proved that the abovementioned conditions for regeneration of the catalyst will remove all impurities on the catalysts and the sample performs like a fresh catalyst. Furthermore, it has been observed that after four cycles of the catalyst regeneration, the conversion efficiency decreased to less than 40%, which is not acceptable. Hence four cycles of regeneration have been chosen for this part

of the study. The liquid products were collected and further analyzed using GC-FID analysis.

3.7 Experiment runs and conditions

Activity measurements of the samples have been performed in a continuous fixed bed plug reactor fabricated, from stainless steel, for this research. The applied feed pump is a JUSCO intelligent HPLC pump. The following describes the procedure for a typical run for the activity evaluation.

1- Turn on the chiller (contains ethylene glycol) at least 4 h before the main experiment to reach the desired temperature (-4 ˚C) for cooling the products which are in the vapor form.

2- Check that the N_2 and H_2 gas cylinders contain enough gas for the experiments.

3- Load the reactor with the silicon pellet, quartz wool and catalyst.

4- Attach the reactor to the rig. Then, tight the thermocouple on the outside of the reactor.

5- Tight the reactor screws to avoid any leaking of the gases.

6- Turn on the flow controller for N_2 and set the desired flow. Then check for gas leakage from the reactor.

7- Turn on the other flow controller for H_2 and do another gas leakage test.

8- Activate the catalyst by flowing H_2/N_2 mixture (80/20) at 500 ˚C for 2 h.

9- After the activation, turn off the H_2 flow controller and let N_2 gas flow for 30 minutes at 500 ˚C.

10- Prepare the feed by mixing 1 vol.% phenol in n-decane. Afterwards, connect the feed to the HPLC pump.

11- Turn off the N_2 and turn on the H_2/N_2 mixture (80/20) at the desired flow rate.

12- Open the feed to reactor valve and turn on the feed pump. Set the pump to the desired flow rate.

13- End the experiment by the time there is no more vapor taking out of the reactor. To do this, turn off the furnace, feed pump and H_2/N_2 flow controller. Turn on the N_2 for 1 hour to dry and cold the reactor.

14- Put the liquid samples in a labeled glass container for further analysis using offline GC-FID.

3.8 Safety aspects

Throughout the experiments, care is taken to prevent the health, fire, reactivity, and contact hazards associated with all the chemicals and hazards related with all the equipment and instruments used in the research project. Besides, normal laboratory safety precaution procedures including the use of appropriate personal protective equipment and use of standard operating procedures and waste disposal system is followed to eliminate and minimize the risk. Appendix C represents the risk assessment survey form for this investigation.

CHAPTER 4: RESULTS AND DISCUSSION

4.1 Introduction

This chapter represents the experimental and analytical results obtained from catalytic HDO of phenol in atmospheric H_2 pressure. The research results have been categorized into three parts include: I- Synthesis and characterization of the catalysts, II- Effect of process parameters on atmospheric HDO of phenol, and III- Stability, regenerability, and mechanism of the reaction. In the first section, the physiochemical properties of prepared catalysts were surveyed by X-ray diffraction (XRD), N_2 physisorption (BET), inductively coupled plasma-optical emission spectrometry (ICP-OES), Energy Dispersive X-Ray Spectroscopy (EDX), H_2 temperature-programmed desorption (H_2-TPD), NH_3 temperature-programmed desorption (NH_3-TPD), thermogravimetry analysis (TGA), H_2 temperature-programmed reduction (H_2-TPR), and field-emission scanning electron microscopy (FESEM). The number in the catalyst names are nominal value and does not represent the real loaded active site on the support surface.

The second section of this chapter surveys the effect of various process parameters on the conversion efficiency and selectivity of the catalytic reaction products. The process parameters have been surveyed in this project are active site loading on the support surface, the reaction temperature, weight hourly space velocity (WHSV), and H_2 volumetric flow rate. Last not the least section of this chapter deals with the results of stability and regenerability tests of the selected catalysts. Besides, the mechanism of the reaction also has been investigated. Additional results and calculations of the study are given in Appendix B.

4.2   Synthesis and Characterization of the catalysts

4.2.1   Catalyst synthesis method selection with XRD analysis

XRD analysis was performed to identify the loaded element as well as its quantity on the surface of the support (SiO_2). Figure 4.1 and Figure 4.2 represent the peak list for method A and B respectively. Zinc hydroxide, zinc oxide and zinc metal were detected in both preparation methods. However, based on the Table 4.1, zinc is the predominant compound on the support surface at method B in comparison to method A that ZnO is predominant compound. Detection of higher zinc metal on the surface of the support in method B might be related to an extra calcination step, before loading the active site. Based on the abovementioned results, Method B has been selected for catalyst preparation and further considerations.

Table 4-1: Comparison of the catalyst characteristics prepared by method A & B using XRD.

Method	Compound Name	Scale Factor	Chemical Formula
Method **A**	Zinc Oxide	0.902	ZnO
	Zinc	0.438	Zn
	Zinc Hydroxide	0.773	$Zn (OH)_2$
Method **B**	Zinc	1.057	Zn
	Zinc Oxide	0.593	ZnO
	Zinc Hydroxide	0.567	$Zn (OH)_2$
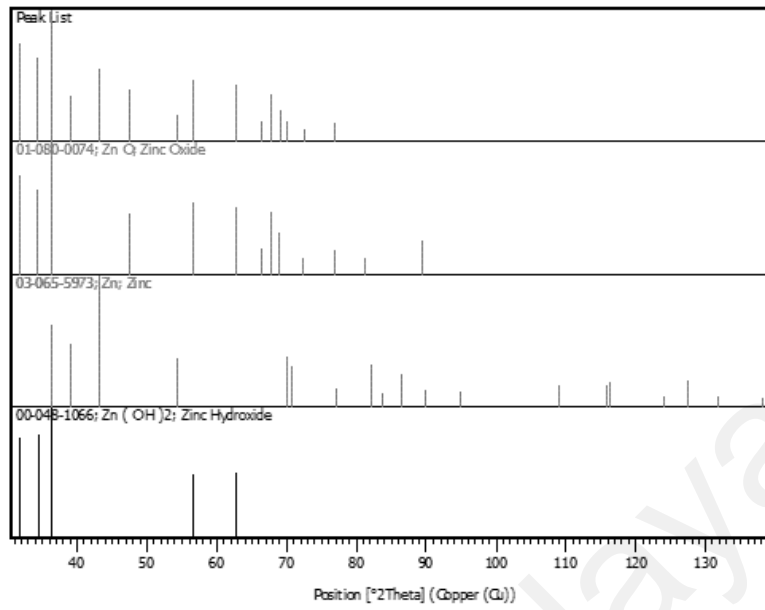
Figure 4.1: XRD Peak list for Catalyst preparation method A.
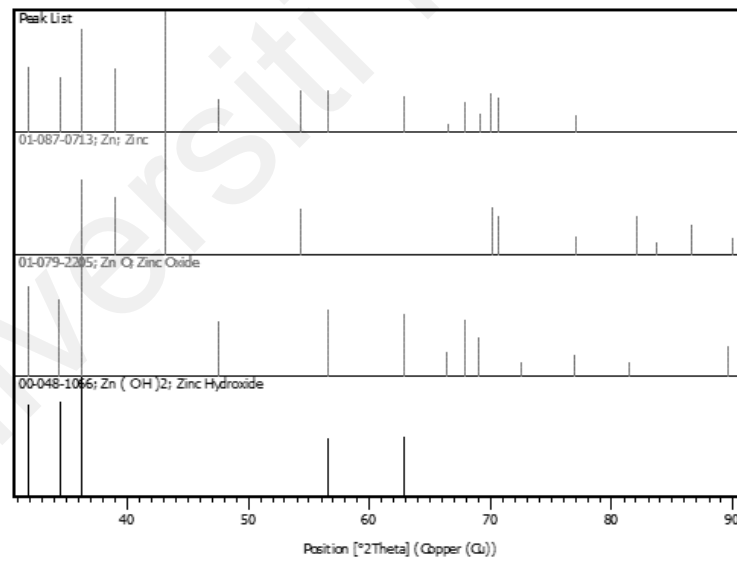
Figure 4.2: XRD Peak list for Catalyst preparation method B.

4.2.2 Crystallography of the catalysts

The XRD patterns of the bare and metalized SiO_2 with various loading percentages are presented in Figure 4.3. The XRD diffractograms confirmed the presence of zinc in

samples (b)–(f). The peaks assigned to the hexagonal (wurtzite) zinc were observed at 2θ = 32°, 34.3°, 36.2°, 47.6°, 56.6°, 62.90°, 66.3°, and 68° (PDF code no: 00-036-1451) with the corresponding crystallographic planes of (100), (002), (101), (102), (110), (103), (200), and (112), respectively (Rusu et al., 2011). Small zinc crystallites were well dispersed given that the diffraction peaks of the (110), (103), (200), and (112) planes of zinc were not detected by XRD. The planes may have formed in negligible amounts or the clusters were too small (less than 5 nm) to be detected by XRD. The average sizes of zinc (100, 002, and 101) crystallites increased with the increase in zinc loading (Table 4.2) because of agglomeration outside the pores (Sacco et al., 2019). All XRD patterns of the samples exhibited similar degrees of crystallinity and minimal peak broadening effect. These characteristics indicated that the addition of 0.5 – 4 wt% zinc negligibly affected the crystallinity of the sample. The XRD peaks of zinc crystallites (Figure 4.3) were not prominent possibly because of the low zinc proportion and the good dispersion of zinc nanoparticles in the SiO_2 support. The existence of zinc in the SiO_2 support was also confirmed via ICP–OES and EDX analyses.
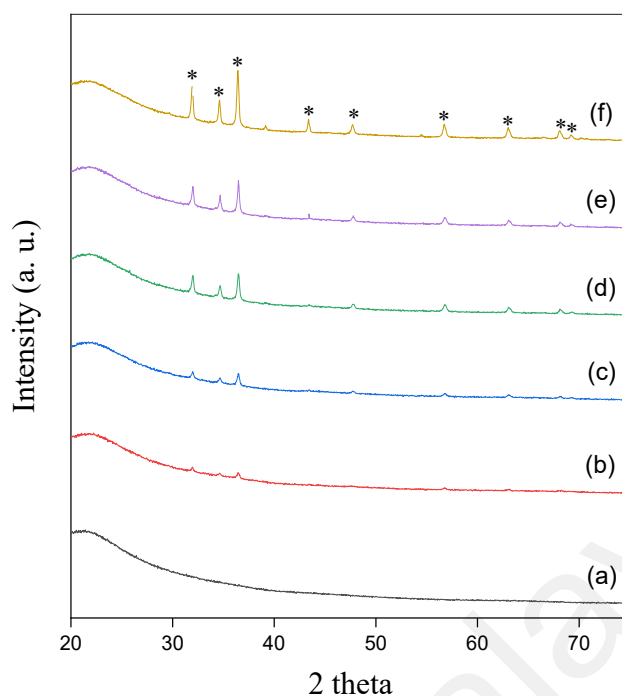
Figure 4.3: XRD patterns of the bare and various percentage of Zn loaded on the SiO_2 surface. (a = bare SiO_2, b = 0.5% Zn/SiO_2, c = 1% Zn/SiO_2, d = 2% Zn/SiO_2, e=3% Zn/SiO_2, f = 4% Zn/SiO_2) where: (*) metallic zinc.

Table 4.2: Physiochemical characteristics of the catalysts and the surface areas of the pure support, for comparison.

Catalyst	S_{BET} Catalyst/ support (m^2/g)	d_{XRD} average (nm) (100,002,101)	Pore volume (cm^3/g)	Pore size (Å)	Theoretical zinc loading (g/kg)	Actual zinc loading (g/kg) (ICP-OES)	Error %
SiO_2	185.5	-	1.300	280.220	-	-	-
0.5% Zn/SiO_2	185.2	48	1.300	280.220	5	4.63	7.4
1% Zn/SiO_2	184.7	49	1.300	280.940	10	9.11	8.9
2% Zn/SiO_2	181	51	1.274	281.906	20	17.50	12.5
3% Zn/SiO_2	173.3	60	1.284	283.819	30	25.31	15.63
4% Zn/SiO_2	153	85	1.265	286.890	40	32.51	18.72

4.2.3 Catalyst surface characterization results by N_2-adsorption analysis

Table 4.2 details the pore size, pore volume, and BET surface area of the calcinated support (SiO_2) and the calcinated impregnated catalysts obtained through N_2 adsorption analysis. The results from N_2-adsorption analyses indicated that the BET surface area of the calcinated support was higher than that of the calcinated impregnated samples. The surface area of SiO_2 was within the surface area range reported by Lei Nie (Nie, 2014).

The BET surface area and pore volume declined after impregnation as previously documented in literature (Oyama et al., 2002; Phillips et al., 2002). Clark et al., investigated the effect of various loadings of molybdenum and phosphide and found that the BET surface area decreased with increasing active site loading (Clark & Oyama, 2003). This finding might be because metal particles blocked pores and therefore decreased the surface area and pore volume. However, pore size increased as the pore volume and BET surface area of the samples decreased with elevating metal loading. Small pores closed selectively with the loading of the active metal on the surfaces of the support. These trends are expected according to literature (Asphaug, 2013). Thus, although pore volume and surface area decreased, the average pore diameter increased because only large pores remained for physisorption. All the samples presented type IV isotherms (isotherm types are shown in Chapter 2, Figure 2.7), which represent a mesoporous structure with multilayer adsorption and capillary condensation. The pore volume distribution plots revealed that most pores were mesoporous and fell in the range of 18–436 Å. All the samples were tested twice to study how the results changed with various analyses, and the results had negligible differences. Table 4.3 represents the annotated sample names, the metal loading and their N_2- adsorption analysis conditions.

Table 4.3: The annotated sample names, the metal loading, and their N_2-adsorption analysis conditions.

No.	Sample	Loading of Zn %	Degas program (˚C & hour)
1	Calcinated support (SiO_2)	0	90 ˚C 1 hour & 200˚C 4 h
2	Calcinated impregnated Zn/SiO_2	0.5	90 ˚C 1 hour & 200˚C 4 h
3	Calcinated impregnated Zn/SiO_2	1	90 ˚C 1 hour & 200˚C 4 h
4	Calcinated impregnated Zn/SiO_2	2	90 ˚C 1 hour & 200˚C 4 h
5	Calcinated impregnated Zn/SiO_2	3	90 ˚C 1 hour & 200˚C 4 h
6	Calcinated impregnated Zn/SiO_2	4	90 ˚C 1 hour & 200˚C 4 h

4.2.4   Metal content analysis using ICP-OES

ICP–OES analysis was performed to investigate the exact metal content of each catalyst. The analysis results for the catalysts are reported in Table 4.2. In all samples, the real metal content was lower than the theoretical content. The differences between the theoretical and the real metal content were within 7%–19%. Based on the results, the error percentages for the prepared catalysts including 0.5%, 1%, 2%, 3%, and 4% zinc were 7.2, 8.9, 12.5, 15.63, and 18.72, respectively.

4.2.5   Metal content analysis using EDX

Table 4.4 provides the EDX values for the bare calcinated SiO_2, 0.5% Zn/SiO_2, 1% Zn/SiO_2, 2% Zn/SiO_2, 3% Zn/SiO_2, and 4% Zn/SiO_2. The EDX values of all the samples provided evidence for the presence of zinc but not for that of bare calcinated SiO_2. Based

on the EDX analysis, the zinc loadings for 0.5% Zn/SiO$_2$, 1% Zn/SiO$_2$, 2% Zn/SiO$_2$, 3% Zn/SiO$_2$, and 4% Zn/SiO$_2$ were approximately 0.46, 0.93, 1.88, 2.59, and 3.37 wt%, respectively.

The accuracy of ICP–OES analysis results is higher than that of EDX analysis results for nonhomogeneous samples. Given that zinc metal was unevenly distributed on the surfaces of the silica, our samples could be considered as nonhomogeneous samples. Therefore, the ICP–OES analysis results were more accurate than the EDX analysis results. Errors existed between the real and the theoretical metal contents obtained through ICP–OES and EDX analyses. These errors were mainly due to the impurity of the zinc metal because it increased with the metal content of the samples.

Table 4.4: EDX results for the bare calcinated SiO$_2$ and 0.5, 1, 2, 3, and 4% Zn/SiO$_2$.

Element	Line Type	Calcinated bare SiO$_2$ Wt%	0.5% Zn/SiO$_2$ Wt%	1% Zn/SiO$_2$ Wt%	2% Zn/SiO$_2$ Wt%	3% Zn/SiO$_2$ Wt%	4% Zn/SiO$_2$ Wt%
O	K series	49.44	49.82	50.80	52.71	41.13	54.13
Si	K series	50.56	49.72	48.27	45.41	55.98	42.20
Zn	L series	-	0.46	0.93	1.88	2.59	3.37
Total:	-	100.00	100.00	100.00	100.00	100.00	100.00

4.2.6 Hydrogen temperature programmed desorption (H$_2$-TPD)

Zn/SiO$_2$ was subjected to H$_2$-TPD analysis at various heating rates using different catalyst samples (0.5% Zn/siO$_2$, 1% Zn/siO$_2$, 2% Zn/SiO$_2$, 3% Zn/SiO$_2$, 4% Zn/SiO$_2$, and SiO$_2$) to investigate relative catalytic activities and to survey the effects of active metal loading and heating rates. As shown in Figures 4.4 and Figure 4.5, the area under the curve represents the amount of H$_2$ desorbed from the catalyst.

Anderson and Nichols (Anderson & Nichols, 1986) investigated the mechanism of hydrogen adsorption on zinc. According to their molecular orbital study, H_2 will adsorb heterolytically as Zn^{2+}—H^- + O_2—H^+ because of energy reasons (most stable state) and configurational reasons. Specifically, heterolytic Zn^{2+} and O^{2-} sites are adjacent and can participate in activating H_2, whereas homolytic Zn^{2+} and O^{2-} sites are widely separated and therefore provide no mechanism for H_2 dissociation. Adsorption is rapid and reversible at room temperature and yields two active species ascribed to surface Zn–H and O–H species (Howard et al., 1984; Tanaka et al., 1981).

As shown in Figure 4.4, H_2 uptake drastically increased with increasing heating rate (30 °C/min). Furthermore, the amounts of hydrogen desorbed from the catalysts increased with increasing amount of metal active sites (up to 3% Zn). This effect is a crucial factor for catalytic activity and indicates that Zn functions as the main metal active site. Figure 4.5 represents the H_2-TPD spectra of various catalyst samples at 30 ˚C/min heating rate. The small H_2 desorption peak exhibited by SiO_2 indicated its ability as a reducible support for H_2 desorption and activation. According to the literature, the reduction in H_2 capture in the 4% Zn/SiO_2 sample may be ascribed to the following mechanism: The high concentration of the active metal in 4% Zn/SiO_2 leads to catalyst aggregation. The catalyst aggregate has reduced selectivity due to its modified structure (the metal is now less accessible, or the ligand is deformed). High catalyst loading causes catalyst–catalyst interactions, such as electron transfer or ligand exchange, which cause catalyst decomposition or generate catalytically inactive species (Das & Deo, 2012; Gomes et al., 2018).

The desorption profiles of all samples, except for those of bare SiO_2 initiated at 400 °C, showed two to three distinct peaks at various temperatures (Table 4.5). The H_2-TPD

profile for 3% Zn/SiO$_2$ showed two high peaks associated with T$_{max}$ at 521 °C and 968 °C. The differences in the amount of spillover hydrogen associated with the active site are the main reason for the significant peaks (Hao et al., 2015). The bare SiO$_2$ profile presented a peak at 872 °C. Therefore, the desorption signal at 872 °C and high temperatures for all samples could be related to the result of surface hydroxyl dehydration. The H$_2$-TPD patterns in this study can be categorized into two regions by using 500 °C as the demarcation interval. The low-temperature desorption could be attributed to chemisorbed hydrogen on Zn, and the high-temperature desorption could be due to H$_2$ spillover from the oxide support to the metal (reverse spillover) (Shin-Kuan, W., 2013).
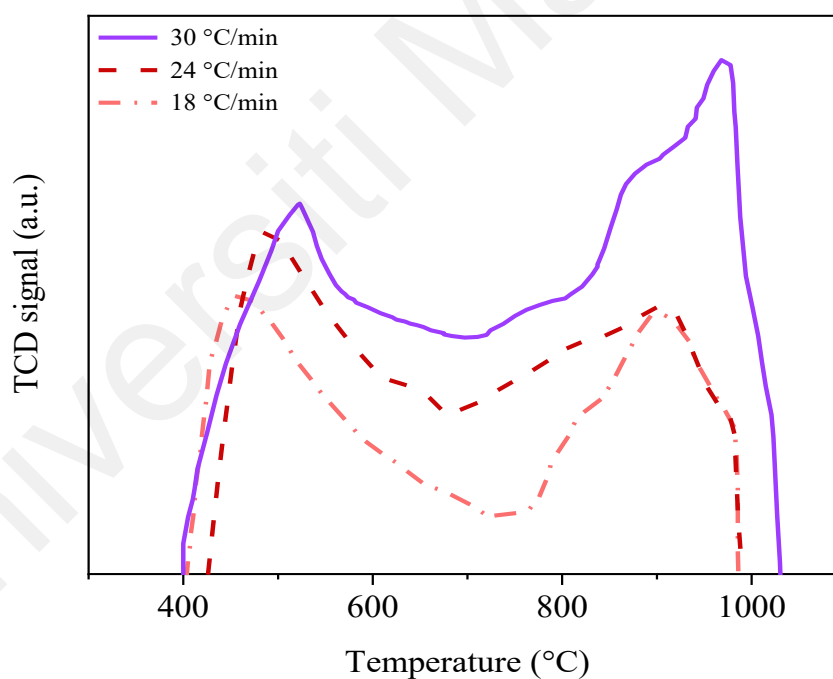
Figure 4.4: H$_2$-TPD spectra of 3% Zn/SiO$_2$ at various heating rates (18, 24, and 30 °C /min).
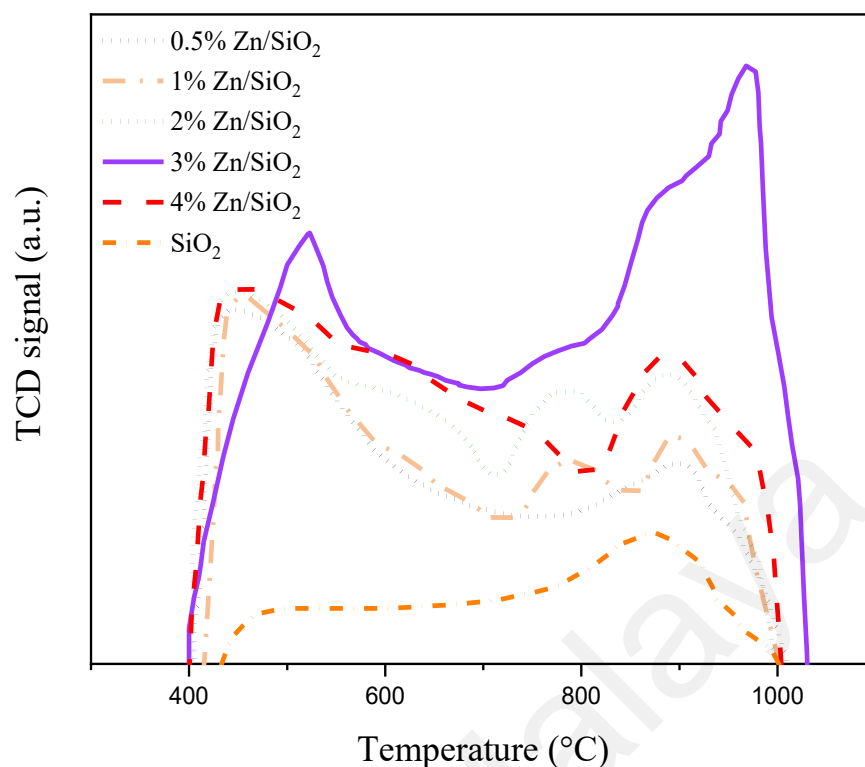
Figure 4.5: H_2-TPD spectra of various catalyst samples at 30 ˚C/min heating rate.

Table 4.5 shows the number of peaks and the peak temperatures for each catalyst and for 3% Zn/SiO$_2$ at various heating rates. As shown in Table 4.5, increasing the active metal loading caused peak temperature to shift to high temperatures. For example, the first peak temperatures for 0.5% and 3% loadings of the zinc were 446 °C and 521 °C, respectively. Furthermore, the elevation of the heating rate from 18 °C to 30 °C provided the same results. Readsorption adds a time increment of treads to the normal time it takes for a desorbing molecule to reach the detector. The elevation of the temperature peak by increasing the active metal loading or heating rate has been reported previously (Schittkowski et al., 2016).

Table 4.5. H_2-TPD analysis results for the catalysts.

Catalyst	Heating rate (°C)	Peak temperature (°C)		
		Peak 1	Peak 2	Peak 3
SiO_2	30	-	-	872
0.5% Zn/SiO_2	30	446	-	897
1% Zn/SiO_2	30	457-466	786	896
2% Zn/SiO_2	30	461	785	885
3% Zn/SiO_2	30	521	890	968
4% Zn/SiO_2	30	465	634	890
3% Zn/SiO_2	24	500	800	899
3% Zn/SiO_2	18	459	815	899

4.2.7 Ammonia temperature programmed desorption (NH₃-TPD)

According to the literature, the hydrodeoxygenation catalyst mainly consists of two functional parts, i.e., a redox component (metal) and acid sites (Yan et al., 2020; X. Zhang et al., 2018; X. Zhu et al., 2011). A synergy of these two components facilitates the hydrogenation and hydrogenolysis processes. Figure 4.6 represents NH₃-TPD profile of the catalysts. It can be observed that all samples absorb NH₃ in a wide temperature range of 100-800 ℃. It can be seen from Table 4.6 and Figure 4.6 that after the 0.5% - 4% Zn were loaded on SiO_2, the total acidity of catalysts is clearly elevated and an increase of the area of NH₃ desorption peak can be observed. Moreover, comparing the desorption peak temperature of the samples, the position of NH₃ desorption peak temperatures have been increased by elevating the zinc doping to the samples. This should be attributed to the interaction and substitution of proton sites on SiO_2 surface structure with the doping zinc metal, resulting in the regeneration of new proton sites on the catalyst. As Table 4.6

indicates, the acidity was significantly increased from 0.108 to 0.490 mmol/g within the increase in zinc loading amount from 0% to 4%. According to Kernajanakon et.al., (2016), loading the optimum amount of active site on the support is crucial and is from 1 to 2.5%. By increasing the loading amount such as 5 and 10%, the acidity of the catalysts decreases due to the covering of acid sites by the generated ZnO cluster. Furthermore, the authors implied that the metal dispersion efficiency on the support could be influenced by the metal loading amount.
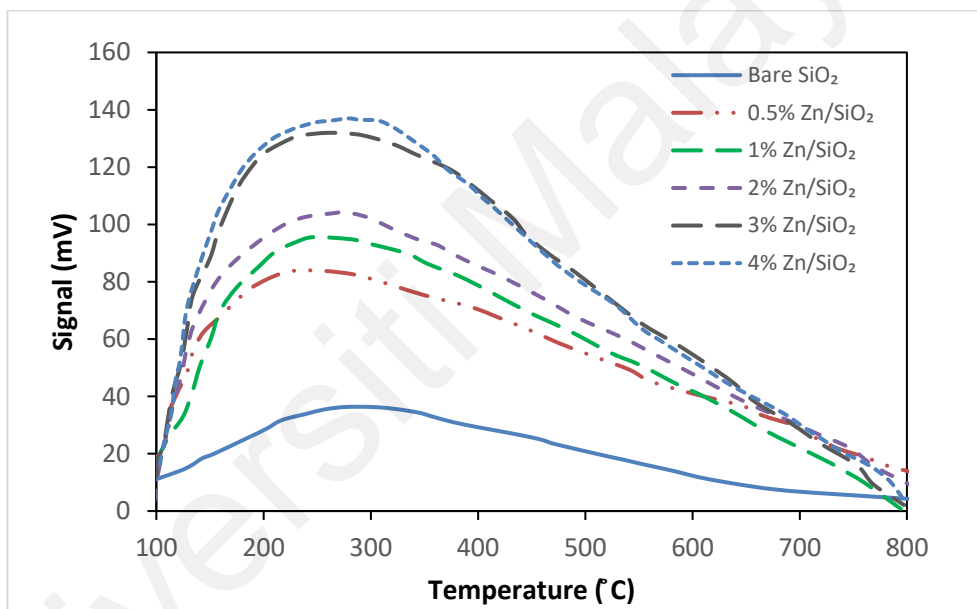
Figure 4.6: NH$_3$-TPD profile of 0.5% Zn/SiO$_2$, 1% Zn/SiO$_2$, 2% Zn/SiO$_2$, 3% Zn/SiO$_2$, 4% Zn/SiO$_2$, and bare SiO$_2$.

Table 4.6: Acidity results of the bare SiO_2 and Zn-doped catalysts.

Catalyst (Nominal Loading)	Acidity of Catalyst (mmol/g)
Bare SiO_2	0.108
0.5% Zn/SiO_2	0.357
1% Zn/SiO_2	0.370
2% Zn/SiO_2	0.422
3% Zn/SiO_2	0.481
4% Zn/SiO_2	0.490

4.2.8 Thermogravimetry (TGA)

The samples were analyzed with TGA analysis in the air in order to determine the extent of the water and organic compounds and their weight loss was recorded as a function of temperature. TGA results of the samples are presented in Figure 4.7. In all cases, the weight loss occurred up to 100℃ which is mainly due to the humidity. As it can be observed from Figure 4.7, Bare SiO_2 has around 2% weight loss whilst the calcinated metalized samples have minor one (less than 1%). This specifies that by loading the support by zinc metal, less humidity can be absorbed and then has lower weight loss during the HDO experiments. No high temperature weight loss has been monitored in TGA analysis which represents that the samples have no organic carbon impurity.
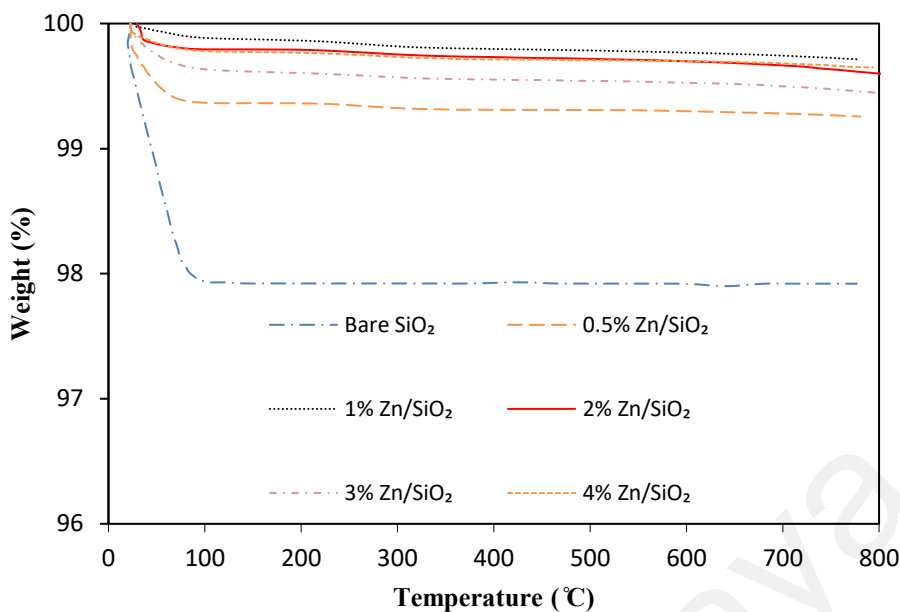
Figure 4.7: Thermogravimetric analysis for the samples as a function of Temperature.

4.2.9 Hydrogen temperature programmed reduction (H₂-TPR)

The reducibility of the silica-supported zinc catalysts was investigated through H_2-TPR (Figure 4.8). The control experiments of the bare support (silica) revealed that the silica did not show any considerable H_2 consumption in the range of 300 °C–700 °C (not shown in Figure 4.8). Consequently, the detected maximum temperature (T_{max}) of H_2 consumption for the samples can be ascribed to the dispersed zinc on the silica surface. The lowest T_{max} (448 °C) was observed for the catalyst with 0.5% zinc loading. The reduction temperature of the catalysts steadily increased with increasing zinc loading likely because of the increase in the crystallite sizes of the catalysts. The XRD results indicated that large Zn crystallites were present on the samples with high zinc loading. Consequently, the 4% Zn/SiO₂ catalyst presented the highest T_{max} among all other samples (530 °C); this finding is in agreement with the aforementioned XRD results.
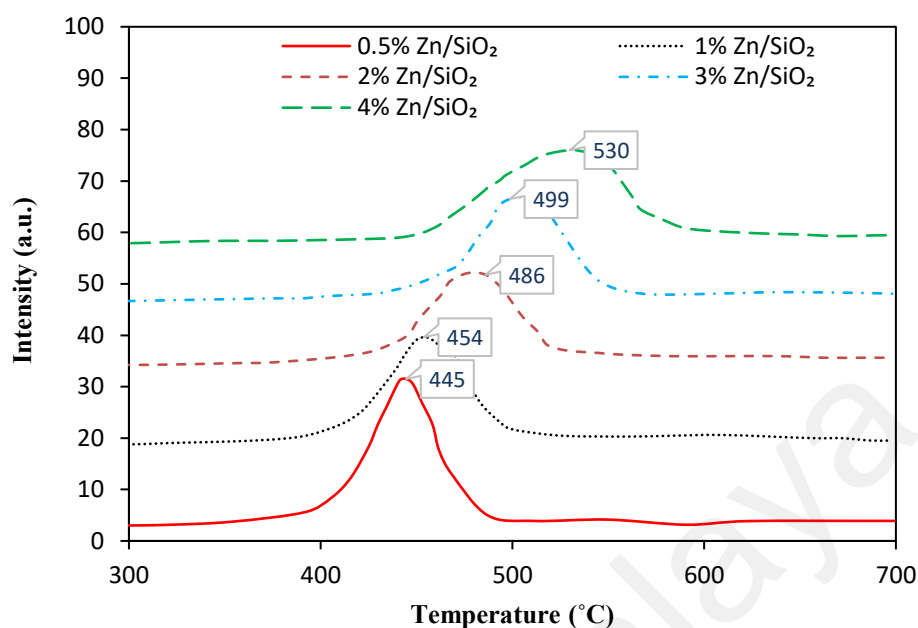
Figure 4.8: H$_2$-TPR profiles of the 0.5% Zn/SiO$_2$, 1% Zn/SiO$_2$, 2% Zn/SiO$_2$, 3% Zn/SiO$_2$, and 4% Zn/SiO$_2$ catalysts.

4.2.10 Topography of the catalysts using FESEM analytical method

Figures 4.9, 4.10, 4.11, and 4.12 represent FESEM images of the bare SiO$_2$, 1% Zn/SiO$_2$, 3% Zn/SiO$_2$, and 4% Zn/SiO$_2$. The micrograph of the bare SiO$_2$ displays large slab shaped particles covered with clumps of SiO$_2$ nanoparticles. As it can be depicted from micrographs 4.8, 4.9, and 4.10, the white spots become more densely colonized and even some of the particles were agglomerated on the surface of the support as the Zn loading was increased to 4% which led to poor dispersion of the Zn over the support. Extra micrographs for the selected catalysts in various magnifications can be find in Appendix A.4.
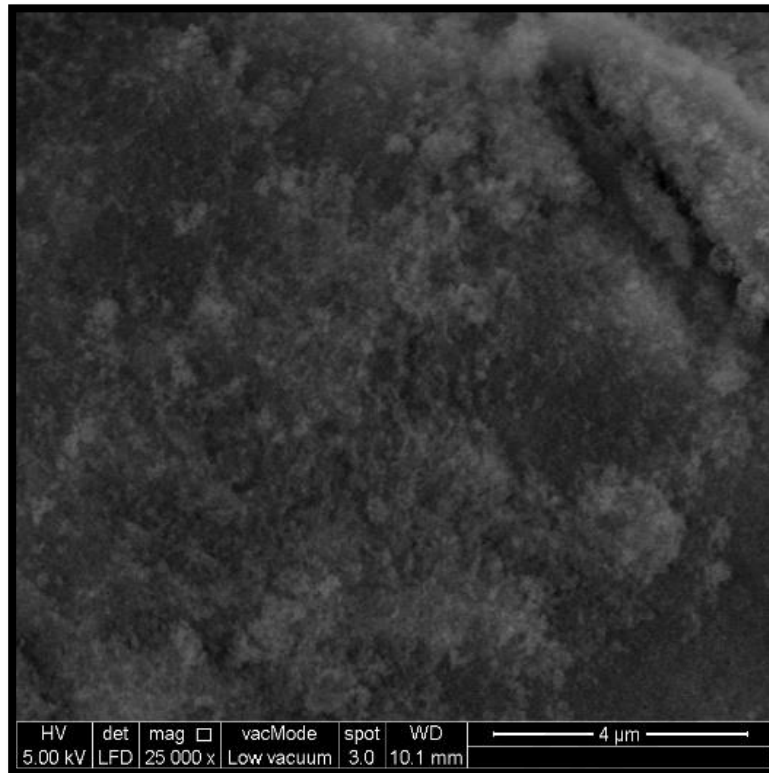
Figure 4.9: FESEM image for bare SiO$_2$.
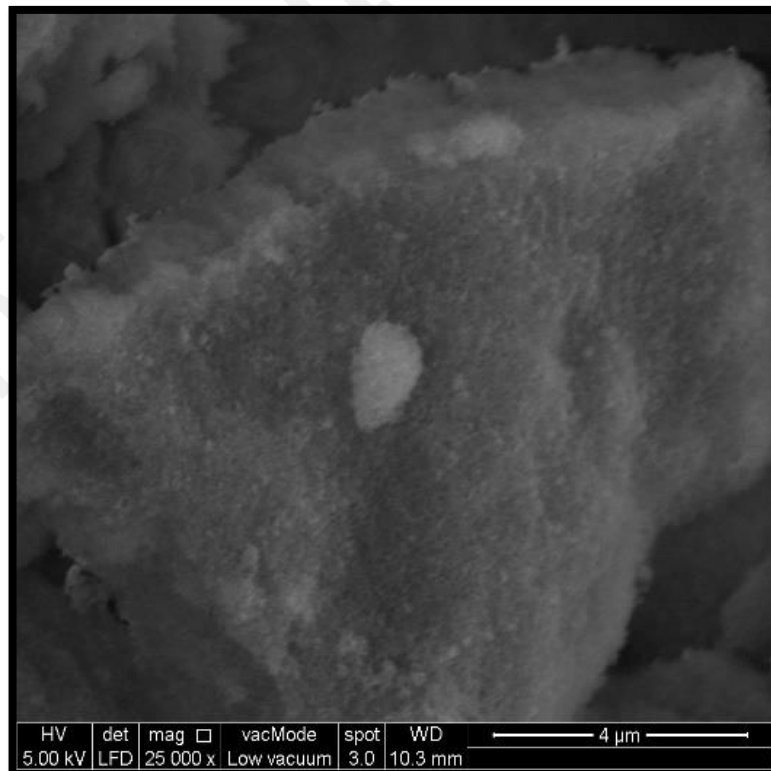
Figure 4.10: FESEM image for 1% Zn/SiO$_2$.
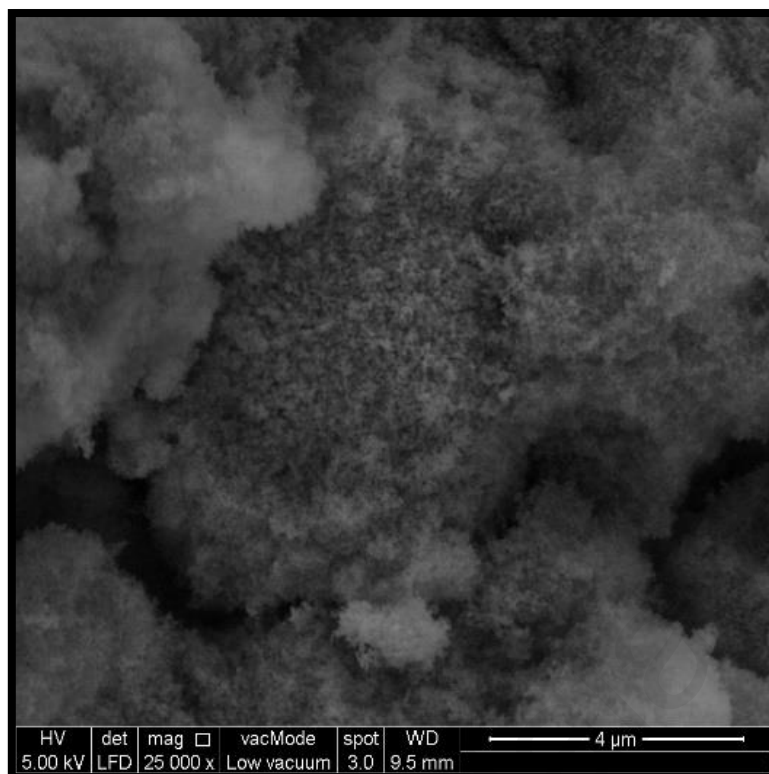
Figure 4.11: FESEM image for 3% Zn/SiO$_2$.
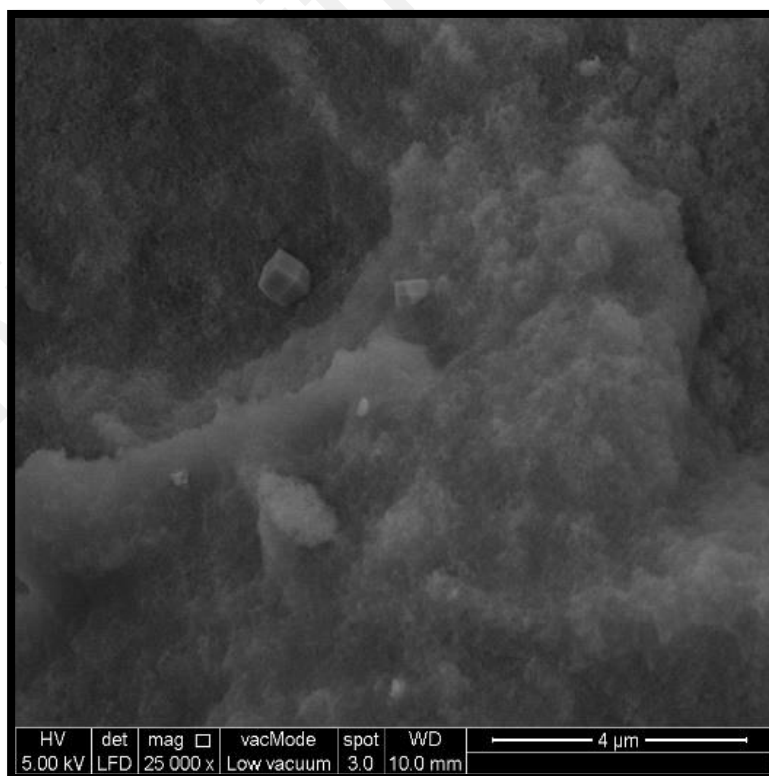
Figure 4.12: FESEM image for 4% Zn/SiO$_2$.

4.3 Effect of process parameters on atmospheric HDO of phenol

The effects of process parameters including zinc load, reaction temperature, WHSV, and H_2 volumetric flow rate were investigated. The WHSV (WHSV = $g_{\text{phenol in the feed per hour}}/g_{\text{catalyst}}$) was changed by the variation in catalyst mass. Details for WHSV calculation can be find in Appendix B.2. The following sections elaborate on the influence of each parameter on conversion efficiency and product selectivity. Several preliminary experiments revealed that the reaction with the supports (SiO_2) alone showed low conversions (<3%), demonstrating that the reactivity of the silica-supported zinc catalysts can be ascribed to metallic zinc and $Zn–SiO_2$ interactions. All the experiments were performed in triplicate, and each tabulated experimental result is the mean of three different replicate experiments.

4.3.1 Chemical compounds characterization and standardization

Before running the experiment samples, preliminary runs were performed in order to find out the run time of each component include acetone (as solvent for GC-FID), phenol, benzene and n-decane. Furthermore, standard curves were prepared for phenol and benzene to find the quantity of the components.

Table 4.7 shows the run time for each component on each applied method in this study. According to the results from each method, all methods can detect the main four components in this study (Acetone, phenol, n-decane, and benzene). However, standard method 8014 A is unable to quantify the benzene in different concentrations. In modified method I, the oven initial temperature has decreased from 80 ˚C to 40 ˚C and initial holding time increased to 2 minutes. Furthermore, the temperature ramp has been increased from 6 ˚C/min to 10 ˚C/min to faster reach the highest set point of the temperature. Upgrading to this method was resulted to quantifying the benzene, but

phenol and n-decane were faced with the same problem of benzene in previous method. In the other words, the amount of n-decane and phenol cannot be detected using modified method I. To solve this problem, modified method II has been created. In this method, the holding time has been increased to 3 minutes from 2 minutes and the temperature ramp increased to 30 ˚C/min from 10 ˚C/min. Also, the maximum temperature was set to 150 ˚C. Using the modified method II, all components have individual run time peak and also can be quantified in different concentration. Appendix B.3 represent the standard curve for phenol, benzene, n-decane, cyclohexane and cyclohexene respectively.

Table 4.7: Run time for each component in each gas chromatography method.

No.	component	Run time		
		Method 8014 A	**Modified method I**	**Modified method II**
1	Acetone	2.349	2.80-2.83	2.94
2	Benzene	2.60	3.04	3.1
3	Cyclohexene	-	-	3.3
4	Cyclohexane	-	-	3.6
5	n-decane	2.96	5.68	5.24
6	Phenol	3.053-3.134	7.08 – 7.72	6.60

4.3.2   Effect of active site (zinc) loading

Figure 4.13 represents the results for the effect of zinc metal loading on the catalyst support for the HDO of phenol (the lines between points are for following the experimental results and do not represent the reaction path). As shown in Figure 4.13, all the catalysts could convert phenol, indicating that this catalyst is active in this process. The conversion efficiency of phenol using xZn/SiO$_2$, with 0.5% - 3% zinc metal loading as the active site, varied from 15% to 80%, respectively (Pourzolfaghar, Abnisa, Daud, et

al., 2020). Table 4.8 represents the data obtained by GC/FID analysis. By increasing the active site loading from 0.5% to 3%, the overall conversion of phenol increased, and the maximum conversion was obtained with 3% loading. By further increasing the zinc loading, the overall conversion slightly decreased. This result indicated that 3% loading was the best amount of zinc metal to be loaded on the catalyst support (SiO_2). The slight reduction in the conversion efficiency on 4% Zn/SiO_2 was related to the occupation of catalyst pores by active metals; this phenomenon decreased the conversion of phenol (De Waele et al., 2018). From the selectivity perspective, the loading of active metals lacked a considerable influence on product selectivity, and the selectivity for the cyclohexane, cyclohexene, and benzene were almost the same. The only exception is the 0.5% loading of Zn, wherein benzene was not detected in the product. Although some benzene was generated, it most likely reduced to generate the cyclohexene and cyclohexane.
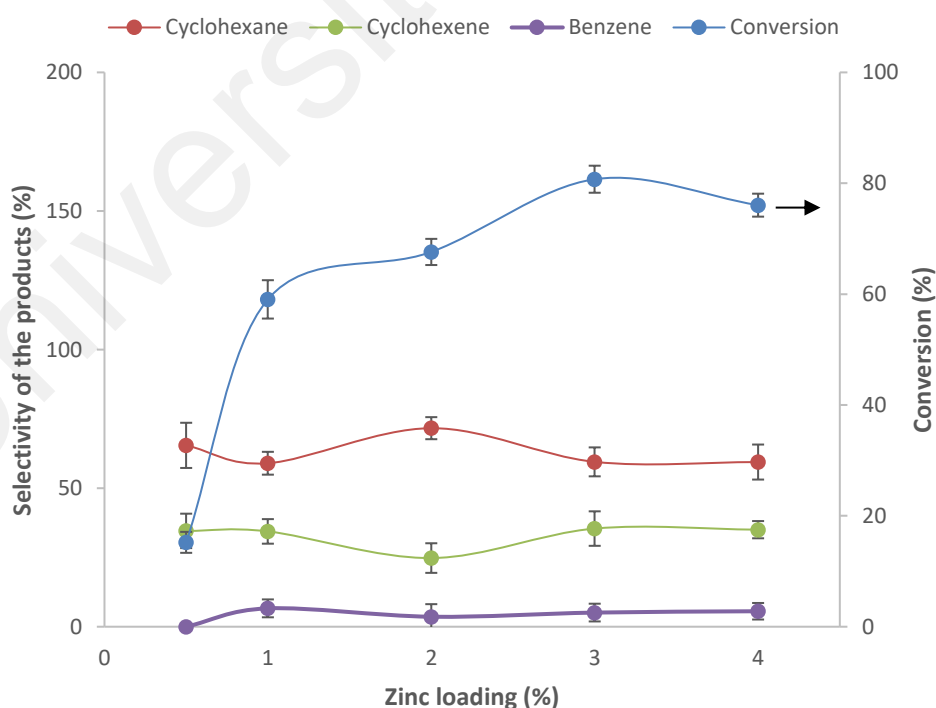
Figure 4.13: Effect of zinc loading on product selectivity and overall conversion efficiency.

Table 4.8: Experimental conditions, conversion efficiency, and selectivity of the products for HDO of phenol in atmospheric H_2 pressure using various loadings of zinc as the active site on the silica surface.

Catalyst	Feed flow rate (mL/min)	WHSV (h^{-1})	H_2 volumetric flow rate (mL/min)	Temp (°C)	Conversion of phenol (%)	Selectivity		
						Benzene	Cyclohexene	Cyclohexane
0.5% Zn/SiO$_2$	0.5	0.32	150	500	15.22	0	34.57	65.43
1% Zn/SiO$_2$	0.5	0.32	150	500	59.05	6.62	34.40	58.98
2% Zn/SiO$_2$	0.5	0.32	150	500	67.61	3.60	24.78	71.62
3% Zn/SiO$_2$	0.5	0.32	150	500	80.73	6.10	25.42	68.48
4% Zn/SiO$_2$	0.5	0.32	150	500	76.05	5.58	35.01	59.41

4.3.3 Effect of reaction temperature

Table 4.9 provides the process conditions for investigating the effect of temperature on the HDO of phenol and the selectivity and efficiency of the products. All the conditions, except for temperature, remained fixed. The temperature was varied from 200 °C – 600 °C. Figure 4.14 depicts product evolution as a function of temperature. The upsurge in the phenol conversion and efficiency of the HDO was consistent with the increase in temperature from 200 °C to 500 °C. Studies have also acknowledged that 500 °C is the best temperature for the conversion of lignin-based oxygenated components, such as lignin, phenol, anisole, and m-cresol (Ausavasukhi et al., 2012; R. N. Olcese et al., 2012a; X. Zhu et al., 2011). The H_2-TPR analysis results also confirmed that the most appropriate temperature for desorption of the H_2 species is 500 °C.
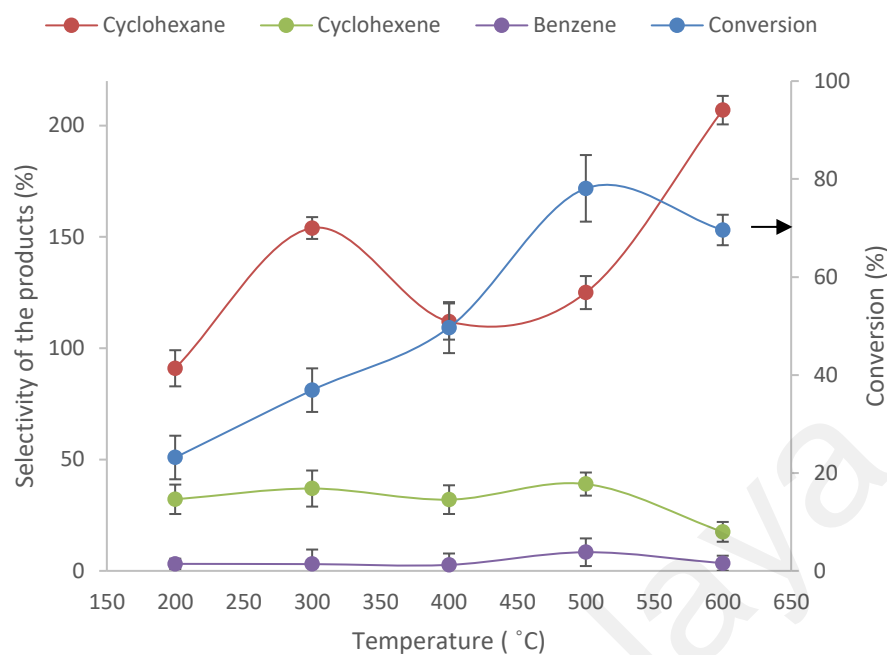
Figure 4.14: Effect of reaction temperature on process products and overall conversion efficiency.

Table 4.9: Experimental conditions, conversion efficiency, and selectivity of the products for HDO of phenol in atmospheric H_2 pressure using various reaction temperatures.

Catalyst	Feed flow rate (mL/min)	WHSV (h^{-1})	H_2 volumetric flow rate (mL/min)	Temp (°C)	Conversion of phenol (%)	Selectivity		
						Benzene	Cyclohexene	Cyclohexane
3% Zn/SiO$_2$	0.5	0.32	150	200	23.15	3.15	25.29	71.57
3% Zn/SiO$_2$	0.5	0.32	150	300	36.90	3.05	18.77	78.18
3% Zn/SiO$_2$	0.5	0.32	150	400	49.67	2.70	21.62	75.68
3% Zn/SiO$_2$	0.5	0.32	150	500	78.10	5.19	24.98	69.83
3% Zn/SiO$_2$	0.5	0.32	150	600	69.60	3.44	7.54	89.02

By increasing the temperature from 500 °C to 600 °C, the selectivity of the cyclohexane increased, whereas the total volume of the products decreased (Figure 4.15).

The contents of phenol and other components were measured using GC–FID analysis. At 600 °C , the thermal decomposition of phenol resulted in the formation of solid carbonaceous materials (coke) as a result of radical recombination and/or polymerization reactions (Y. Wang et al., 2013). The product volume decreased by approximately 10% at 200 °C, 300 °C, and 400 °C. Nevertheless, at 500 °C, the product volume decreased by 30%. At 600 °C, only 5.6% of the product was recovered, and 94.4% was converted into coke. Therefore, despite the increased selectivity at 600 °C, this temperature is an unacceptable range because the formation of coke is a serious problem in the upgrading or processing of bio-oil. Coke deactivates the catalysts for bio-oil upgrading and plugs the downstream equipment of gasification systems.
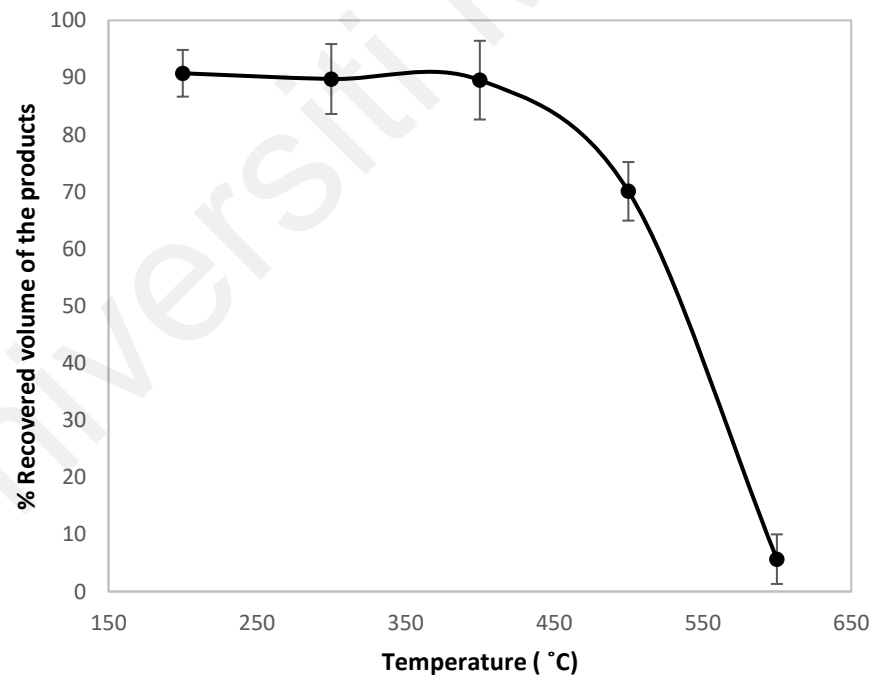
Figure 4.15: Volume of the recovered products at various operation temperatures.

4.3.4 Effect of Weight Hourly Space Velocity (WHSV)

The data illustrating Zn/SiO_2-catalyzed phenol conversion at various values of WHSV are displayed in Figure 4.16. High space velocities led to the low overall conversion of phenol into products with low/no oxygen molecules because of the reduced residence time of the reactants in the reactor. However, the selectivity of products persisted with increasing WHSV. Therefore, the WHSV affected only the conversion of phenol without significantly disturbing the selectivity of the products. Table 4.10 represent the experimental conditions, conversion efficiency, and selectivity of the products using various weight hourly space velocity (WHSV). As it can be observed from Table 4.10, in order to have various WHSV values, the feed flow rates were varied from 0.5 mL/min to 1.4 mL/min. The amount of the catalyst (1 g) was fixed during the experiments. By elevating the WHSV value, the conversion efficiency of the HDO reaction decreased continuously. The highest conversion efficiency belongs to the test with WHSV of 0.32 h^{-1} and the lowest, as expected, belongs to the experiment with WHSV of 0.89 h^{-1}. The selectivity of cyclohexane was varied from 59.10% to 69.22% which were belong to the highest and lowest WHSV values, respectively.
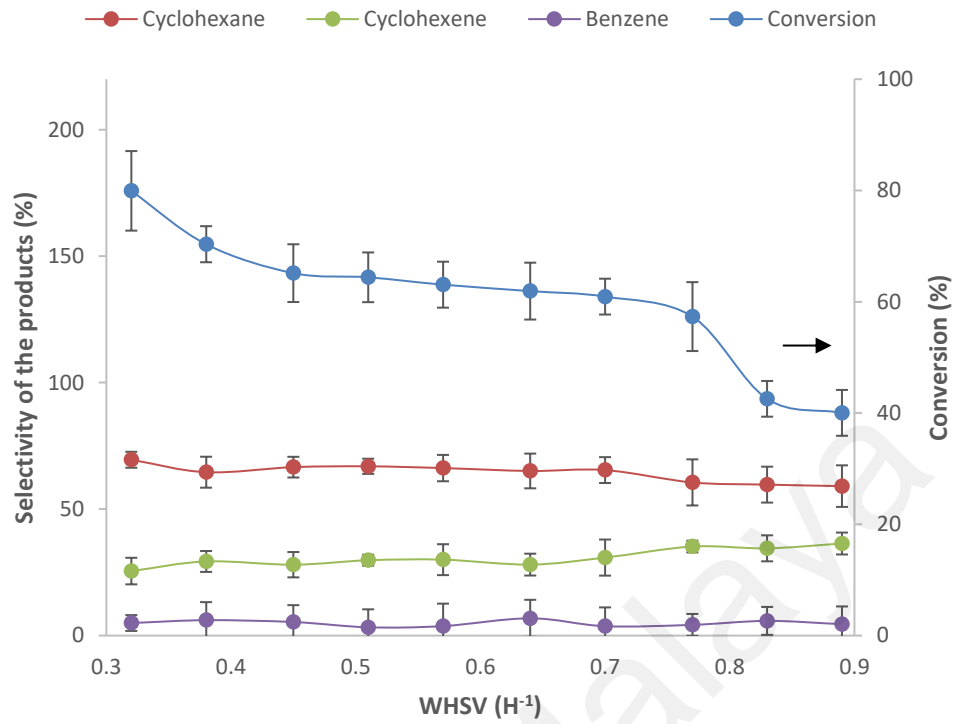
Figure 4.16: Conversion of phenol catalyzed by 3% Zn/SiO$_2$ at various values of WHSV.

Table 4.10: Experimental conditions, conversion efficiency, and selectivity of the products for HDO of phenol in atmospheric H_2 pressure using various weight hourly space velocity (WHSV).

Catalyst	Feed flow rate (mL/min)	WHSV (h^{-1})	H_2 volumetric flow rate (mL/min)	Temp (°C)	Conversion of phenol (%)	Selectivity		
						Benzene	Cyclohexene	Cyclohexane
3% Zn/SiO$_2$	0.5	0.32	150	500	79.93	4.97	25.51	69.52
3% Zn/SiO$_2$	0.6	0.38	150	500	70.34	6.09	29.31	64.60
3% Zn/SiO$_2$	0.7	0.45	150	500	65.14	5.37	28.03	66.60
3% Zn/SiO$_2$	0.8	0.51	150	500	64.39	3.28	29.79	66.93
3% Zn/SiO$_2$	0.9	0.57	150	500	63.07	3.75	30.02	66.23
3% Zn/SiO$_2$	1	0.64	150	500	61.91	6.84	28.08	65.10
3% Zn/SiO$_2$	1.1	0.70	150	500	60.92	3.71	30.85	65.44
3% Zn/SiO$_2$	1.2	0.77	150	500	57.33	4.24	35.20	60.56
3% Zn/SiO$_2$	1.3	0.83	150	500	42.55	5.81	34.50	59.69
3% Zn/SiO$_2$	1.4	0.89	150	500	40.03	4.51	36.40	59.10

4.3.5   Effect of H$_2$ volumetric flow rate

The effect of hydrogen volumetric flow rate on conversion and yield was investigated at 500 °C with the feed flow rate of 0.5 mL/min; WHSV (h^{-1}) of 0.32; and H$_2$ flow rates of 0, 150, 300, 600, and 900 mL/min (Figure 4.17 & Table 4.11). The conversion of phenol on 3% Zn/SiO$_2$ in the absence of hydrogen differed noticeably from that in any hydrotreatment methods, evidencing the role of hydrogen in the reaction. The phenol conversion rate was 30.24% in the absence of H$_2$ and was 79.93% at 150 ml/min H$_2$ flow. In the absence of hydrogen, almost no HDO products were trapped (except about 11% of cyclohexen + cyclohexane). Polycyclic aromatic hydrocarbons (PAH) are the main

products given that the key role of H_2 in HDO is to reduce the formation of coke precursors (PAH from phenol conversion) (R. N. Olcese et al., 2012b).

However, the effect of hydrogen became negligible under the H_2 flow rate of 150–900 mL/min. This result indicated that hydrogen adsorption on the surface of the catalyst had reached saturation. The slight variation in the yields of products including benzene, cyclohexene, and cyclohexane indicated that the selectivity of the products is independent of hydrogen concentration; this result is consistent with previously reported results (E.-J. Shin & Keane, 1998).
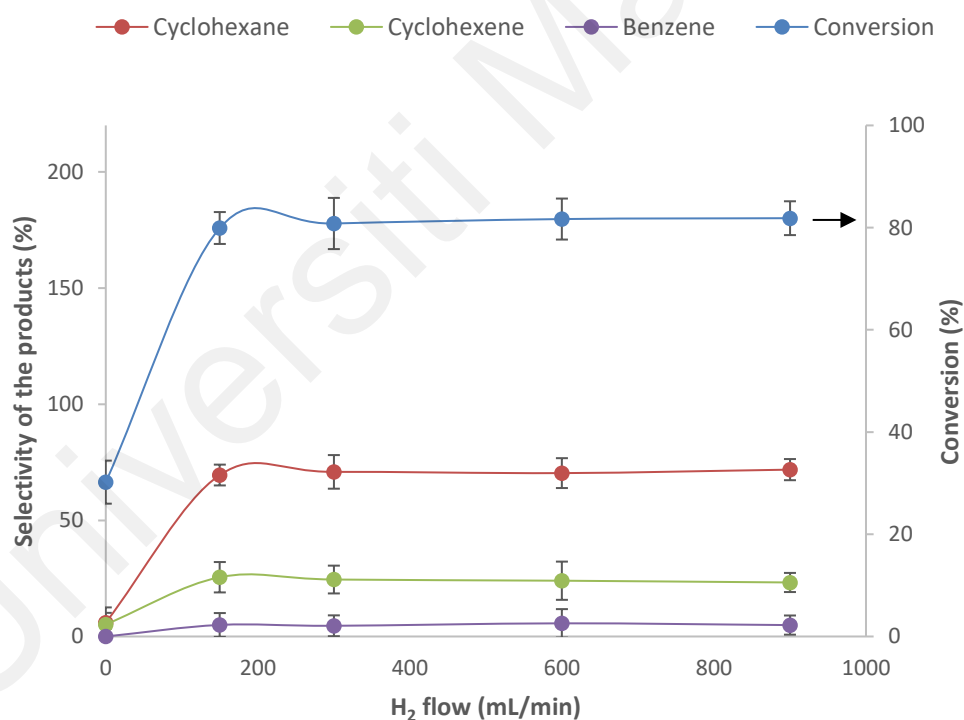
Figure 4.17: Effect of H_2 flow rate on product conversion and selectivity.

Table 4.11: Experimental conditions, conversion efficiency, and selectivity of the products for HDO of phenol in atmospheric H_2 pressure using various hydrogen volumetric flow rate.

Catalyst	Feed flow rate (mL/min)	WHSV (h⁻¹)	H₂ volumetric flow rate (mL/min)	Temp (°C)	Conversion of phenol (%)	Selectivity		
						Benzene	Cyclohexene	Cyclohexane
3% Zn/SiO₂	0.5	0.32	0	500	30.24	0	5.2	6
3% Zn/SiO₂	0.5	0.32	150	500	79.93	4.96	25.51	69.52
3% Zn/SiO₂	0.5	0.32	300	500	80.81	4.60	24.53	70.86
3% Zn/SiO₂	0.5	0.32	600	500	81.68	5.66	24.01	70.32
3% Zn/SiO₂	0.5	0.32	900	500	81.85	4.91	23.26	71.83

4.4 Stability, regenerability and mechanism of the reaction

4.4.1 Stability of the catalysts

The catalyst with higher reactivity, 3%Zn/SiO$_2$, was selected for the stability studies of phenol HDO. The conversion of phenol was calculated based on collected reaction data at different time-on-stream (TOS) up to 600 min to identify the variation of catalytic activity with TOS as shown in Figure 4.18. As it can be illustrated from the Figure, the catalyst was highly active up to 240 min with a minor decrease inactivity. After that, the catalyst activity was decreased gradually with increasing TOS. After about 340 min of TOS, a variation of conversion was found to be insignificant and was around 43% up to 600 min. Moreover, the variation of selectivity of major products was also insignificant after 420 mins of TOS. In terms of the selectivity of the products, after 420 min TOS, the selectivity of the cyclohexane slightly decreased with a minor increase in the selectivity on cyclohexene. Henceforth, from the stability results, it could be concluded that the

Silica supported zinc with 3% loading is highly active until 340 min and after that it must be replaced or regenerated (Pourzolfaghar, Abnisa, Wan Daud, et al., 2020).
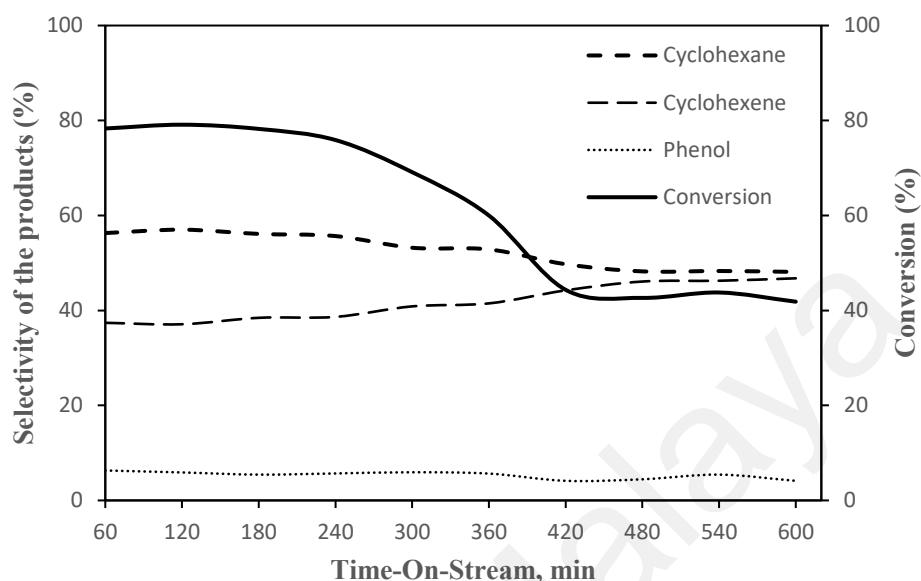
Figure 4.18: Variation of activity and selectivity of major products for HDO of phenol with TOS. Catalyst 3%Zn/SiO$_2$; Temperature 500 ℃; pressure 1 atm; WHSV (h^{-1}) 0.32; feed flow rate (mL/min) 0.5; and H$_2$ volumetric flow rate (mL/min) 150.

4.4.2   Regenrability of the catalysts

The applied catalyst for the stability test has been used for reusability study. The spent catalyst was regenerated by calcination at 500 ℃ for one hour under the air atmosphere after each cycle. The freshly calcinated sample was then examined by the HDO of phenol. This procedure was continued until four cycles of regeneration. Figure 4.19 represents the results of the regeneration study. As it can be perceived from the Figure, the catalyst has been recovered fully and had almost the same results as the fresh catalyst in its first and second regeneration steps. In the third and fourth cycles of regeneration, the conversion efficiency of the catalyst has been eliminated. The main reason for eliminating the phenol conversion efficiency after the third regeneration cycle might be because of coking and occupying the pores of the support.
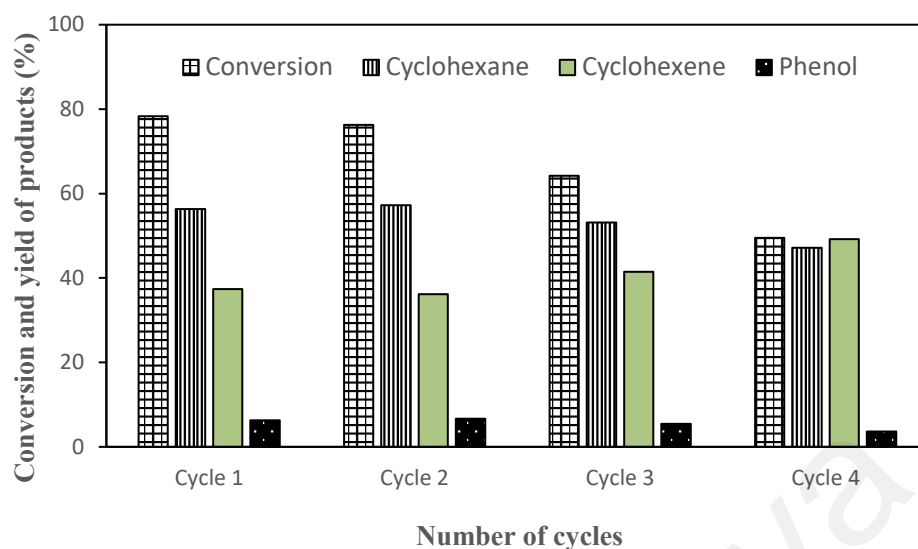
Figure 4.19: Catalyst reusability study showing the conversion and yield of products for hydrodeoxygenation of phenol over 3%Zn/SiO$_2$. Temperature 500℃; pressure 1 atm; WHSV (h^{-1}) 0.32; feed flow rate (mL/min) 0.5; and H$_2$ volumetric flow rate (mL/min) 150.

4.4.3   Mechanism of the reaction

Consistent with studies on pathways for the phenol conversion during HDO, two important routes were reported (Figure 4.20) (Boullosa-Eiras et al., 2014; Bu et al., 2012; Echeandia et al., 2010; C. Zhao et al., 2011). The initial route is based on hydrogenation domination, and the second is based on hydrogenolysis. Route 1 progresses through the stepwise hydrogenation of the aromatic ring to generate cyclohexanone as the principal product. Cyclohexanol is generated as a secondary product through the additional hydrogenation of cyclohexanone (a ketone). Hydrogenolysis results in cyclohexene formation and oxygen removal. Moreover, cyclohexane, methylcyclopentane, and n-hexane may form during additional hydrogenation.

The second route is instigated by the direct hydrogenolysis of the phenol's C–O bond to form benzene as the primary product. In the initial stage, oxygen is removed. Cyclohexene forms through hydrogenation. A series of reactions would ensure through

the formation of cyclohexane, methylcyclopentane, and/or n-hexane (Bu et al., 2012; Deutsch & Shanks, 2012; Echeandia et al., 2010; Massoth et al., 2006). The crucial impact of experimental conditions and catalyst type on the reaction mechanism route has been acknowledged by numerous studies. Although Route 2 is classically preferred in cases wherein noble metals, such as sulfided NiMo catalysts (Nie, 2014), are used (Wildschut et al., 2010; C. Zhao et al., 2009), Route 1 is preferred when considering sulfided CoMo catalysts (Gevert et al., 1987). Moreover, Route 1 is highly preferred for low pressures and high temperatures (E. J. Shin & Keane, 2000). Route 1 is the appropriate mechanism for this process given the presence of benzene in the products; the absence of cyclohexanone and cyclohexanol in the products (not detected by GC/MC in preliminary tests); and the use of nonnoble metal catalysts (xZn/SiO$_2$), atmospheric pressure, and high temperature.
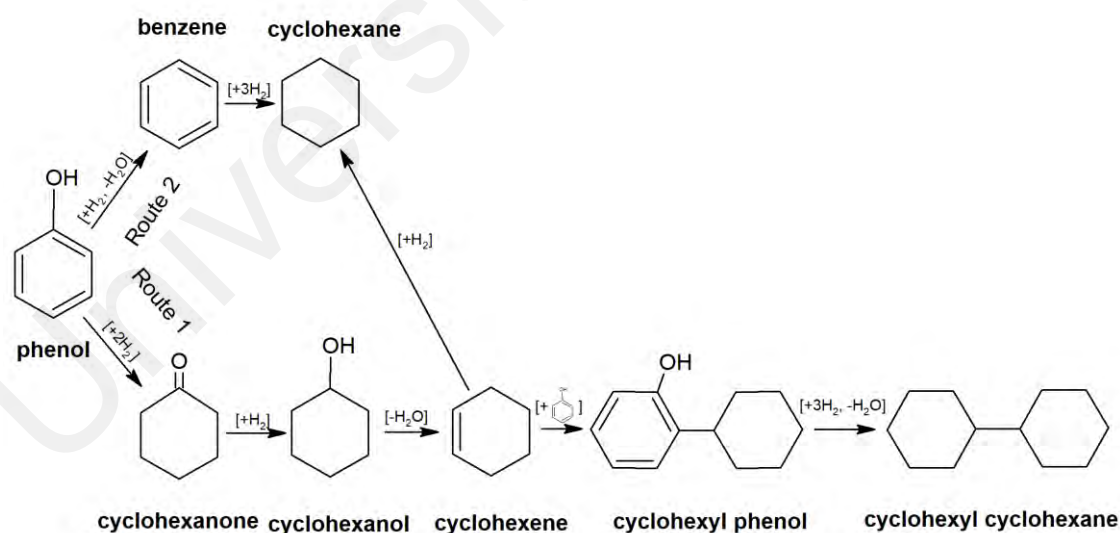
Figure 4.20: Possible reaction mechanisms for the HDO of phenol.

Figure 4.21 represent a schematic for reaction mechanism of HDO of phenol on Zn/SiO$_2$ and the phenol adsorption on the catalyst surface.
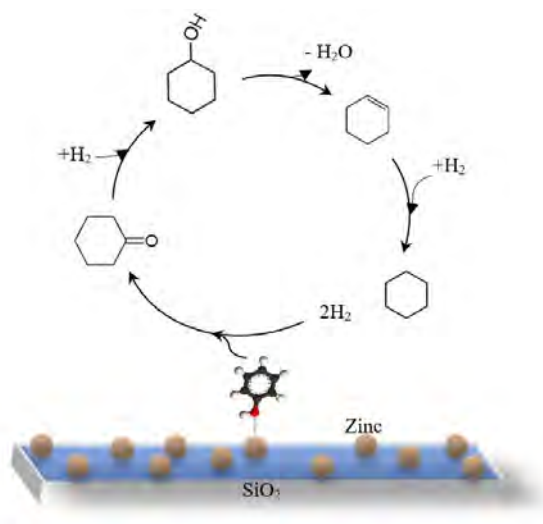
Figure 4.21: A schematic for reaction mechanism of HDO of phenol on Zn/SiO₂.

4.5 Discussion

4.5.1 Overview of the characterization studies

The catalyst characterization studies along with topography analysis of the samples revealed that the zinc metal is a promising active site to be applied for hydrodeoxygenation of oxygenated compounds such as phenol. It also revealed that the physicochemical properties of zinc-supported catalysts depended on their active site content. The incorporation of zinc as an active site over SiO_2 mostly involved the filling of pores with zinc, which occupied up to 6.58% of the surface area, according to the BET results. High surface area and large porosities of the samples, analyzed by N_2-adsorption analysis, make the surface reactions possible during the HDO process. XRD analysis revealed that the comparable degrees of crystallinity and slight peak broadening of all XRD diffractograms are indicative of insignificantly transformation of the crystallinity of the samples.

Thermogravimetry analysis exposed that the silica-supported zinc catalysts are highly stable at high temperatures up to 800 ˚C, which is a key factor for a catalyst to be applied for HDO reactions at high reaction temperatures. Significant H_2 consumption of the samples in the range of 400 – 550 ˚C explored by H_2-TPR proved that the catalysts have decent reducibility due to the zinc metal. Furthermore, as it can be perceived from Figure 4.8, all the samples have one broad peak, which is representative of the one-step reduction of the active metal. H_2-TPD analysis demonstrated that all samples are able to completely desorb the hydrogen molecules which is a critical factor for a catalyst to be applied in an industrial scale. Furthermore, this effect is a crucial feature for catalytic activity and indicates that Zn functions as the main metal active site. Based on the literature (Karnjanakom et al., 2016), the surface acidity of a catalyst plays an important role in the reactivity and selectivity of the HDO reactions. In other words, higher acidity results in a

higher conversion efficiency and selectivity of the products. NH_3-TPD analysis proved that the total acidities of the samples were in the range of 0.108–0.490 mmol/g. Elevating the active site doping resulted in a higher value for the total acidity, and the sample with 4% of Zn represented the highest surface acidity of 0.490 mmol/g. The topography analysis micrographs (Figure 4.10 and 4.11) of the selected samples (1% and 3%) showed no sign of agglomeration of the zinc metals on the silica surface. Agglomeration is an imperative reason for a reduction in conversion efficiency (Huynh et al., 2016).

4.5.2 Optimization study

Along with the characterization analysis, reactivity analysis revealed that the highest conversion efficiency could be achieved using the sample with 3% metal loading (80%), which was predictable based on the finding from characterization studies. Table 5.1 shows all independent process variables (zinc load, reaction temperature, WHSV, and H_2 volumetric flow rate) and their conversion efficiencies in different ranges. Furthermore, the amount of phenol in the reactor per minute ($q_{phenol,in}$) as well as the amount of phenol out of the reactor per minute ($q_{phenol, out}$) in mol, have been calculated and furnished in the Table 5.1.

The OFAT (one factor at a time) methodology or monothetic analysis has been used to design the testing of the independent factors. In the first step, the effect of the active site loading has been studied. According to the results, the sample with 3% active site, represented the highest conversion efficiency up to 80%. Elevating the active metal loading resulted in diminishing of the conversion efficiency, which based on the characterization results, it was predictable. According to the literature, the slight reduction in the conversion efficiency was related to the occupation of catalyst pores by active metals; this phenomenon decreased the conversion of phenol (De Waele et al., 2018). The

occupation of the catalyst pores can be observed in Figure 4.12, the micrograph of 4% Zn/SiO_2 catalyst.

Table 4.12: Experimental conditions and results.

Catalyst	Feed flow rate (mL/min)	WHSV (h^{-1})	H_2 volumetric flow rate (mL/min)	Temp (˚C)	Conversion of phenol (%)	$q_{phenol,in}$ mol/min	$q_{phenol,out}$ mol/min
Effect of the zinc load							
0.5% Zn/SiO_2	0.5	0.32	150	500	15.22	5.68484E-05	8.65232E-06
1% Zn/SiO_2	0.5	0.32	150	500	59.05	5.68484E-05	3.3569E-05
2% Zn/SiO_2	0.5	0.32	150	500	67.61	5.68484E-05	3.84352E-05
3% Zn/SiO_2	0.5	0.32	150	500	80.73	5.68484E-05	4.58937E-05
4% Zn/SiO_2	0.5	0.32	150	500	76.05	5.68484E-05	4.32332E-05
Effect of the reaction temperature							
3% Zn/SiO_2	0.5	0.32	150	200	23.15	5.68484E-05	1.31604E-05
3% Zn/SiO_2	0.5	0.32	150	300	36.9	5.68484E-05	2.0977E-05
3% Zn/SiO_2	0.5	0.32	150	400	49.67	5.68484E-05	2.82366E-05
3% Zn/SiO_2	0.5	0.32	150	500	78.1	5.68484E-05	4.43986E-05
3% Zn/SiO_2	0.5	0.32	150	600	69.6	5.68484E-05	3.95665E-05
Effect of the WHSV							
3% Zn/SiO_2	0.5	0.32	150	500	79.93	5.68484E-05	4.54389E-05
3% Zn/SiO_2	0.6	0.38	150	500	70.34	6.8218E-05	4.79846E-05
3% Zn/SiO_2	0.7	0.45	150	500	65.14	7.95877E-05	5.18434E-05
3% Zn/SiO_2	0.8	0.51	150	500	64.39	9.09574E-05	5.85675E-05
3% Zn/SiO_2	0.9	0.57	150	500	63.07	0.000102327	6.45377E-05
3% Zn/SiO_2	1	0.64	150	500	61.91	0.000113697	7.03897E-05
3% Zn/SiO_2	1.1	0.7	150	500	60.92	0.000125066	7.61905E-05
3% Zn/SiO_2	1.2	0.77	150	500	57.33	0.000136436	7.82188E-05
3% Zn/SiO_2	1.3	0.83	150	500	42.55	0.000147806	6.28914E-05
3% Zn/SiO_2	1.4	0.89	150	500	40.03	0.000159175	6.37179E-05
Effect of the H_2 volumetric flow rate							
3% Zn/SiO_2	0.5	0.32	0	500	30.24	5.68484E-05	1.71909E-05
3% Zn/SiO_2	0.5	0.32	150	500	79.93	5.68484E-05	4.54389E-05
3% Zn/SiO_2	0.5	0.32	300	500	80.81	5.68484E-05	4.59392E-05
3% Zn/SiO_2	0.5	0.32	600	500	81.68	5.68484E-05	4.64337E-05
3% Zn/SiO_2	0.5	0.32	900	500	81.85	5.68484E-05	4.65304E-05

Agglomeration of the active metal in some parts of the support surface, has occupied many of the surface pores. According to Popov et al., (Popov et al., 2013), 350 ˚C is a

typical temperature for the conventional HDO process. However, from thermodynamic point of view, by eliminating the pressure of the process, temperature should be elevated to make up the lack of pressure. Consequently, higher temperature, in comparison to the typical range of temperature, was predictable for this process. However, optimizing the process temperature is crucial since elevating the temperature, specially above 400 ˚C, will increase the process cost as well as the formation of the coke (Cheng et al., 2016). Table 5.1 also has compared the performance of 3% Zn/SiO_2 at various WHSV from 0.32 to 0.89 h^{-1} at favored conditions (Temperature 500 ℃; pressure 1 atm; and H_2 volumetric flow rate (mL/min) 150). The highest conversion efficiency reached at the lowest WHSV. This indicates that the higher contact time will results to higher hydrodeoxygenation of the oxygenated products (Infantes-Molina et al., 2015). Increasing the volumetric flow rate of the hydrogen, had negligible effect by increasing the value greater than 150 mL/min. Consequently, the optimized process conditions for hydrodeoxygenation of 1% phenol in n-decane at atmospheric pressure of hydrogen are 500 ℃ (reaction temperature); 150 mL/min (H_2 volumetric flow rate); 0.32 h^{-1} (WHSV); and 3% (active metal loading). Figure 4.22 represents a comparison of different affective variable applied in this investigation and their effects on the total HDO efficiency of the phenol.
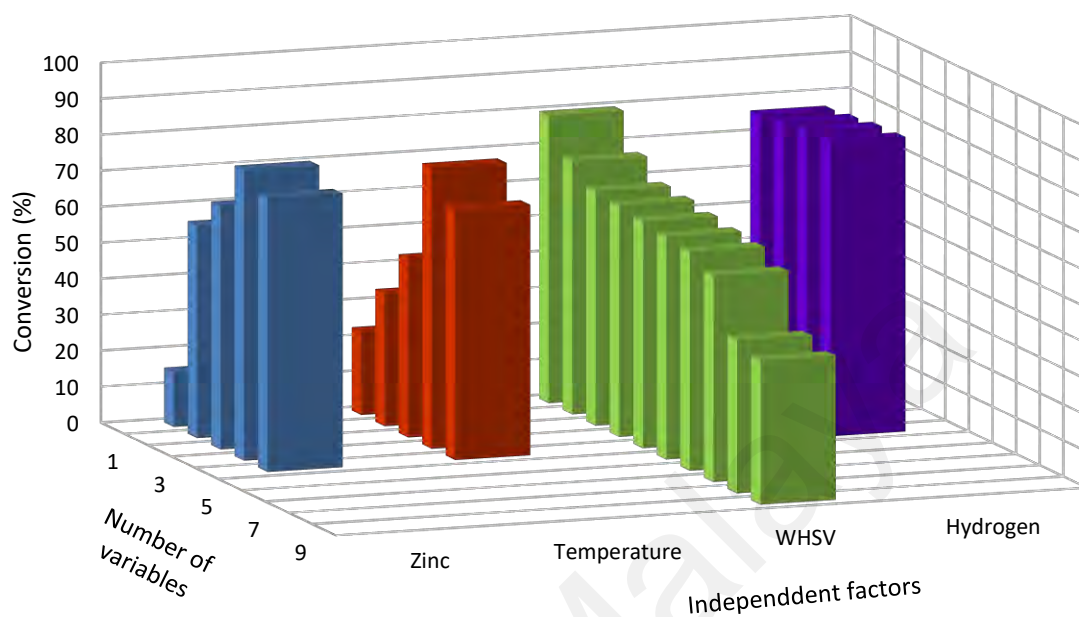
Figure 4.22: Effect of various process parameters on the total HDO efficiency of the phenol.

4.5.3 Catalyst stability study

The activity and optimization of the heterogeneous catalysts have been evaluated using a continues type reactor. However, not only the activity of the catalyst, but also its stability is an important factor in the assessment for a potential application (De Vylder et al., 2019). This means that the catalyst should exhibit a stable activity throughout its lifetime or be easily regenerated to a similar activity level. To this purpose, the stability and regenerability tests were performed using 3% Zn/SiO_2 catalyst. The time-on-stream investigation showed that the silica-supported zinc was highly active up to 240 min of phenol HDO, with a conversion efficiency up to 80%, and after 420 min of TOS, the activity decreased to around a conversion rate of 43%. Deposition of the impurities and

coke on the surface of the catalysts is responsible for the deactivation of the catalysts. Reusability tests revealed that the catalyst displayed outstanding reusability and could be regenerated fully after several reusing rounds.

CHAPTER 5: CONCLUSIONS AND RECOMMENDATIONS

In this research project, the catalytic gas-phase hydrodeoxygenation of phenol has been performed at atmospheric pressure of hydrogen gas using silica supported zinc catalysts. The catalyst characterization study using various analytical techniques including XRD, BET, TGA, H_2-TPD, H_2-TPR, NH_3-TPD, EDX, and ICP-OES along with topography analysis of the samples using the FESEM method revealed that the zinc metal is a promising active site to be applied for hydrodeoxygenation of oxygenated compounds such as phenol. Zinc is an abundant element in the earth's crust, which makes it a promising candidate as a cost-effective active site. Along with the characterization analysis, reactivity analysis revealed that the Zn/SiO_2 is an active and selective catalyst for converting phenol into aromatic hydrocarbons.

The effects of various independent variables were examined to explore the optimal process conditions. The hydrogen volumetric flow rate (150–900 ml/min) only slightly affects product distribution and conversion efficiency. Temperature (200 ˚C-600 ˚C) increases the reaction conversion efficiency without changing the selectivity. Among all loading amounts, 3% loading of the active metal (zinc) represents the highest conversion efficiency. Hence, the optimization study indicated that a process with 3% Zn/SiO_2 as the catalyst, temperature at 500 ˚C, WHSV of 0.32 h^{-1}, and H_2 volumetric flow rate of 150 mL/min provides the highest possible conversion efficiency of phenol into aromatic hydrocarbons. The HDO conversion of 80% and cyclohexane yield of 69% have been achieved under the above-mentioned conditions. The time-on-stream investigation showed that the silica-supported zinc was highly active up to 240 min of phenol HDO, with a conversion efficiency up to 80%, and after 420 min of TOS, the activity decreased to around a conversion rate of 43%.

Reusability tests revealed that the catalyst displayed outstanding reusability and could be regenerated fully after several reusing rounds. Zn/SiO_2 is a multipurpose catalyst that functions in catalytic reactors straightforwardly. Moreover, this catalyst is cheap and ecofriendly and could be a prospective catalyst for the production of aromatics from phenol through lignin fast pyrolysis followed by the HDO of the vapor.

Further investigation on the reaction mechanism and kinetics of these catalysts, and also regeneration studies are required in the future to facilitate the progress of bio-oil oxygenated compounds using silica-supported zinc catalysts.

REFERENCES

Abnisa, F., Arami-Niya, A., Wan Daud, W. M. A., Sahu, J. N., & Noor, I. M. (2013). Utilization of oil palm tree residues to produce bio-oil and bio-char via pyrolysis. *Energy Conversion and Management*, *76*, 1073–1082. https://doi.org/10.1016/j.enconman.2013.08.038

Abnisa, F., Daud W.M.A. Wan, W. M. A. W., Husin, W. N. W., & Sahu, J. N. (2011). Utilization possibilities of palm shell as a source of biomass energy in Malaysia by producing bio-oil in pyrolysis process. *Biomass and Bioenergy*, *35*(5), 1863–1872. https://doi.org/10.1016/j.biombioe.2011.01.033

Abnisa, F., Wan Daud, W. M. A., Arami-Niya, A., Ali, B. S., & Sahu, J. N. (2014). Recovery of Liquid Fuel from the Aqueous Phase of Pyrolysis Oil Using Catalytic Conversion. *Energy & Fuels*, *28*(5), 3074–3085. https://doi.org/10.1021/ef5003952

Adams, P., Bridgwater, T., Lea-Langton, A., Ross, A., & Watson, I. (2018). Biomass conversion technologies. In *Greenhouse Gas Balances of Bioenergy Systems* (pp. 107–139). Elsevier.

Adjaye, J. D., & Bakhshi, N. N. (1995). Production of hydrocarbons by catalytic upgrading of a fast pyrolysis bio-oil. Part II: Comparative catalyst performance and reaction pathways. *Fuel Processing Technology*, *45*(3), 185–202. https://doi.org/10.1016/0378-3820(95)00040-E

Ali, N., Zhang, Q., Liu, Z.-Y., Li, F.-L., Lu, M., & Fang, X.-C. (2020). Emerging technologies for the pretreatment of lignocellulosic materials for bio-based products. *Applied Microbiology and Biotechnology*, *104*(2), 455–473.

Anderson, A. B., & Nichols, J. A. (1986). Hydrogen on zinc oxide. Theory of its heterolytic adsorption. *Journal of the American Chemical Society*, *108*(16), 4742–4746.

Anggoro, D. D., Buchori, L., Sasongko, S. B., & Oktavianty, H. (2019). Basicity Optimization of KF/Ca-MgO Catalyst using Impregnation Method. *Bulletin of Chemical Reaction Engineering & Catalysis*, *14*(3), 678–682.

Asphaug, S. (2013). Catalytic Hydrodeoxygenation of Bio-oils with Supported MoP-Catalysts. *Thesis Chemical Engineering, Norwegian University of Science and Technology (NTNU)*, June.

Ausavasukhi, A., Huang, Y., To, A. T., Sooknoi, T., & Resasco, D. E. (2012). Hydrodeoxygenation of m-cresol over gallium-modified beta zeolite catalysts. *Journal of Catalysis*, *290*, 90–100. https://doi.org/10.1016/j.jcat.2012.03.003

Badawi, M., Paul, J. F., Cristol, S., Payen, E., Romero, Y., Richard, F., Brunet, S., Lambert, D., Portier, X., Popov, A., Kondratieva, E., Goupil, J. M., El Fallah, J., Gilson, J. P., Mariey, L., Travert, A., & Maugé, F. (2011). Effect of water on the stability of Mo and CoMo hydrodeoxygenation catalysts: A combined experimental and DFT study. *Journal of Catalysis*, *282*(1), 155–164. https://doi.org/https://doi.org/10.1016/j.jcat.2011.06.006

Boullosa-Eiras, S., Lødeng, R., Bergem, H., Stöcker, M., Hannevold, L., & Blekkan, E. A. (2014). Catalytic hydrodeoxygenation (HDO) of phenol over supported molybdenum carbide, nitride, phosphide and oxide catalysts. *Catalysis Today*, *223*, 44–53. https://doi.org/10.1016/j.cattod.2013.09.044

Bridgewater, A. V. (2004). Biomass fast pyrolysis. *Thermal Science*, *8*(2), 21–50.

Bridgwater, A. V. (2012). Review of fast pyrolysis of biomass and product upgrading. *Biomass and Bioenergy*, *38*, 68–94. https://doi.org/10.1016/j.biombioe.2011.01.048

Bu, Q., Lei, H., Zacher, A. H., Wang, L., Ren, S., Liang, J., Wei, Y., Liu, Y., Tang, J., Zhang, Q., & Ruan, R. (2012). A review of catalytic hydrodeoxygenation of lignin-derived phenols from biomass pyrolysis. *Bioresource Technology*, *124*, 470–477. https://doi.org/10.1016/j.biortech.2012.08.089

Bui, P., Cecilia, J. A., Oyama, S. T., Takagaki, A., Infantes-Molina, A., Zhao, H., Li, D., Rodríguez-Castellón, E., & Jiménez López, A. (2012). Studies of the synthesis of transition metal phosphides and their activity in the hydrodeoxygenation of a biofuel model compound. *Journal of Catalysis*, *294*, 184–198. https://doi.org/10.1016/j.jcat.2012.07.021

Bui, P. P., Takagaki, A., Kikuchi, R., & Oyama, S. T. (2016). Kinetic and Infrared Spectroscopy Study of Hydrodeoxygenation of 2-Methyltetrahydrofuran on a Nickel Phosphide Catalyst at Atmospheric Pressure. *ACS Catalysis*, acscatal.6b02396. https://doi.org/10.1021/acscatal.6b02396

Chandra-Sekhar, V., Shee, D., & Maity, S. K. (2014). Kinetics of hydrodeoxygenation of octanol over supported nickel catalysts: a mechanistic study. *RSC Adv.*, *4*(78), 41612–41621. https://doi.org/10.1039/C4RA06826B

Chen, C. J., Lee, W. S., & Bhan, A. (2016). Mo2C catalyzed vapor phase hydrodeoxygenation of lignin-derived phenolic compound mixtures to aromatics under ambient pressure. *Applied Catalysis A: General*, *510*, 42–48. https://doi.org/10.1016/j.apcata.2015.10.043

Chen, L., Janssens, T. V. W., Skoglundh, M., & Grönbeck, H. (2019). Interpretation of NH 3-TPD Profiles from Cu-CHA Using First-Principles Calculations. *Topics in Catalysis*, *62*(1–4), 93–99.

Cheng, S., Wei, L., Julson, J., Muthukumarappan, K., Kharel, P. R., & Boakye, E. (2017). Hydrocarbon bio-oil production from pyrolysis bio-oil using non-sulfide Ni-Zn/Al2O3catalyst. *Fuel Processing Technology*, *162*, 78–86. https://doi.org/10.1016/j.fuproc.2017.04.001

Cheng, S., Wei, L., Zhao, X., & Julson, J. (2016). Application, deactivation, and regeneration of heterogeneous catalysts in bio-oil upgrading. *Catalysts*, *6*(12), 195.

Chiaramonti, D., Bonini, M., Fratini, E., Tondi, G., Gartner, K., Bridgwater, A. V., Grimm, H. P., Soldaini, I., Webster, A., & Baglioni, P. (2003). Development of emulsions from biomass pyrolysis liquid and diesel and their use in engines - Part 1: Emulsion production. *Biomass and Bioenergy*, *25*(1), 85–99. https://doi.org/10.1016/S0961-9534(02)00183-6

Chiaramonti, David, Oasmaa, A., & Solantausta, Y. (2007). Power generation using fast pyrolysis liquids from biomass. *Renewable and Sustainable Energy Reviews*, *11*(6), 1056–1086. https://doi.org/https://doi.org/10.1016/j.rser.2005.07.008

Choudhary, T. V., & Phillips, C. B. (2011). Renewable fuels via catalytic hydrodeoxygenation. *Applied Catalysis A: General*, *397*(1–2), 1–12. https://doi.org/10.1016/j.apcata.2011.02.025

Clark, P. A., & Oyama, S. T. (2003). Alumina-supported molybdenum phosphide hydroprocessing catalysts. *Journal of Catalysis*, *218*(1), 78–87. https://doi.org/10.1016/S0021-9517(03)00086-1

Courty, P., & Marcilly, C. (1983). A scientific approach to the preparation of bulk mixed oxide catalysts. In *Studies in Surface Science and Catalysis* (Vol. 16, pp. 485–519). Elsevier.

Croteau, R., Kutchan, T. M., & Lewis, N. G. (2000). Secondary Metabolites. *Biochemistry Molecular Biology of Plants*, *7*(7), 1250–1318. https://doi.org/10.1016/j.phytochem.2011.10.011

Cui, B., Zhang, J., Liu, S., Liu, X., Xiang, W., Liu, L., Xin, H., Lefler, M. J., & Licht, S. (2017). Electrochemical synthesis of ammonia directly from N 2 and water over iron-based catalysts supported on activated carbon. *Green Chemistry*, *19*(1), 298–304.

Czajczyńska, D., Anguilano, L., Ghazal, H., Krzyżyńska, R., Reynolds, A. J., Spencer, N., & Jouhara, H. (2017). Potential of pyrolysis processes in the waste management sector. *Thermal Science and Engineering Progress*, *3*, 171–197. https://doi.org/https://doi.org/10.1016/j.tsep.2017.06.003

Czernik, S., & Bridgwater, A. V. (2004). Overview of applications of biomass fast pyrolysis oil. *Energy and Fuels*, *18*(2), 590–598. https://doi.org/10.1021/ef034067u

Das, T., & Deo, G. (2012). Effects of metal loading and support for supported cobalt catalyst. *Catalysis Today*, *198*(1), 116–124.

de Jongh, P., & de Jong, K. (2018). Synthesis of Solid Supports and Catalysts. *Catalysis: An Integrated Textbook for Students*.

de Miguel Mercader, F., Groeneveld, M. J., Kersten, S. R. A., Geantet, C., Toussaint, G., Way, N. W. J., Schaverien, C. J., & Hogendoorn, K. J. A. (2011). Hydrodeoxygenation of pyrolysis oil fractions: process understanding and quality assessment through co-processing in refinery units. *Energy & Environmental Science*, *4*(3), 985–997.

De, S., Saha, B., & Luque, R. (2015). Hydrodeoxygenation processes: Advances on catalytic transformations of biomass-derived platform chemicals into hydrocarbon fuels. *Bioresource Technology*, *178*, 108–118. https://doi.org/10.1016/j.biortech.2014.09.065

De Vylder, A., Lauwaert, J., Van Auwenis, S., De Clercq, J., & Thybaut, J. W. (2019). Catalyst Stability Assessment in a Lab-Scale Liquid-Solid (LS) [2] Plug-Flow Reactor.

Catalysts, *9*(9), 755.

De Waele, J., Galvita, V. V., Poelman, H., Detavernier, C., & Thybaut, J. W. (2018). PdZn nanoparticle catalyst formation for ethanol dehydrogenation: Active metal impregnation vs incorporation. *Applied Catalysis A: General*, *555*(November 2017), 12–19. https://doi.org/10.1016/j.apcata.2018.02.005

Debdoubi, A., El Amarti, A., Colacio, E., Blesa, M. J., & Hajjaj, L. H. (2006). The effect of heating rate on yields and compositions of oil products from esparto pyrolysis. *International Journal of Energy Research*, *30*(15), 1243–1250. https://doi.org/10.1002/er.1215

Demirbas, A. (2007). The influence of temperature on the yields of compounds existing in bio-oils obtained from biomass samples via pyrolysis. *Fuel Processing Technology*, *88*(6), 591–597. https://doi.org/10.1016/j.fuproc.2007.01.010

Deutsch, K. L., & Shanks, B. H. (2012). Hydrodeoxygenation of lignin model compounds over a copper chromite catalyst. *Applied Catalysis A: General*, *447–448*, 144–150. https://doi.org/10.1016/j.apcata.2012.09.047

Do, P. T. M., Foster, A. J., Chen, J., & Lobo, R. F. (2012). Bimetallic effects in the hydrodeoxygenation of meta-cresol on γ-Al2O3 supported Pt–Ni and Pt–Co catalysts. *Green Chemistry*, *14*(5), 1388. https://doi.org/10.1039/c2gc16544a

Echeandia, S., Arias, P. L., Barrio, V. L., Pawelec, B., & Fierro, J. L. G. (2010). Synergy effect in the HDO of phenol over Ni-W catalysts supported on active carbon: Effect of tungsten precursors. *Applied Catalysis B: Environmental*, *101*(1–2), 1–12. https://doi.org/10.1016/j.apcatb.2010.08.018

Elliott, D. C. (2007). Historical developments in hydroprocessing bio-oils. *Energy and Fuels*, *21*(3), 1792–1815. https://doi.org/10.1021/ef070044u

Eschenbacher, A., Saraeian, A., Shanks, B. H., Jensen, P. A., Li, C., Duus, J. Ø., & Ahrenfeldt, J. (2020). Enhancing bio-oil quality and energy recovery by atmospheric hydrodeoxygenation of wheat straw pyrolysis vapors using Pt and Mo-based catalysts. *Sustainable Energy & Fuels*, *4*(4), 1991–2008.

Everard, J. D., & Loescher, W. H. (2017). Primary Products of Photosynthesis, Sucrose and Other Soluble Carbohydrates. In *Encyclopedia of Applied Plant Sciences* (Second Edi, Vol. 2). Elsevier. https://doi.org/10.1016/B978-0-12-394807-6.00095-2

Fanchiang, W. L., & Lin, Y. C. (2012). Catalytic fast pyrolysis of furfural over H-ZSM-5 and Zn/H-ZSM-5 catalysts. *Applied Catalysis A: General*, *419–420*, 102–110. https://doi.org/10.1016/j.apcata.2012.01.017

Friščić, T. (2011). Metal-organic frameworks: mechanochemical synthesis strategies. *Encyclopedia of Inorganic and Bioinorganic Chemistry*, 1–19.

Furimsky, E. (2000). Catalytic hydrodeoxygenation. *Applied Catalysis A: General*, *199*(2), 147–190. https://doi.org/10.1016/S0926-860X(99)00555-4

Gevert, B. S., Otterstedt, J.-E., & Massoth, F. E. (1987). Kinetics of the HDO of methyl-substituted phenols. *Applied Catalysis*, *31*(1), 119–131. https://doi.org/https://doi.org/10.1016/S0166-9834(00)80671-5

Gollakota, A. R. K., Reddy, M., Subramanyam, M. D., & Kishore, N. (2016). A review on the upgradation techniques of pyrolysis oil. *Renewable and Sustainable Energy Reviews*, *58*, 1543–1568. https://doi.org/10.1016/j.rser.2015.12.180

Gomes, J. F., Lopes, A., Bednarczyk, K., Gmurek, M., Stelmachowski, M., Zaleska-Medynska, A., Quinta-Ferreira, M. E., Costa, R., Quinta-Ferreira, R. M., & Martins, R. C. (2018). Effect of noble metals (Ag, Pd, Pt) loading over the efficiency of TiO2 during photocatalytic ozonation on the toxicity of parabens. *ChemEngineering*, *2*(1), 4.

Goo, K. Z., Leong, L. K., Yap, Y. H., Lin, K.-S., & Chiang, C.-L. (2020). Direct Ultrasound Synthesis of Vanadyl Pyrophosphate Catalyst for Partial Oxidation of N-Butane to Maleic Anhydride. *Journal of Computational and Theoretical Nanoscience*, *17*(2–3), 925–933.

Graċa, I., Lopes, J. M., Cerqueira, H. S., & Ribeiro, M. F. (2013). Bio-oils upgrading for second generation biofuels. *Industrial and Engineering Chemistry Research*, *52*(1), 275–287. https://doi.org/10.1021/ie301714x

Guo, X.-Y., Yan, Y.-J., & Li, T.-C. (2004). Influence of catalyst type and regeneration on upgrading of crude bio-oil through catalytical thermal cracking. *Guocheng Gongcheng Xuebao/The Chinese Journal of Process Engineering*, *4*(1), 53–58. https://www.scopus.com/inward/record.uri?eid=2-s2.0-2042544073&partnerID=40&md5=797664aa3f35089f70ae83435bc7af39

Gutierrez, A., Kaila, R. K., Honkela, M. L., Slioor, R., & Krause, A. O. I. (2009). Hydrodeoxygenation of guaiacol on noble metal catalysts. *Catalysis Today*, *147*(3), 239–246. https://doi.org/https://doi.org/10.1016/j.cattod.2008.10.037

Haneveld, J., Tas, N. R., Brunets, N., Jansen, H. V, & Elwenspoek, M. (2008). Capillary filling of sub-10nm nanochannels. *Journal of Applied Physics*, *104*(1), 14309. https://doi.org/10.1063/1.2952053

Hao, Y., Wang, X., Perret, N., Cárdenas-lizana, F., Keane, M. A., Hao, Y., Wang, X., Perret, N., Cárdenas-lizana, F., Ca, F., Hao, Y., Wang, X., & Keane, M. A. (2015). *Support effects in the gas phase hydrogenation of butyronitrile over palladium Support effects in the gas phase hydrogenation of butyronitrile over palladium*. *0758*. https://doi.org/10.1179/2055075814Y.0000000002

He, Z., & Wang, X. (2012). Hydrodeoxygenation of model compounds and catalytic systems for pyrolysis bio-oils upgrading. *Catalysis for Sustainable Energy, Versita*, *1*, 28–52. https://doi.org/10.2478/cse-2012-0004

Howard, J., Braid, I. J., & Tomkinson, J. (1984). Spectroscopic studies of hydrogen adsorbed on zinc oxide (kadox 25). *Journal of the Chemical Society, Faraday Transactions 1: Physical Chemistry in Condensed Phases*, *80*(1), 225–235.

Huber, G. W., Iborra, S., & Corma, A. (2006). Synthesis of transportation fuels from

biomass: Chemistry, catalysts, and engineering. *Chemical Reviews*, *106*(9), 4044–4098. https://doi.org/10.1021/cr068360d

Hurst, N. W., Gentry, S. J., Jones, A., & McNicol, B. D. (1982). Temperature programmed reduction. *Catalysis Reviews Science and Engineering*, *24*(2), 233–309.

Hutchings, G. J., & Védrine, J. C. (2004). Heterogeneous catalyst preparation. In *Basic principles in applied catalysis* (pp. 215–258). Springer.

Huynh, T. M., Armbruster, U., Kreyenschulte, C. R., Nguyen, L. H., Phan, B. M. Q., Nguyen, D. A., & Martin, A. (2016). Understanding the performance and stability of supported Ni-Co-based catalysts in phenol HDO. *Catalysts*, *6*(11), 176.

Infantes-Molina, A., Gralberg, E., Cecilia, J. A., Finocchio, E., & Rodríguez-Castellón, E. (2015). Nickel and cobalt phosphides as effective catalysts for oxygen removal of dibenzofuran: role of contact time, hydrogen pressure and hydrogen/feed molar ratio. *Catalysis Science & Technology*, *5*(6), 3403–3415.

Jacobson, K., Maheria, K. C., & Kumar Dalai, A. (2013). Bio-oil valorization: A review. *Renewable and Sustainable Energy Reviews*, *23*, 91–106. https://doi.org/10.1016/j.rser.2013.02.036

Jiamin, W., Xudong, F., Xiwei, X., Yujian, W., Wu, Y., Xu, X., Sun, Y., Jiang, E., Fan, X., & Tu, R. (2020). *Gas-phase hydrodeoxygenation of guaiacol over Ni-based HUSY zeolite catalysts under atmospheric H2 pressure.*

Jiang, E., Cheng, S., Tu, R., He, Z., Jia, Z., Long, X., Wu, Y., & Sun, Y. (2020). High yield self-nitrogen-oxygen doped hydrochar derived from microalgae carbonization in bio-oil: properties and potential applications. *Bioresource Technology*, 123735.

Joshi, N., & Lawal, A. (2012). Hydrodeoxygenation of acetic acid in a microreactor. *Chemical Engineering Science*, *84*, 761–771. https://doi.org/10.1016/j.ces.2012.09.018

Karnjanakom, S., Bayu, A., Hao, X., Kongparakul, S., Samart, C., Abudula, A., & Guan, G. (2016). Selectively catalytic upgrading of bio-oil to aromatic hydrocarbons over Zn, Ce or Ni-doped mesoporous rod-like alumina catalysts. *Journal of Molecular Catalysis A: Chemical*, *421*, 235–244. https://doi.org/10.1016/j.molcata.2016.06.001

Katikaneni, S., Adjaye, J., & Bakhshi, N. (1995). Performance of aluminophosphate molecular sieve catalysts for the production of hydrocarbons from wood-derived and vegetable oils. *Energy & Fuels*, *7*, 1065–1078. https://doi.org/10.1021/ef00054a021

Ko, C. H., Park, S. H., Jeon, J. K., Suh, D. J., Jeong, K. E., & Park, Y. K. (2012). Upgrading of biofuel by the catalytic deoxygenation of biomass. *Korean Journal of Chemical Engineering*, *29*(12), 1657–1665. https://doi.org/10.1007/s11814-012-0199-5

Komiyama, M. (1985). Design and preparation of impregnated catalysts. *Catalysis Reviews Science and Engineering*, *27*(2), 341–372.

Korea, R., Jechan, S., & Chem, G. (2019). *As featured in:* https://doi.org/10.1039/c9gc01210a

Krutof, A., & Hawboldt, K. A. (2020). Thermodynamic model of fast pyrolysis bio-oil advanced distillation curves. *Fuel*, *261*, 116446.

Lee, W. S., Wang, Z., Wu, R. J., & Bhan, A. (2014). Selective vapor-phase hydrodeoxygenation of anisole to benzene on molybdenum carbide catalysts. *Journal of Catalysis*, *319*, 44–53. https://doi.org/10.1016/j.jcat.2014.07.025

Leofanti, G., Padovan, M., Tozzola, G., & Venturelli, B. (1998). Surface area and pore texture of catalysts. *Catalysis Today*, *41*(1–3), 207–219.

Li, Ye, Li, Z., Wang, H., & Cai, N. (2020). CaO carbonation kinetics determined using micro-fluidized bed thermogravimetric analysis. *Fuel*, *264*, 116823.

Li, Yuning, Liu, S., Xie, S., & Xu, L. (2009). Promoted metal utilization capacity of alkali-treated zeolite: Preparation of Zn/ZSM-5 and its application in 1-hexene aromatization. *Applied Catalysis A: General*, *360*(1), 8–16. https://doi.org/10.1016/j.apcata.2009.02.039

Li, Z., Jiang, E., Xu, X., Sun, Y., & Tu, R. (2020). Hydrodeoxygenation of phenols , acids , and ketones as model bio-oil for hydrocarbon fuel over Ni-based catalysts modi fi ed by Al , La and Ga. *Renewable Energy*, *146*, 1991–2007. https://doi.org/10.1016/j.renene.2019.08.012

Li, Z., Yi, W., Li, Z., Bai, X., Fu, P., Tian, C., & Zhang, Y. (2020). Hydrodeoxygenation of bio-oil and model compounds for production of chemical materials at atmospheric pressure over nickel-based zeolite catalysts. *Energy Sources, Part A: Recovery, Utilization, and Environmental Effects*, 1–13.

Limayem, A., & Ricke, S. C. (2012). Lignocellulosic biomass for bioethanol production: Current perspectives, potential issues and future prospects. *Progress in Energy and Combustion Science*, *38*(4), 449–467. https://doi.org/10.1016/j.pecs.2012.03.002

Liu, C., Wang, H., Karim, A. M., Sun, J., & Wang, Y. (2014). Catalytic fast pyrolysis of lignocellulosic biomass. *Chem. Soc. Rev.*, *43*(22), 7594–7623. https://doi.org/10.1039/C3CS60414D

Luzgin, M. V., Rogov, V. A., Arzumanov, S. S., Toktarev, A. V., Stepanov, A. G., & Parmon, V. N. (2009). Methane aromatization on Zn-modified zeolite in the presence of a co-reactant higher alkane: How does it occur? *Catalysis Today*, *144*(3–4), 265–272. https://doi.org/10.1016/j.cattod.2008.08.043

Ma, Z., Wei, L., Zhou, W., Jia, L., Hou, B., Li, D., & Zhao, Y. (2015). Overview of catalyst application in petroleum refinery for biomass catalytic pyrolysis and bio-oil upgrading. *RSC Advances*, *5*(107), 88287–88297.

Malani, R. S., Shinde, V., Ayachit, S., Goyal, A., & Moholkar, V. S. (2019). Ultrasound–assisted biodiesel production using heterogeneous base catalyst and mixed non–edible oils. *Ultrasonics Sonochemistry*, *52*, 232–243.

Massoth, F. E., Politzer, P., Concha, M. C., Murray, J. S., Jakowski, J., & Simons, J. (2006). Catalytic hydrodeoxygenation of methyl-substituted phenols: Correlations of kinetic parameters with molecular properties. *Journal of Physical Chemistry B*, *110*(29), 14283–14291. https://doi.org/10.1021/jp057332g

Mbaraka, I. K., & Shanks, B. H. (2006). Conversion of oils and fats using advanced mesoporous heterogeneous catalysts. *Journal of the American Oil Chemists' Society*, *83*(2), 79–91. https://doi.org/10.1007/s11746-006-1179-x

Mirzayanti, Y. W., Prajitno, D. H., & Roesyadi, A. (2017). Catalytic hydrocracking of Kapuk seed oil (Ceiba pentandra) to produce biofuel using Zn-Mo supported HZSM-5 catalyst. *IOP Conference Series: Earth and Environmental Science*, *67*(1), 012023. https://doi.org/10.1088/1755-1315/67/1/012023

Mo, J., Sha, J., Li, D., Li, Z., & Chen, Y. (2019). Fluid release pressure for nanochannels: the Young–Laplace equation using the effective contact angle. *Nanoscale*, *11*(17), 8408–8415.

Mohan, D., Pittman, C. U., & Steele, P. H. (2006). Pyrolysis of wood/biomass for bio-oil: A critical review. *Energy and Fuels*, *20*(3), 848–889. https://doi.org/10.1021/ef0502397

Mølgaard, P., Carvalho, D., Hudson, W. P., Danvad, C., Arendt, P., Birkedal, J., & Degn, A. (2014). *Catalysis Science & Technology*. https://doi.org/10.1039/c4cy00522h

Molina, B. D. (2014). *Alkali promoted molybdenum (IV) sulfide based catalysts, development and characterization for alcohol synthesis from carbon monoxide and hydrogen*.

Mortensen, P. M., Gardini, D., Damsgaard, C. D., Grunwaldt, J.-D., Jensen, P. A., Wagner, J. B., & Jensen, A. D. (2016). Deactivation of Ni-MoS2 by bio-oil impurities during hydrodeoxygenation of phenol and octanol. *Applied Catalysis A: General*, *523*, 159–170. https://doi.org/https://doi.org/10.1016/j.apcata.2016.06.002

Mortensen, P. M., Grunwaldt, J. D., Jensen, P. A., & Jensen, A. D. (2013). Screening of catalysts for hydrodeoxygenation of phenol as a model compound for bio-oil. *ACS Catalysis*, *3*(8), 1774–1785. https://doi.org/10.1021/cs400266e

Mortensen, P. M., Grunwaldt, J. D., Jensen, P. A., Knudsen, K. G., & Jensen, A. D. (2011). A review of catalytic upgrading of bio-oil to engine fuels. *Applied Catalysis A: General*, *407*(1–2), 1–19. https://doi.org/10.1016/j.apcata.2011.08.046

Munnik, P., de Jongh, P. E., & de Jong, K. P. (2015). Recent Developments in the Synthesis of Supported Catalysts. *Chemical Reviews*, *115*(14), 6687–6718. https://doi.org/10.1021/cr500486u

Naik, S. N., Goud, V. V., Rout, P. K., & Dalai, A. K. (2010). Production of first and second generation biofuels: A comprehensive review. *Renewable and Sustainable Energy Reviews*, *14*(2), 578–597. https://doi.org/10.1016/j.rser.2009.10.003

Ni, Y., Sun, A., Wu, X., Hai, G., Hu, J., Li, T., & Li, G. (2011). The preparation of nano-sized H[Zn, Al]ZSM-5 zeolite and its application in the aromatization of methanol.

Microporous and Mesoporous Materials, *143*(2–3), 435–442. https://doi.org/10.1016/j.micromeso.2011.03.029

Nie, L. (2014). *Catalytic Hydrodeoxygenation of Phenolic Compounds of Importance in Bio-oil Upgrading*.

Nimmanwudipong, T., Aydin, C., Lu, J., Runnebaum, R. C., Brodwater, K. C., Browning, N. D., Block, D. E., & Gates, B. C. (2012). Selective hydrodeoxygenation of guaiacol catalyzed by platinum supported on magnesium oxide. *Catalysis Letters*, *142*(10), 1190–1196. https://doi.org/10.1007/s10562-012-0884-3

Nimmanwudipong, T., Runnebaum, R. C., Block, D. E., & Gates, B. C. (2011a). Catalytic reactions of guaiacol: Reaction network and evidence of oxygen removal in reactions with hydrogen. *Catalysis Letters*, *141*(6), 779–783. https://doi.org/10.1007/s10562-011-0576-4

Nimmanwudipong, T., Runnebaum, R. C., Block, D. E., & Gates, B. C. (2011b). Catalytic Conversion of Guaiacol Catalyzed by Platinum Supported on Alumina: Reaction Network Including Hydrodeoxygenation Reactions. *Energy & Fuels*, *25*(8), 3417–3427. https://doi.org/10.1021/ef200803d

No, S. Y. (2014). Application of bio-oils from lignocellulosic biomass to transportation, heat and power generation - A review. *Renewable and Sustainable Energy Reviews*, *40*, 1108–1125. https://doi.org/10.1016/j.rser.2014.07.127

Oasmaa, A., Peacocke, C., Gust, S., Meier, D., & McLellan, R. (2005). Norms and standards for pyrolysis liquids. End-user requirements and specifications. *Energy & Fuels*, *19*(5), 2155–2163.

Olbrich, W., Boscagli, C., Raffelt, K., Zang, H., Dahmen, N., & Sauer, J. (2016). Catalytic hydrodeoxygenation of pyrolysis oil over nickel-based catalysts under H 2/CO 2 atmosphere. *Sustainable Chemical Processes*, *4*(1), 9.

Olcese, R., Bettahar, M. M., Malaman, B., Ghanbaja, J., Tibavizco, L., Petitjean, D., & Dufour, A. (2013). Gas-phase hydrodeoxygenation of guaiacol over iron-based catalysts. Effect of gases composition, iron load and supports (silica and activated carbon). *Applied Catalysis B: Environmental*, *129*, 528–538. https://doi.org/10.1016/j.apcatb.2012.09.043

Olcese, R. N., Bettahar, M., Petitjean, D., Malaman, B., Giovanella, F., & Dufour, A. (2012a). Gas-phase hydrodeoxygenation of guaiacol over Fe/SiO 2 catalyst. *Applied Catalysis B: Environmental*, *115–116*, 63–73. https://doi.org/10.1016/j.apcatb.2011.12.005

Olcese, R. N., Bettahar, M., Petitjean, D., Malaman, B., Giovanella, F., & Dufour, A. (2012b). Gas-phase hydrodeoxygenation of guaiacol over Fe/SiO2 catalyst. *Applied Catalysis B: Environmental*, *115–116*, 63–73. https://doi.org/https://doi.org/10.1016/j.apcatb.2011.12.005

Olcese, R. N., Francois, J., Bettahar, M. M., Petitjean, D., & Dufour, A. (2013). Hydrodeoxygenation of guaiacol, a surrogate of lignin pyrolysis vapors, over iron based catalysts: Kinetics and modeling of the lignin to aromatics integrated process.

Energy and Fuels, *27*(2), 975–984. https://doi.org/10.1021/ef301971a

Oyama, S. T., Clark, P., Teixeira da Silva, V. L. S., Lede, E. J., & Requejo, F. G. (2002). XAFS characterization of highly active alumina-supported molybdenum phosphide catalysts (MoP/Al2O3) for hydrotreating. *Journal of Physical Chemistry B*, *105*(21), 4961–4966. https://doi.org/10.1021/jp004500q

Parsell, T. H., Owen, B. C., Klein, I., Jarrell, T. M., Marcum, C. L., Haupert, L. J., Amundson, L. M., Kenttämaa, H. I., Ribeiro, F., Miller, J. T., & Abu-Omar, M. M. (2013). Cleavage and hydrodeoxygenation (HDO) of C–O bonds relevant to lignin conversion using Pd/Zn synergistic catalysis. *Chem. Sci.*, *4*(2), 806–813. https://doi.org/10.1039/C2SC21657D

Pattiya, A. (2018). *1 - Fast pyrolysis* (L. B. T.-D. T. L. for E. A. Rosendahl (ed.); pp. 3–28). Woodhead Publishing. https://doi.org/https://doi.org/10.1016/B978-0-08-101029-7.00001-1

Perego, C., & Villa, P. (1997). Catalyst preparation methods. *Catalysis Today*, *34*(3–4), 281–305.

Phillips, D. C., Sawhill, S. J., Self, R., & Bussell, M. E. (2002). Synthesis, characterization, and hydrodesulfurization properties of silica-supported molybdenum phosphide catalysts. *Journal of Catalysis*, *207*(2), 266–273. https://doi.org/10.1006/jcat.2002.3524

Popov, A., Kondratieva, E., Mariey, L., Goupil, J. M., El Fallah, J., Gilson, J. P., Travert, A., & Maugé, F. (2013). Bio-oil hydrodeoxygenation: Adsorption of phenolic compounds on sulfided (Co)Mo catalysts. *Journal of Catalysis*, *297*, 176–186. https://doi.org/10.1016/j.jcat.2012.10.005

Pourzolfaghar, H., Abnisa, F., Daud, W. M. A. W., & Aroua, M. K. (2020). Gas-phase hydrodeoxygenation of phenol over Zn/SiO2 catalysts: Effects of zinc load, temperature, weight hourly space velocity, and H2 volumetric flow rate. *Biomass and Bioenergy*, *138*, 105556. https://doi.org/10.1016/j.biombioe.2020.105556

Pourzolfaghar, H., Abnisa, F., Wan Daud, W. M. A., Aroua, M. K., & Mahlia, T. M. I. (2020). Catalyst Characteristics and Performance of Silica-Supported Zinc for Hydrodeoxygenation of Phenol. *Energies*, *13*(11), 2802.

Prasomsri, T., Nimmanwudipong, T., & Roman-Leshkov, Y. (2013). Effective hydrodeoxygenation of biomass-derived oxygenates into unsaturated hydrocarbons by MoO3 using low H2 pressures. *Energy & Environmental Science*, *6*(6), 1732–1738. https://doi.org/10.1039/C3EE24360E

Prasomsri, T., Shetty, M., Murugappan, K., & Román-Leshkov, Y. (2014). Insights into the catalytic activity and surface modification of MoO 3 during the hydrodeoxygenation of lignin-derived model compounds into aromatic hydrocarbons under low hydrogen pressures. *Energy & Environmental Science*, *7*(8), 2660. https://doi.org/10.1039/C4EE00890A

Ren, H., Chen, Y., Huang, Y., Deng, W., Vlachos, D. G., & Chen, J. G. (2014). Tungsten carbides as selective deoxygenation catalysts: experimental and computational

studies of converting C3 oxygenates to propene. *Green Chem.*, *16*(2), 761–769. https://doi.org/10.1039/C3GC41256C

Resasco, D. E. (2011). *Anisole and Guaiacol Hydrodeoxygenation over Monolithic Pt À Sn Catalysts*. *25*, 4155–4162.

Romero, Y., Richard, F., & Brunet, S. (2010). Hydrodeoxygenation of 2-ethylphenol as a model compound of bio-crude over sulfided Mo-based catalysts: Promoting effect and reaction mechanism. *Applied Catalysis B: Environmental*, *98*(3), 213–223. https://doi.org/https://doi.org/10.1016/j.apcatb.2010.05.031

Romero, Y., Richard, F., Renème, Y., & Brunet, S. (2009). Hydrodeoxygenation of benzofuran and its oxygenated derivatives (2,3-dihydrobenzofuran and 2-ethylphenol) over NiMoP/Al2O3catalyst. *Applied Catalysis A: General*, *353*(1), 46–53. https://doi.org/10.1016/j.apcata.2008.10.022

Rover, M., Hall, P., Johnston, P., Smith, R., & Brown, R. (2015). Stabilization of bio-oils using low temperature, low pressure hydrogenation. *Fuel*, *153*, 224–230. http://www.sciencedirect.com/science/article/pii/S0016236115002021

Ruddy, D. A., Schaidle, J. A., Ferrell III, J. R., Wang, J., Moens, L., & Hensley, J. E. (2014). Recent advances in heterogeneous catalysts for bio-oil upgrading via "ex situ catalytic fast pyrolysis": catalyst development through the study of model compounds. In *Green Chemistry* (Vol. 16, Issue 2). https://doi.org/10.1039/c3gc41354c

Runnebaum, R. C., Nimmanwudipong, T., Block, D. E., & Gates, B. C. (2012). Catalytic conversion of compounds representative of lignin-derived bio-oils: a reaction network for guaiacol, anisole, 4-methylanisole, and cyclohexanone conversion catalysed by Pt/γ-Al2O3. *Catalysis Science & Technology*, *2*(1), 113. https://doi.org/10.1039/c1cy00169h

Rusu, D. I., Rusu, G. G., & Luca, D. (2011). Structural Characteristics and Optical Properties of Thermally Oxidized Zinc Films. *Acta Physica Polonica, A.*, *119*(6).

Saber, M., Nakhshiniev, B., & Yoshikawa, K. (2016). A review of production and upgrading of algal bio-oil. *Renewable and Sustainable Energy Reviews*, *58*, 918–930. https://doi.org/10.1016/j.rser.2015.12.342

Sacco, O., Vaiano, V., Sannino, D., Picca, R. A., & Cioffi, N. (2019). Ag modified ZnS for photocatalytic water pollutants degradation: Influence of metal loading and preparation method. *Journal of Colloid and Interface Science*, *537*, 671–681.

Schittkowski, J., Buesen, D., Toelle, K., & Muhler, M. (2016). The Temperature-Programmed Desorption of H 2 from Cu/ZrO 2. *Catalysis Letters*, *146*(5), 1011–1017.

Schmal, M. (2016). Catalyst Preparation. In *Heterogeneous Catalysis and its Industrial Applications* (pp. 161–187). Springer.

Şenol, O. I., Ryymin, E. M., Viljava, T. R., & Krause, A. O. I. (2007). Effect of hydrogen sulphide on the hydrodeoxygenation of aromatic and aliphatic oxygenates on

sulphided catalysts. *Journal of Molecular Catalysis A: Chemical*, *277*(1–2), 107–112. https://doi.org/10.1016/j.molcata.2007.07.033

Shafaghat, H., Rezaei, P. S., & Ashri Wan Daud, W. M. (2015). Effective parameters on selective catalytic hydrodeoxygenation of phenolic compounds of pyrolysis bio-oil to high-value hydrocarbons. *RSC Adv.*, *5*(126), 103999–104042. https://doi.org/10.1039/C5RA22137D

Shemfe, M., Gu, S., & Fidalgo, B. (2017). Techno-economic analysis of biofuel production via bio-oil zeolite upgrading: An evaluation of two catalyst regeneration systems. *Biomass and Bioenergy*, *98*, 182–193. https://doi.org/https://doi.org/10.1016/j.biombioe.2017.01.020

Shetty, M., Murugappan, K., Prasomsri, T., Green, W. H., & Román-Leshkov, Y. (2015). Reactivity and stability investigation of supported molybdenum oxide catalysts for the hydrodeoxygenation (HDO) of m-cresol. *Journal of Catalysis*, *331*, 86–97. https://doi.org/10.1016/j.jcat.2015.07.034

Shin-Kuan, W., et al. (2013). *Atmospheric Hydrodeoxygenation of Guaiacol over Alumina-, Zirconia-, and Silica-Supported Nickel Phosphide Catalysts*. *1*, 349–358.

Shin, E.-J., & Keane, M. A. (1998). Catalytic hydrogen treatment of aromatic alcohols. *Journal of Catalysis*, *173*(2), 450–459.

Shin, E. J., & Keane, M. A. (2000). Gas-phase hydrogenation/hydrogenolysis of phenol over supported nickel catalysts. *Industrial and Engineering Chemistry Research*, *39*(4), 883–892. https://doi.org/10.1021/ie990643r

Sio, Z., & Yue-juan, W. (2017). *Zn/SiO 2 气相催化裂解 1,1,2- 三氯乙烷脱 HCl ：酸性与失活*. *33*(5), 1017–1026. https://doi.org/10.3866/PKU.WHXB201702082

Smiešková, A., Rojasová, E., Hudec, P., & Šabo, L. (2004). Aromatization of light alkanes over ZSM-5 catalysts: Influence of the particle properties of the zeolite. *Applied Catalysis A: General*, *268*(1–2), 235–240. https://doi.org/10.1016/j.apcata.2004.03.043

Soares, A. P. V., Portela, M. F., & Kiennemann, A. (2005). Methanol selective oxidation to formaldehyde over iron-molybdate catalysts. *Catalysis Reviews*, *47*(1), 125–174.

Soni, V. K., Dhara, S., Krishnapriya, R., Choudhary, G., Sharma, P. R., & Sharma, R. K. (2020). Highly selective Co3O4/silica-alumina catalytic system for deoxygenation of triglyceride-based feedstock. *Fuel*, *266*, 117065.

Sun, J., Karim, A. M., Zhang, H., Kovarik, L., Li, X. S., Hensley, A. J., McEwen, J. S., & Wang, Y. (2013). Carbon-supported bimetallic Pd-Fe catalysts for vapor-phase hydrodeoxygenation of guaiacol. *Journal of Catalysis*, *306*, 47–57. https://doi.org/10.1016/j.jcat.2013.05.020

Tanaka, K., Aomura, K., Okuhara, T., & Miyahara, K. (1981). Orientation in the addition of HD molecules to buta-1, 3-diene over ZnO catalyst. A method of judging heterolytic and homolytic dissociation of hydrogen in catalysis. *Journal of the*

Chemical Society, Faraday Transactions 1: Physical Chemistry in Condensed Phases, 77(7), 1697–1706.

Thommes, M., Kaneko, K., Neimark, A. V, Olivier, J. P., Rodriguez-Reinoso, F., Rouquerol, J., & Sing, K. S. W. (2015). Physisorption of gases, with special reference to the evaluation of surface area and pore size distribution (IUPAC Technical Report). *Pure and Applied Chemistry*, 87(9–10), 1051–1069.

Valencia, D., Conde, R. I., García, B., Ramírez-verduzco, L. F., & Aburto, J. (2019). Development of bio-inspired supports based on Ca e SiO 2 and their use in hydrodeoxygenation of palmitic acid. *Renewable Energy*, *xxxx*. https://doi.org/10.1016/j.renene.2019.10.087

Viswanadham, N., Pradhan, A. R., Ray, N., Vishnoi, S. C., Shanker, U., & Prasada Rao, T. S. R. (1996). Reaction pathways for the aromatization of paraffins in the presence of H-ZSM-5 and Zn/H-ZSM-5. *Applied Catalysis A: General*, 137(2), 225–233. https://doi.org/10.1016/0926-860X(95)00287-1

Vorobiev, E., & Lebovka, N. (2020). Biomass Feedstocks. In *Processing of Foods and Biomass Feedstocks by Pulsed Electric Energy* (pp. 337–398). Springer.

Wan, S., Pham, T., Zhang, S., Lobban, L., Resasco, D., & Mallinson, R. (2013). Direct catalytic upgrading of biomass pyrolysis vapors by a dual function Ru/TiO 2 catalyst. *AIChE Journal*, 59(7), 2275–2285. https://doi.org/10.1002/aic.14038

Wang, H., Male, J., & Wang, Y. (2013). Recent advances in hydrotreating of pyrolysis bio-oil and its oxygen-containing model compounds. *ACS Catalysis*, 3(5), 1047–1070. https://doi.org/10.1021/cs400069z

Wang, W. yan, Yang, Y. quan, Bao, J. guo, & Luo, H. an. (2009). Characterization and catalytic properties of Ni-Mo-B amorphous catalysts for phenol hydrodeoxygenation. *Catalysis Communications*, 11(2), 100–105. https://doi.org/10.1016/j.catcom.2009.09.003

Wang, Y., Mourant, D., Hu, X., Zhang, S., Lievens, C., & Li, C. (2013). Formation of coke during the pyrolysis of bio-oil. *Fuel*, 108, 439–444. https://doi.org/10.1016/j.fuel.2012.11.052

Whiffen, V. (2013). *A Study of Metal Phosphides for the Hydrodeoxygenation of Phenols and Pyrolysis Oil by*. *July*.

Wildschut, J., Melián-Cabrera, I., & Heeres, H. J. (2010). Catalyst studies on the hydrotreatment of fast pyrolysis oil. *Applied Catalysis B: Environmental*, 99(1–2), 298–306. https://doi.org/10.1016/j.apcatb.2010.06.036

Williams, P. T., & Horne, P. A. (1994). Characterisation of oils from the fluidised bed pyrolysis of biomass with zeolite catalyst upgrading. *Biomass and Bioenergy*, 7(1), 223–236. https://doi.org/http://dx.doi.org/10.1016/0961-9534(94)00064-Z

Wimmers, O. J., Arnoldy, P., & Moulijn, J. A. (1986). Determination of the reduction mechanism by temperature-programmed reduction: application to small iron oxide (Fe2O3) particles. *The Journal of Physical Chemistry*, 90(7), 1331–1337.

Wu, S. K., Lai, P. C., & Lin, Y. C. (2014). Atmospheric hydrodeoxygenation of guaiacol over nickel phosphide catalysts: Effect of phosphorus composition. *Catalysis Letters*, *144*(5), 878–889. https://doi.org/10.1007/s10562-014-1231-7

Wu, S. K., Lai, P. C., Lin, Y. C., Wan, H. P., Lee, H. T., & Chang, Y. H. (2013). Atmospheric hydrodeoxygenation of guaiacol over alumina-, zirconia-, and silica-supported nickel phosphide catalysts. *ACS Sustainable Chemistry and Engineering*, *1*(3), 349–358. https://doi.org/10.1021/sc300157d

Xu, Y., Cui, S., Long, J., Gong, J., Da, Z., Zhang, J., Zhu, Y., Luo, Y., & Jinlian, T. (2017). *Catalytic cracking catalyst having a higher selectivity, processing method and use thereof*. Google Patents.

Yan, P., Li, M. M.-J., Kennedy, E., Adesina, A., Zhao, G., Setiawan, A., & Stockenhuber, M. (2020). The role of acid and metal sites in hydrodeoxygenation of guaiacol over Ni/Beta catalysts. *Catalysis Science & Technology*, *10*(3), 810–825.

Yang, J., Li, S., Zhang, L., Liu, X., Wang, J., Pan, X., Li, N., Wang, A., Cong, Y., Wang, X., & Zhang, T. (2017a). Hydrodeoxygenation of furans over Pd-FeOx/SiO2 catalyst under atmospheric pressure. *Applied Catalysis B: Environmental*, *201*, 266–277. https://doi.org/10.1016/j.apcatb.2016.08.045

Yang, J., Li, S., Zhang, L., Liu, X., Wang, J., Pan, X., Li, N., Wang, A., Cong, Y., Wang, X., & Zhang, T. (2017b). Hydrodeoxygenation of furans over Pd-FeOx/SiO2 catalyst under atmospheric pressure. *Applied Catalysis B: Environmental*, *201*, 266–277. https://doi.org/https://doi.org/10.1016/j.apcatb.2016.08.045

Yang, Y. Q., Tye, C. T., & Smith, K. J. (2008). Influence of MoS2 catalyst morphology on the hydrodeoxygenation of phenols. *Catalysis Communications*, *9*(6), 1364–1368. https://doi.org/10.1016/j.catcom.2007.11.035

Yi-hao, H. U., Tong-yang, S., Yue-juan, W., Geng-shen, H. U., Guan-qun, X. I. E., & Meng-fei, L. U. O. (2017). *Zn / SiO 2 Gas Phase Catalytic Cracking 1 , 1 , 2-Trichloroethane Dehydrochlorination : Acidity and Inactivation*. 1–11.

Yiwen, F., Ji, T., Xiaochang, H., Weibin, S., Yibing, S., & Changyong, S. U. N. (2010). Aromatization of Dimethyl Ether over Zn / H-ZSM-5 Catalyst. *Chinese Journal of Catalysis*, *31*(3), 264–266. https://doi.org/10.1016/S1872-2067(09)60046-2

Zanuttini, M. S., Dalla Costa, B. O., Querini, C. A., & Peralta, M. A. (2014). Hydrodeoxygenation of m-cresol with Pt supported over mild acid materials. *Applied Catalysis A: General*, *482*, 352–361. https://doi.org/10.1016/j.apcata.2014.06.015

Zanuttini, M. S., Lago, C. D., Querini, C. A., & Peralta, M. A. (2013). Deoxygenation of m-cresol on Pt/??-Al2O3 catalysts. *Catalysis Today*, *213*, 9–17. https://doi.org/10.1016/j.cattod.2013.04.011

Zhang, J., Matsubara, K., Yun, G.-N., Zheng, H., Takagaki, A., Kikuchi, R., & Oyama, S. T. (2017). Comparison of phosphide catalysts prepared by temperature-programmed reduction and liquid-phase methods in the hydrodeoxygenation of 2-methylfuran. *Applied Catalysis A: General*, *548*, 39–46.

https://doi.org/https://doi.org/10.1016/j.apcata.2017.06.009

Zhang, Q., Chang, J., Wang, T., & Xu, Y. (2007). Review of biomass pyrolysis oil properties and upgrading research. *Energy Conversion and Management*, *48*(1), 87–92. https://doi.org/10.1016/j.enconman.2006.05.010

Zhang, X., Tang, W., Zhang, Q., Wang, T., & Ma, L. (2018). Hydrodeoxygenation of lignin-derived phenoic compounds to hydrocarbon fuel over supported Ni-based catalysts. *Applied Energy*, *227*, 73–79.

Zhang, X., Zhang, Q., Wang, T., Li, B., Xu, Y., & Ma, L. (2016). Efficient upgrading process for production of low quality fuel from bio-oil. *Fuel*, *179*, 312–321. https://doi.org/10.1016/j.fuel.2016.03.103

Zhao, C., He, J., Lemonidou, A. A., Li, X., & Lercher, J. A. (2011). Aqueous-phase hydrodeoxygenation of bio-derived phenols to cycloalkanes. *Journal of Catalysis*, *280*(1), 8–16. https://doi.org/10.1016/j.jcat.2011.02.001

Zhao, C., Kou, Y., Lemonidou, A. A., Li, X., & Lercher, J. A. (2009). Highly selective catalytic conversion of phenolic bio-oil to alkanes. *Angewandte Chemie - International Edition*, *48*(22), 3987–3990. https://doi.org/10.1002/anie.200900404

Zhao, H. Y., Li, D., Bui, P., & Oyama, S. T. (2011). Hydrodeoxygenation of guaiacol as model compound for pyrolysis oil on transition metal phosphide hydroprocessing catalysts. *Applied Catalysis A: General*, *391*(1–2), 305–310. https://doi.org/10.1016/j.apcata.2010.07.039

Zhao, X., Wei, L., Cheng, S., Cao, Y., Julson, J., & Gu, Z. (2015). Catalytic cracking of carinata oil for hydrocarbon biofuel over fresh and regenerated Zn/Na-ZSM-5. *Applied Catalysis A: General*, *507*, 44–55. https://doi.org/https://doi.org/10.1016/j.apcata.2015.09.031

Zhou, G., Jensen, P. A., Le, D. M., Knudsen, N. O., & Jensen, A. D. (2016a). Atmospheric hydrodeoxygenation of biomass fast pyrolysis vapor by MoO3. *ACS Sustainable Chemistry & Engineering*, *4*(10), 5432–5440.

Zhou, G., Jensen, P. A., Le, D. M., Knudsen, N. O., & Jensen, A. D. (2016b). Atmospheric Hydrodeoxygenation of Biomass Fast Pyrolysis Vapor by MoO3. *ACS Sustainable Chemistry and Engineering*, *4*(10), 5432–5440. https://doi.org/10.1021/acssuschemeng.6b00757

Zhu, M., & Wachs, I. E. (2018). A perspective on chromium-Free iron oxide-based catalysts for high temperature water-gas shift reaction. *Catalysis Today*, *311*, 2–7.

Zhu, X., Lobban, L. L., Mallinson, R. G., & Resasco, D. E. (2011). Bifunctional transalkylation and hydrodeoxygenation of anisole over a Pt/HBeta catalyst. *Journal of Catalysis*, *281*(1), 21–29. https://doi.org/10.1016/j.jcat.2011.03.030